Mathematical Characterization of Skin Absorption

Dissertation zur Erlangung des Grades des Doktors der Naturwissenschaften der Naturwissenschaftlich-Technischen Fakultät III Chemie, Pharmazie, Bio- und Werkstoffwissenschaften der Universität des Saarlandes

UNIVERSITÄT DES SAARLANDES

von

Dominik Selzer

Saarbrücken, 2014

Tag des Kolloquiums:	19.03.2015
Dekan:	Prof. Dr.-Ing. Dirk Bähre
Mitglieder des Promotionsausschusses:	Prof. Dr. Claus-Michael Lehr (Vorsitz)
	Prof. Dr. Ulrich F. Schäfer
	Prof. Dr.-Ing. Stefan Diebels
	Dr. Martin Frotscher

Eidesstattliche Erklärung

"Hiermit versichere ich an Eides statt, dass ich diese Arbeit 'Mathematical Characterization of Skin Absorption' selbstständig und nur unter Angabe der angegebenen Quellen und Verweise angefertigt habe. Die aus anderen Quellen oder indirekt übernommenen Daten und Konzepte sind unter Angabe der Quellen gekennzeichnet. Ich habe diese Arbeit bisher weder im In- noch im Ausland in gleicher oder ähnlicher Form in einem Verfahren zur Erlangung eines akademischen Grades vorgelegt."

Saarbrücken, November 2014

Dominik Selzer

Abstract

Work on the mathematical modeling and data analysis of skin absorption with focus on finite dosing is presented within this thesis. It could be shown that correction of experimental data based on the area of application should be taken into consideration depending on the drug's lipophilic character. Next, the influence of the lateral compartment for finite dose in-vitro skin mass balance was examined with the help three mathematical models that could satisfyingly predict or describe the experimental data. Moreover, for two model drugs high amounts of substance could be found in the lateral skin compartment. Finally, a diffusion model was developed to predict in-vivo concentration-depth profiles (C-DP) with model input parameters gathered from in-vitro experiments. In addition, work on prediction of keratin binding is presented using an extended database. Furthermore, it could be shown that skin topography might have a considerable impact on skin absorption. Finally, a mathematical equation to correct Raman signal attenuation to improve non-invasive C-DPs of human skin is presented. In summary, it can be stated that the concepts and investigations at hand could improve experimental data, experimental setups and mathematical models in the field of skin absorption.

Kurzzusammenfassung

Arbeiten auf dem Gebiet der mathematischen Modellierung und Analyse von Hautabsorption, mit einem Fokus auf finite Dosierung, werden in dieser Arbeit vorgestellt. Es konnte gezeigt werden, dass Abhängig von der Lipophilie der Substanz, die Korrektur experimenteller Daten, basierend auf der Applikationsfläche, in Betracht gezogen werden sollte. Der Einfluss des lateralen Kompartiments auf die *in-vitro* Massenbilanz bei finiter Dosierung wurde mit Hilfe dreier mathematischer Modelle untersucht, die experimentelle Daten befriedigend vorhersagen oder beschreiben konnten. Für zwei Modellsubstanzen konnten hohe Substanzmengen im lateralen Hautkompartiment gefunden werden. Zuletzt wurde ein Diffusionsmodell, basierend auf aus *in-vitro* Experimenten stammenden Modelleingabeparametern, entwickelt, um *in-vivo* Konzentrations-Schicht-Tiefenprofile (KST) vorherzusagen. In Ergänzung werden Arbeiten auf dem Gebiet der Vorhersage von Keratin-Bindung mit Hilfe einer erweiterten Datenbank vorgestellt. Außerdem konnte gezeigt werden, dass die Hauttopographie Auswirkungen auf die Hautabsorption haben kann. Abschließend wird eine mathematische Gleichung zur Signaldämpfungskorrektur bei Raman-Spektroskopie vorgestellt, um nichtinvasive Messungen von KST der menschlichen Haut zu verbessern. Zusammenfassend lässt sich sagen, dass die hier gezeigten Konzepte und Untersuchungen zur Verbesserung experimenteller Daten, Versuche und mathematischer Modelle im Bereich der Hautabsorption beigetragen konnten.

Table of contents

Abbreviations

A	Application area
$c(x,t)$	Concentration at position x and time t
Co	Initial concentration
CAF	Caffeine
D	Apparent diffusion coefficient
DSL	Deeper skin layers (viable epidermis and parts of the dermis)
FD-C	Franz diffusion-cell
FFA	Flufenamic acid
FTS	Full thickness skin
h	Height
HSE	Heat-separated epidermis
J	Flux
J_{peak}	Peak flux
J_{SS}	Steady-state flux
k	Boltzmann's constant
$K_{i/j}$	Partition coefficient regarding compartment i and j
$K_{o/w}$	Octanol-water partition coefficient
k_p	Permeability
l	Length
$m(t)$	Accumulated permeated mass at time t
MW	Molecular weight
$Q(t)$	Amount released over time t
RSE	Residual standard error
SB-M	Saarbücken penetration model

SC	*Stratum corneum*
SE	Standard error
S_v	Saturated concentration in layer v
t	Time
T	Temperature
t_{lag}	Lag-time
V	Volume
VE	Viable epidermis
Ω_i	Compartment i
$\Gamma_{i,j}$	Interface between compartment i and j

1 Introduction

Parts of this chapter have been published in:

Selzer, D., Abdel-Mottaleb, M. M. A., Hahn, T., Schaefer, U. F., & Neumann, D. (2013). Finite and Infinite Dosing: Difficulties in Measurements, Evaluations and Predictions. *Adv Drug Deliver Rev*, 65(2), 278–294.

Selzer, D., Schaefer, U. F., Lehr, C.-M., Hansen, S. (2013) Basic Mathematics in Skin Absorption. In H. Maibach (Ed.), Percutaneous Penetration Enhancers: *Springer Press* (in press)

Schaefer, U. F., Selzer, D., Hansen, S., Lehr, C.-M. (2013) Human native and reconstructed skin preparations for in vitro penetration and permeation studies. In H. Maibach (Ed.), Percutaneous Penetration Enhancers: *Springer Press* (in press)

1.1 Transdermal absorption

1.1.1 Skin morphology

The human skin is by far the largest visible organ of the body (approximately 2 m^2). On the one hand it forms an effective barrier between the organism and the environment, preventing invasion of pathogens and impeding the absorption of chemicals, on the other hand it prevents the unregulated loss of water and solutes from inside.

Furthermore, the skin is responsible for metabolism and several other functions like the regulation of heat balance, sense of touch and protection against injuries. The outer skin can roughly be divided into three layers of epithelial tissue:

- Epidermis
- Dermis
- Subcutis

For in-depth information about the structure and function of the human skin the reader is kindly referred to [1, 2].

1.1.1.1 Epidermis

The epidermis is the outermost layer and is responsible for the protective and waterproofing properties of the skin. It features a thickness of about 100 – 150 µm. One specialty is the lack of blood vessels so that the deepest layers are nourished by diffusion from capillaries from the upper layers of the subjacent dermis. The main types of cells that are located inside the epidermis are Langerhans cells, Merkel cells and melanocytes, whereas the largest part (90%) ascribes to the keratinocytes [3]. The Langerhans cells are responsible for the immune response of the whole skin and Merkel cells are associated with the sense of touch. The human epidermis can be further subdivided into two main layers, the *stratum corneum* (SC) and the viable epidermis.

The *stratum corneum* is the outermost layer of the epidermis, featuring a thickness of usually 10 – 25 µm (depending on body site) under physiological conditions, while it may swell to several times this thickness when immersed in water for longer periods of time. Despite the fact that it accounts to only a small fraction of total skin thickness the SC is by far the most effective barrier of the skin. Applying mechanical damage to the skin (e.g. via scalpel blade, sandpaper abrasion, adhesive tape stripping and suction blister top removal) showed a strong increase in permeability [4]. The SC is composed of large, nonviable, cornified plate-like envelopes (corneocytes) filled with keratin (fibrous structural proteins) which are arranged in layers (15 – 25) [5]. They are almost non-permeable, are embedded in a continuous lipid matrix and originate from the basal layer of the epidermis, the *stratum germinativum*. Due to this shape one can model this layer as a *bricks and mortar model* (Figure 1-1) where the bricks are the corneocytes and the mortar is the lipid matrix [6]. The keratin helps to provide a certain hydration level (approximately 30% *in-vivo* [7]) by preventing water evaporation.

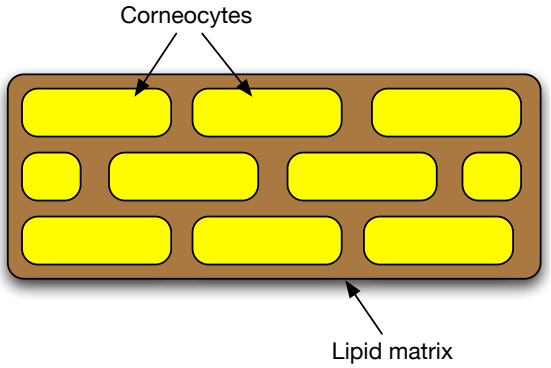

Figure 1-1 *Bricks and mortar model* of the *stratum corneum* (not drawn to scale).

Finally the viable epidermis can be subdivided into several layers (from top to bottom, Figure 1-2):

- *Stratum lucidum* (only in palms of hands and bottom of feet)
- *Stratum granulosum*
- *Stratum spinosum*
- Basal membrane (*stratum germinativum*)

The viable epidermis provides protection against exposure to ultraviolet light (via production of melanin – a pigment).

1.1.1.2 Dermis

The dermis has a thickness of 3 – 5 mm and thus forms the thickest layer of the skin. It is mainly composed of fibroblasts which are responsible for the production of collagen and elastin fibres. Sensory nerves, blood and lymphatic vessels, hair follicles and sweat glands are also located inside this thick layer. The elastic fibers are responsible for the flexibility of the skin and the ability to adapt to pressure.

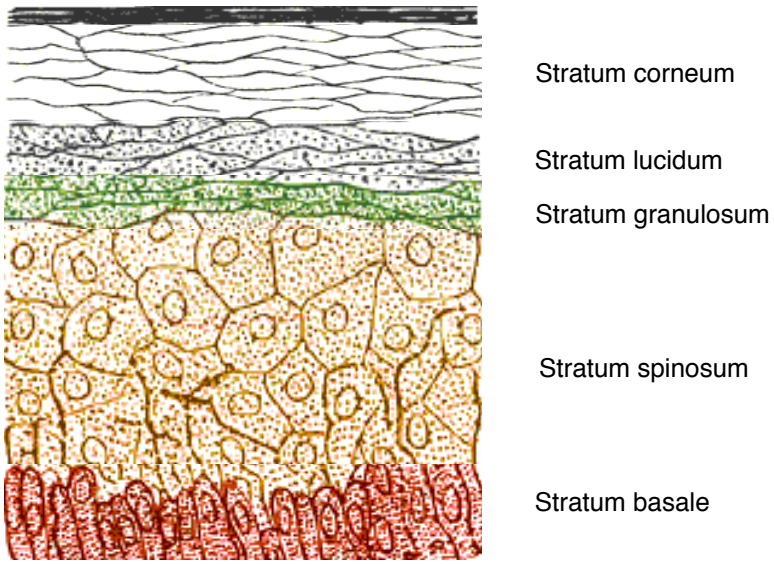

Figure 1-2 Simplified morphology of the epidermis. Adapted from [8].

1.1.1.3 Subcutis

The subcutaneous fat layer acts as a conjunction between the overlying dermis and the underlying body tissue. The thickness highly depends on the site of the body and physical condition of the person. It is composed of loose fat, connective tissue, blood vessels and nerves [1]. The main purpose of this layer is to isolate the body, provide mechanical protection against physical shock and serve as an energy reservoir.

1.1.2 Transport pathways through the skin

While for healthy skin the barrier function is typically located in the *stratum corneum*, the bottleneck for invasion of very lipophilic substances shifts down to the conjunction of *stratum corneum* and viable epidermis due to their reduced solubility in the aqueous epidermis layers [9].

Based on the anatomical structure of the skin, two basically different pathways for substance invasion are to be considered:

- Diffusion across the intact SC, the outermost layer of the skin.
- Invasion via skin appendages such as hair follicles or glands.

Normally, the route through the intact SC accounts for the main pathway of skin absorption, especially if small and dissolved molecules are concerned. However, for nanoparticles or submicron-sized drug delivery systems, for example liposomes and nanoparticles, the appendageal pathway may be predominant [10-12]. An additional mechanical rubbing, e.g. a massage, will improve the appendageal delivery. Moreover, for healthy skin it has been reported that nanoparticles > 10 nm are unlikely to overcome the *stratum corneum* barrier [13].

Governed by the anatomical structure of the intact *stratum corneum* the following absorption pathways are feasible: The intercellular route and the transcellular route. The intercellular route is associated with the lipid bilayer structures in between the corneocytes and is considered to be the predominating invasion route, particularly if steady state conditions are assumed. It has been shown that transepidermal water loss is strongly increased and the permeability is strongly enhanced after lipid extraction of the epidermis [14, 15]. Due to the liquid crystalline structures of the lipid matrix surrounding the corneocytes, the intercellular route provides hydrophilic as well as lipophilic domains offering the possibility that both lipophilic and hydrophilic entities diffuse via this pathway. Although the intercellular route is very tortuous and therefore much longer (e.g. a factor of approximately 13 in comparison to the macroscopic thickness of the SC for an unexpanded membrane [16]), the diffusion is relatively fast in this region due to an enhanced diffusivity in comparison to

the corneocytes. Furthermore, this pathway can easily be modulated by penetration enhancers.

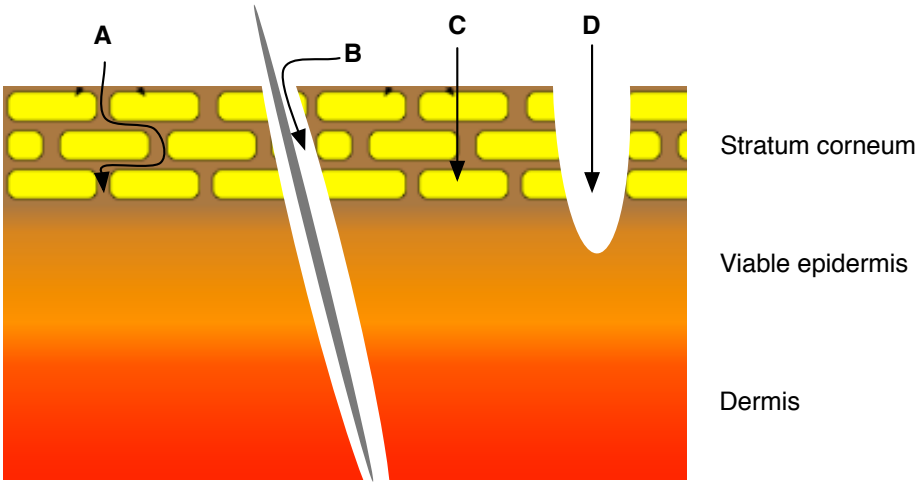

Figure 1-3 Illustration of the four possible substance absorption routes in human skin (adapted from [17]). A: Intercellular diffusion, B: Transport pathway trough hair follicles and sweat glands, C: Transcellular pathway, D: Micro-scale holes in the skin.

The transcellular route is normally regarded negligible because diffusion in the solid corneocytes is low and the necessity to partition several times between the lipid bilayers and the more hydrophilic corneocytes. Both phenomena result in a reduced absorption with the exception if penetration enhancers are used which might increase the permeability of the corneocytes.

As a result of the various possibilities for substance invasion through and into the *stratum corneum, in-vitro* skin absorption experiments must take into account these different pathways.

In diseased skin the barrier function is reduced because of structural changes in the *stratum corneum*. For example, the lipid bilayer structure is partly lost or the number of *stratum corneum* layers may be reduced. An illustrated overview with regard to the different transport pathways is given in Figure 1-3.

1.2 Experimental methods to investigate transdermal drug transport

As an easy accessible organ, for a long time our skin is used for the application of cosmetics and furthermore also for the topical application of drugs [18]. Primarily, however, the skin is actually a protective organ hindering the invasion of foreign substances from the environment to our body and to maintain homeostasis. Therefore, different reasons exist to monitor the fate of compounds in contact with the skin. For example, to assure that no absorption occurs (cosmetics or hazardous substances) or vice versa to demonstrate that skin absorption does take place, indeed (drug delivery). While the motivation and scope for skin absorption studies might be different, the same experimental setups can be used to gather the desired information. In contrast to clinical studies or animal experiments, *in-vitro* skin absorption studies allow the screening of different formulations, without any ethical restrictions, which is a particular problem for cosmetics where animal experiments have been banned [19, 20]. Actually, information about xenobiotic *in-vitro* skin absorption is requested explicitly by the EU initiative REACH – Registration, Evaluation, Authorization and Restriction of Chemicals [21]. Besides these advantages, the major drawback of *in-vitro* skin absorption studies is the absence of peripheral blood flow that cannot be simulated completely. Furthermore, concerning risk assessment the acceptance of *in-vitro* skin absorption data by the authorities are different.

In the European Union, dermal absorption data for many pesticides has been estimated by *in-vitro* experiments [22, 23]. In contrast NAFTA countries (the USA, Canada and Mexico [24]) do not accept *in-vitro* skin absorption data alone for risk assessment. However, most of the skin absorption data published in the field of cosmetic and pharmaceutical sciences is based on in vitro skin absorption studies.

The following sections address common *in-vitro* test systems and analytical methods for the two major types of skin absorption experiments: "Skin permeation" and "skin penetration" experiments. Skin permeation measurements focus on the amount of substance transported across the skin (or parts of the skin) over time. This is especially important for questions regarding systemic delivery of drugs or risk assessment with respect to exposure to hazardous substances.

In contrast, skin penetration measurements deal with the investigation of drug concentration distribution in different skin layers over time. These investigations are typically important to answer questions regarding local application of drugs.

1.2.1 Methods to investigate skin permeation

In-vitro skin permeation experiments are generally performed using diffusion cells, whose donor and acceptor compartments are separated by excised skin or one or more of its composing layers. The cells are usually made of glass although other materials are in use as well. Diffusion cells can be classified into two major types, static and flow through cells. In static cells, donor, membrane and acceptor may be arranged either vertically as in the well-known Franz diffusion cell (Figure 1-4 A) [25] or horizontally (side by side) as in the (Teflon) Bronaugh cell (Figure 1-4 B) [26].

Usually, the acceptor solution is stirred by magnetic stir bars and the whole system is thermostatically controlled. Side by side cells can be used for measurement of permeation from one stirred solution through a membrane into another stirred solution which might be advantageous for, e.g., testing permeation from a saturated solution in the presence of excess solid [27].

Flow through cells are usually similar to the upright Franz diffusion cells but with certain modifications that allow the continuous replacement of the acceptor solution with the aid of a pump (Figure 1-4 C). This might be useful for permeants of very low solubility as a tool to provide sink conditions such as in the case of highly lipophilic drugs that easily saturate the acceptor solution in the static type of cells [28, 29]. Another possible advantage of the flow through system is achieved by using a tissue culture medium as acceptor solution that continuously flows under the skin, so that local metabolism can be studied and the system has higher similarity to the *in-vivo* situation [30]. However, care should be taken to avoid high dilution that might lead to detection or analytical problems. Furthermore, parameters like flow rate or sampling interval can have a considerable impact on the curve shape and hence on the estimated parameters [31]. Detailed review of the different types and design of diffusion cells are available in literature [32].

When performing permeation experiments, samples from the acceptor solution are withdrawn after pre-determined time intervals and assessed for cumulative amount of permeant. The amount of substance in the barrier itself is usually not determined.

Different preparations and layers of excised skin may be used as the barrier, for example *stratum corneum* sheets or epidermis or dermatomed skin.

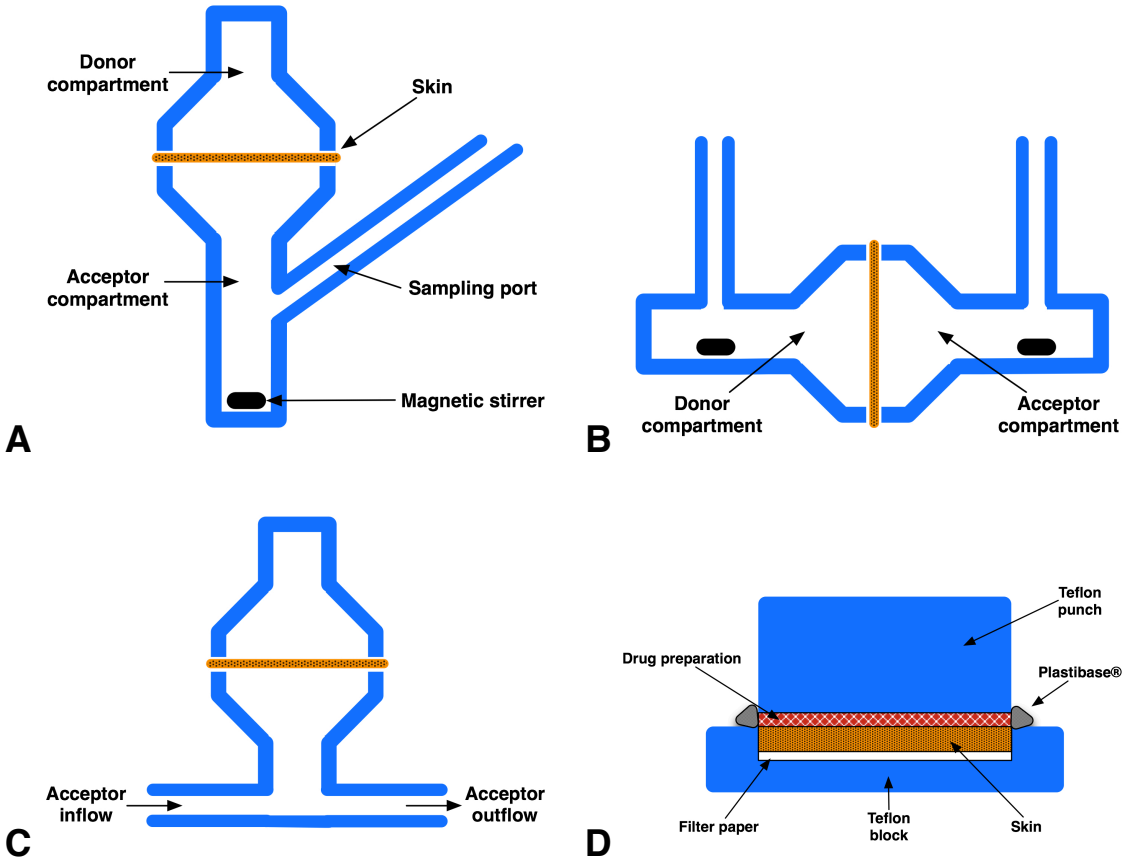

Figure 1-4 Sketch of a static vertical Franz diffusion-cell (A), static side-by-side diffusion cell, flow through cell (C) and Saarbruecken penetration model (D).

1.2.2 Methods to investigate skin penetration

While the total amounts of permeant in the acceptor solution and in the barrier already allow for assessing the transport process across the skin, the concentration-depth profile of a permeant in the different skin layers may be even more valuable. Concentration-depth profiles are time dependent and vary with the permeant's physicochemical properties.

One of the most commonly performed experiments to evaluate the change in permeant concentration within the SC both *in-vitro* and *in-vivo* is tape stripping [27]. In short, drug formulations are applied to the skin and after a pre-determined time tape stripping is performed. Subsequently, the drug may be extracted from the tapes to quantify the amount of drug which has penetrated into the SC.

The removal of sequential layers of the SC using adhesive tapes is considered to be minimally invasive and suitable for bioequivalence studies [33, 34]. A good correlation between the amount of drug recovered on the strips and that having entered systemic circulation was also found [35, 36]. *In-vivo*, tape stripping can be performed with minimal discomfort and relative ease on the volar forearm of healthy volunteers [36]. To improve the contact of the tape to the skin *in-vitro*, pressure on the tape may be applied using a roller [11] or a defined weight [37, 38]. For further information on the tape stripping procedure, the reader is kindly referred to [39, 40]. To establish concentration-depth profiles in the SC, the thickness of the removed layer and the location in the skin are required. Here, difficulties arise primarily from the change in cohesion between the corneocytes with SC depth. For example, the outer layers seem to be less densely bound and therefore can be easily removed in comparison to the deeper more intact layers [41]. As a consequence, the amount of SC removed per tape strip follows an exponential decay curve [42, 43].

1.2.2.1 The Saarbrücken penetration model

The Saarbrücken penetration model (SB-M) is a model to study the rate and extent of drug penetration into the *stratum corneum* and the deeper skin layers *in-vitro* [38]. In this type of experiment, a semisolid drug formulation or a piece of filter paper soaked in a drug solution is applied to the skin surface placed in a Teflon block on a

filter paper soaked with Ringer solution to prevent drying of the skin. Subsequently, a Teflon punch containing the formulation is placed on the skin and charged with a weight for two minutes in order to improve the contact between the skin and the drug preparation [38, 44]. Thus, this setup avoids the relatively non-physiologic hydration which may occur when using FD-Cs. The skin itself is the only acceptor for the penetrating drug and the penetration of the drug into the different skin layers is followed by skin segmentation and further analysis of the drug concentration in these segments. Therefore, data obtained from SB-M are mainly related to the drug concentration in the different skin layers without giving any details about drug permeation or flux through the skin, which can be better investigated using a FD-C. However, a direct correlation between the penetration data obtained from SB-M and the permeation parameters from FD-Cs for the lipophilic drug flufenamic acid was found [45].

1.2.2.2 Optical methods

Optical methods such as confocal laser scanning microscopy (CLSM) or confocal Raman spectroscopy may be used as well to obtain semi-quantitative concentration-depth profiles. Both are non-invasive imaging techniques that can be applied both *in-vitro* and *in-vivo*. However, until now quantitative measurements are not possible. With CLSM, images parallel to the skin surface at different depths are recorded that can then be reconstructed to obtain a three dimensional image for different skin structures and any permeant that penetrated the skin without any mechanical sectioning of the skin [46]. As CLSM is mainly used to visualize the fate of fluorescent substances or carriers through the skin, experiments are mostly performed under infinite dose conditions (see next section) [11, 47].

Raman spectroscopy has long been recognized as a standard method in analytical pharmacy and chemistry. In pharmaceutics and biopharmaceutics, it has been widely used to study biological skin samples [48] and in clinical dermatology, to study, e.g. atopic dermatitis [49] and basal cell carcinoma [50]. Similar to CLSM, confocal Raman spectroscopy may be used to obtain concentration-depth profiles [51, 52]. An advantage of this technique is that it is not necessary to label the diffusing molecules as long as they are Raman-active.

Due to the optical density of skin, CLSM and confocal Raman spectroscopy do not allow inspection of deeper skin layers.

1.2.3 Infinite and finite dosing

Two scenarios may be distinguished according to the amount of substance applied to the skin, infinite and finite dosing. In the case of infinite dosing, the applied dose is so large that depletion of the permeant in the donor chamber caused by evaporation or diffusion into and through the barrier is negligibly small. Consequently, the dose is considered to be constant and infinite [27]. In infinite dose experiments, the permeant is often applied in comparatively large volumes, which may exert an occlusive effect and thus lead to an increased permeability, although this effect may already be observed for thin layers [53].

In contrast to infinite dose experiments with an infinitely large donor, in the finite dose regime, only a limited amount of the donor formulation is applied to the skin surface. The application of a finite dose supposedly best resembles the *in-vivo* situation when applying e.g., an ointment. Furthermore, special effects like the influence of evaporation of excipients can be observed.

Per definition in the Organisation for Economic Co-Operation and Development (OECD) guideline 428 [54] and the guidance document 28 [55], finite dose skin absorption experiments are characterized by the application of ≤ 10 µl/cm^2 of a liquid formulation to the skin. For semisolid and solid substances, values range from 1 to 10 mg/cm^2 [54-56].

For substances with low permeability, it may be difficult to observe donor depletion and to obtain the curve shapes characteristic for finite dosing [57].

1.3 Mathematical background of analyzing skin absorption processes

It is usually assumed that the travel of molecules through the skin membrane is governed simply by passive diffusion due to the absence of active transporters. From an atomistic point of view diffusion is based on Brownian motion of particles in virtue of their thermal energy. From an empirical and more macroscopic understanding the driving force of molecular movement is a concentration gradient of the diffusant in a medium and can be mathematically described by laws derived by Adolf Fick in 1855.

Fick's first law (Equation 1-1) relates the diffusion flux J (e.g. in mol/m^{2}s) to the concentration gradient. Here D, the diffusion coefficient, is a proportionality constant usually given in m^2/s and c the concentration at point x in space and time t.

$$J(x,t) = -D\nabla c(x,t) \qquad \text{Equation 1-1}$$

Assuming conservation of mass one can derive Fick's second law of diffusion (Equation 1-2).

$$\frac{\partial c(x,t)}{\partial t} = \nabla\big(\mathrm{D}\,\nabla c(x,t)\big) \qquad \text{Equation 1-2}$$

In this general equation the diffusion coefficient may vary in dependence of location and/or concentration. Additional terms can be included to address e.g. binding phenomena [58], enzymatic reactions [59], corneocyte desquamation [60] or general convective transport to model elimination or clearance of molecules into the systematic circulation [61]. For the one-dimensional case and a homogenous medium (constant diffusivity) Equation 1-2 simplifies to:

$$\frac{\delta c(x,t)}{\delta t} = \frac{\delta}{\delta x}\left(D\,\frac{\delta}{\delta x}c(x,t)\right) \qquad \text{Equation 1-3}$$

Homogeneity is often a strong simplification but a typical assumption for easy analytical models to describe transdermal drug transport. These parabolic partial differential equations can often be solved analytically for various initial and boundary conditions and various solutions are presented in Sections 1.3.1 and 1.3.2. As mentioned before, these conditions often denote simplifications and are only true for the description of a specific experimental setup (e.g. infinite dose or finite dose conditions with certain initial conditions). This is a fundamental issue and must be always kept in mind when applying mathematical models in general. More flexible but complex models that allow the application to a wider range of scenarios can be solved by applying numerical concepts and are addressed in section 1.3.4.

For the inhomogeneous and more general case the diffusion flux at a cross-section x at time t is directed from sites of higher chemical potential to sites of lower chemical potential (Equation 1-4 [62, 63]). Inhomogeneous media transitions change the classical diffusion problem to a diffusion-partition problem.

$$J(x,t) = -\frac{D}{kT}c(x,t)\frac{\delta\varphi(x,t)}{\delta x} \qquad \text{Equation 1-4}$$

Here, $\varrho(x,t)$ is the chemical potential of the substance, T the temperature and k is Boltzmann's constant. For the homogeneous case with $\varrho(x,t) = kT\ ln(c(x,t)$ and a constant diffusivity Equation 1-4 simplifies to the standard diffusion equation as stated in Equation 1-3.

The general case equation that describes the diffusion-partion problem with the chemical potential defined as $\varrho(x,t) = kT\ \ln((c(x,t)/K(x))$ and the position-dependent partition coefficient $K(x)$ is given by Equation 1-5 [62].

$$\frac{\delta c(x,t)}{\delta t} = \frac{\delta}{\delta x}\left(D\frac{\delta}{\delta x}c(x,t) - D(x)c(x,t)\frac{\delta}{\delta x}\ln K(x)\right) \qquad \text{Equation 1-5}$$

Besides studies with variable partition and/or diffusion coefficients inside a certain skin layer [62] it is more common (especially for more complex multi-layer models) to assign specific diffusion coefficients to the different layers and specific partition coefficients to the interfaces of two adjacent layers. The presented solutions of the diffusion equation and determination of distinctive parameters almost exclusively

depend on predicted, fitted or experimentally determined diffusivities and partition coefficients. Therefore, at least a basic understanding of the relationship between molecular properties and the aforementioned parameters is essential when it comes to the preparation, setup and evaluation of transdermal skin transport.

For spherical particles in a continuous fluid, the diffusion coefficient can be calculated by using the well-known Stokes-Einstein relation (Equation 1-6) with viscosity η of the solvent and particle radius *r*.

$$D = \frac{kT}{6\pi\eta r}$$

Equation 1-6

For the diffusion in polymers it could be found empirically that for a small particles the following relationship holds [64]:

$$D = D_m^0 MW^{-n}$$

Equation 1-7

Here, *MW* is the solute molecular weight and *n* and $D^O{}_m$ are constants characteristics of the membrane at a specific temperature. Other theories derived from polymer research have also been applied successfully to the field of describing diffusivities in the skin domain. For deeper insight the interested reader is kindly referred to [65].

Where the diffusivity *D* denotes the speed of a diffusant through a membrane and is inversely related to the weight of the solute, the partition coefficient *K* accounts for jumps in concentrations at the interface of two adjacent skin layers and is often related to a measure of solute lipophilicity, most commonly the logarithmic octanol-water partition coefficient. *K* is a thermodynamic parameter reflecting the relative affinity of a solute for a certain phase over another phase. Hence, the partition coefficient between layer m_2 and layer m_1 can be defined as

$$K_{\frac{m2}{m1}} = \frac{C_{m2}^{eq}}{C_{m1}^{eq}}$$

Equation 1-8

with C_{m2}^{eq} and C_{m1}^{eq} being the respective solute concentrations at the interface of the

two adjacent phases at equilibrium. In general, the partition coefficient is concentration-dependent but if the solubilities in the two phases are relatively low (which holds true for many cases) this effect can be neglected and the partition coefficient can be defined by using the saturation concentrations S_{m_1} and S_{m_2} in the different layers [66] with

$$K_{\frac{m2}{m1}} = \frac{S_{m2}}{S_{m1}} \qquad \text{Equation 1-9}$$

A typical strategy is to establish a relationship between an easy to observe parameter that mimics the membrane properties and the parameter of interest. A prominent example is the ocanol/water partition coefficient $K_{o/w}$ that could be related to the *stratum corneum* lipid phase/water partition coefficient K_{lip} with the help of a linear free energy relationship [67]:

$$K_{lip} = aK_{o/w}^{b} \qquad \text{Equation 1-10}$$

Here, the constants a and b correspond to characteristics of the relationship between aqueous vehicle and lipid phase of the *stratum corneum*. It is obvious that this relationship strongly depends on the physico-chemical properties of the layers at the interface (e.g. donor/SC or viable epidermis/*stratum corneum*).

It must be noted that representation of diffusivity and partition coefficient in a certain skin layer by a single number basically averages several transport mechanisms (e.g. several different routes trough the *stratum corneum* or implicit binding phenomena) of the diffusant. This important fact must be kept in mind when developing and applying mathematical models as well as trying to generalize basic relationships, such as Equation 1-7 and Equation 1-10. Since literally all mathematical models heavily oversimplify the underlying physics, parameters derived from mathematical concepts might obfuscate the governing mechanics.

1.3.1 Mathematical analysis of skin permeation

As mentioned before, permeation experiments are usually performed to measure the amount permeated through the barrier over time in relation to the diffusion area. For an *in-vitro* setup this relates to the accumulated mass in an acceptor compartment. Typical concentration/mass/flux versus time profiles for the infinite, semi-infinite (volume larger than 10 µl/cm², but with a depletion of the donor which is already perceptive) and finite dose cases are depicted in Figure 1-5. These theoretical calculations were performed using the DSkin® software[1]. An aqueous donor/acceptor with a drug diffusion coefficient of 6.33E-5 cm²/sec, *stratum corneum* lipid channel diffusion coefficient of 1.87E-8 cm²/sec and partition coefficient of 6.56 was used for simulations. The initial donor concentration was set to 1 mg/ml and the donor volume for the semi-infinite dose and finite dose scenario was set the 2 µl and 20 µl respectively for an area of diffusion of 1.767 cm². A tortious *stratum corneum* lipid path length of 180 µm was assumed which corresponds to a swollen membrane for an *in-vitro* setup [16]. Perfect sink conditions of the acceptor compartment are assumed.

The chosen values correspond to a model compound of approximate 300 Da with a $\log K_{O/W}$ of 2 in an aqueous vehicle and model parameters were estimated by DSkin®. The concentration-over-time profile depicted in Figure 1-5 A shows the characteristic depletion of the donor for the finite dose case and less pronounced for the semi-infinite case. The barrier mass-over-time curve for an infinite dose setup does reach a plateau as soon as the steady-state is reached (Figure 1-5 B). As opposed to this, the mass of the finite dose case decreases after reaching a maximum (Figure 1-5 B). In case of the infinite dose setup the accumulated mass inside the acceptor compartment reaches the typical straight steady-state line (Figure 1-5 C). This corresponds to a plateau of the flux-over-time profile (Figure 1-5 D). In contrast the finite dose scenario will reach a theoretical mass plateau in the acceptor compartment if all substance has traveled through the membrane. Obviously the flux reaches a max-

[1] DSkin® http://www.scientific-consilience.com (Developer: D. Selzer)

imum and subsequently decreases with time. For the simulation of the semi-infinite dose case shown in Figure 1-5 D the applied volume per area was set slightly higher than the finite dose threshold defined by the OECD [54, 55]. This shows clearly that the assumption of an infinite dose (no significant depletion) does not automatically hold by applying fixed volume-based rules.

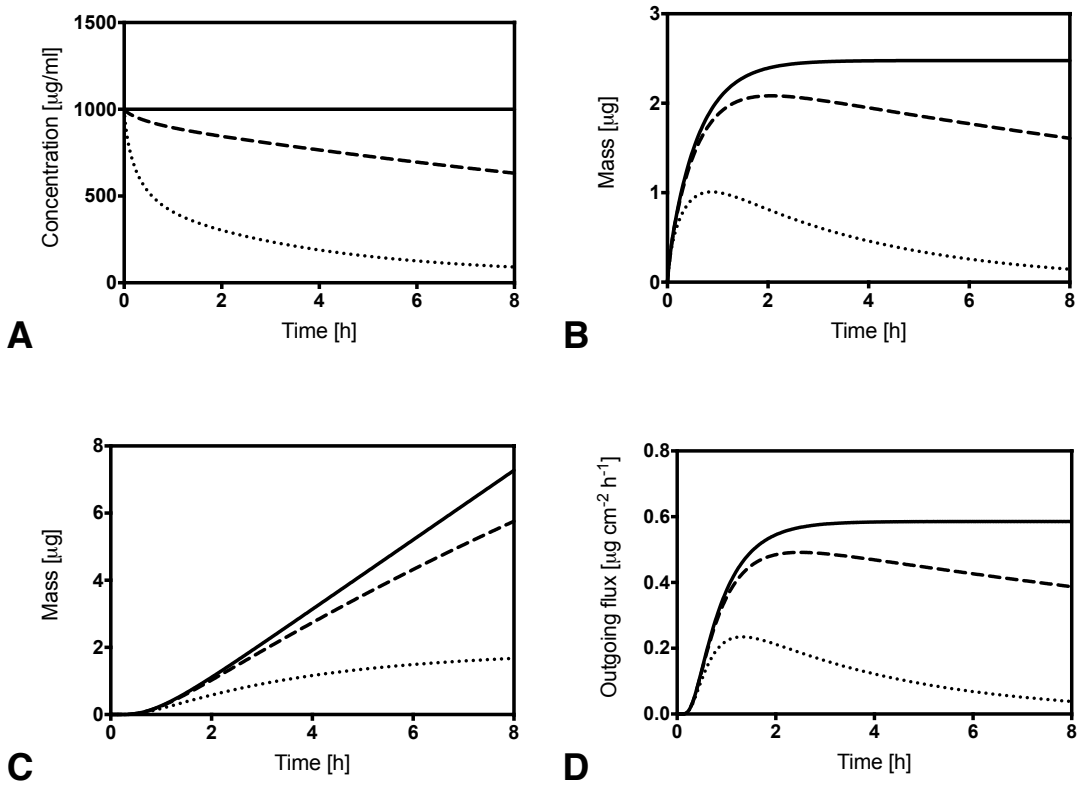

Figure 1-5 Theoretical change of concentration in the donor compartment over time (A), change of mass inside the *stratum corneum* (B), accumulated mass inside the acceptor compartment (C) and change of *stratum corneum* outgoing flux (D) for infinite (solid line), semi-infinite (dashed line) and finite dosing (dotted line). Simulations were performed using the DSkin® software.

This is crucial when applying the mathematical concepts since choosing faulty assumptions can lead to serious misinterpretation of experimental data. One has to keep in mind that even if small volumes of highly concentrated solutions are applied and the permeation is low, the system might behave like an infinite dose case due to the fact that significant donor depletion only occurs at very long experimental time periods in relation to the permeated solute amount in the acceptor compartment. Investigation of infinite and finite dose experiments typically differ concern-

ing their parameters of interest and application of mathematical concepts (e.g. analytical solutions of the diffusion equation are always tailored to certain boundary and initial conditions). In the next two sections analytical solutions of the diffusion equation and mathematical concepts for the most typical experimental settings are summarized. For an exhaustive compilation of solutions regarding the diffusion equation for various boundary and initial condition the author kindly refers to [63].

1.3.1.1 Investigations of infinite dose experiments

Analysis of infinite dose *in-vitro* skin permeation is typically accomplished by measuring the cumulative amount of substance inside the acceptor compartment over time. For short times the amount increases exponentially until reaching a steady line (the steady-state) with constant flux J_{SS} (see Figure 1-6). From a mathematical point of view a few assumptions must be made to derive an analytical solution for the diffusion equation by defining initial and boundary conditions. In this case we assume a constant and steady concentration in the donor compartment, perfect sink conditions (zero concentration in the acceptor at all times) and that no compound of interest is located inside the barrier at time $t = 0$.

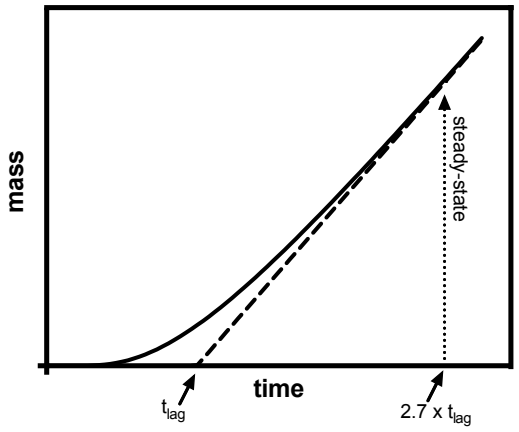

Figure 1-6 Accumulated mass over time in the acceptor compartment of an infinite dose experiment (solid line) and linear part of the steady state phase (dashed line). The intersection of the linearized steady state phase and time-axis denotes the lag-time.

By incorporating these rules, for a homogenous membrane the absorption curve can be described by an analytical solution of Ficks second law of diffusion [63, 68] with

$$m(t) = A \times K \times l \times C_0 \left[K \times l \times t - \frac{1}{6} - \frac{2}{\pi^2} \sum_{n=1}^{\infty} \frac{(-1)^n}{n^2} \exp\left(-\frac{Dn^2\pi^2 t}{l^2} \right) \right] \quad \text{Equation 1-11}$$

Here A denotes the area of application, K is the partition coefficient between donor and barrier, C_o is the concentration of applied formulation in the donor which is assumed not to change significantly during experimental time periods, D is the macroscopic diffusion coefficient, l is the macroscopic thickness of the barrier and t is the time after application. It is obvious that with t leaning towards infinity (and hence reaching the steady-state) the solution simplifies to the linear part of the steady-state (Figure 1-6) with

$$m(t) = A\frac{DK}{l}C_0\left(t - \frac{l^2}{6D}\right) \quad \text{Equation 1-12}$$

From Equation 1-12 we can examine important parameters when it comes to analysis of infinite dose experiments. The first parameter is the so-called apparent permeability coefficient k_p which is often given in units of cm/h and is defined as

$$k_p = \frac{DK}{l} \quad \text{Equation 1-13}$$

It is independent of area of application and initial concentration and hence a direct parameter for the strength of permeation for a compound through a certain barrier from a specific vehicle under infinite dose and perfect sink conditions. Mathematically it denotes a normalization of steady-state flux J_{SS} with

$$k_p = \frac{J_{SS}}{C_0} \quad \text{Equation 1-14}$$

Such parameters might heavily depend on experimental conditions. Hence, this has to be kept in mind when comparing parameters (inter-laboratory and intra-laboratory). Although k_p may be a useful and popular parameter when it comes to examination of permeation experiments it can be sometimes misleading when comparing the permeation of several compounds [66, 69]. The apparent permeability coefficient k_p describes an intrinsic property of a solute to permeate across a specific medium (for example the skin) which is independent of the dose but influ-

enced by the applied vehicle. Therefore comparisons are only possible between compounds which are applied in identical vehicles. In 2006 Sloan et al. introduced a change of paradigm when it comes to explaining experimental data [70]. They suggested using the more expressive parameter J_{max} which denotes the maximum possible flux of a solute through a barrier for comparing permeability. By using J_{max} it is possible to overcome the limitations addressed before with:

$$J_{max} = k_p \times S_v = D \times \frac{S_m}{l} \qquad \text{Equation 1-15}$$

Here, S_V is the saturated permeant concentration in the vehicle and S_M is the solubility of the solute within the barrier. In other words, by removing the influence of the partition coefficient between skin and vehicle, J_{max} should be independent of the vehicle applied. Thus, it describes an intrinsic permeability of a solute in a certain medium making it an ideal parameter to compare permeability of different solutes. Obviously, this is the case as long as the vehicle does not affect the transport kinetics in the barrier [71]. In contrast to epidermal k_p which is optimally correlated to the molecular weight and lipophilicity of a compound [72-74], Magnusson et al. could show that molecular weight is the main determinant when is comes to predicting solute maximum flux [75].

A further parameter to characterize infinite dose absorption is the so-called lag-time t_{lag} given by

$$t_{lag} = \frac{l^2}{6D} \qquad \text{Equation 1-16}$$

It is a measure that relates to the time it takes for a compound to travel trough the barrier and ro establish a steady-state. A word of caution is necessary concerning the meaning of t_{lag}. t_{lag} does not directly represent the time when the steady-state is achieved (see Figure 1-6), however it can be approximated by multiplying t_{lag} with 2.7 (Crank showed that steady- $\frac{Dt}{l^2} = 0.45$ state is achieved when approximately (Crank,1975)).

1.3.1.2 Investigations of finite dose experiments

In contrast to the infinite dose exposure scenario a typical finite dose absorption profile does not reach a steady-state, but builds a mass plateau inside the acceptor compartment at late time points (Figure 1-5 C). Finite dose experiments also show a characteristic depletion of donor concentration (Figure 1-5 A) and increase in flux until reaching the so-called peak flux J_{peak} at time t_{peak} (Figure 1-7). As opposed to the infinite dose case, deduction and application of an analytical solution for the description of absorption curves requires a more sound mathematical foundation. Based on the theory of heat flow by Carslaw and Jaeger a description of the flux of the compound leaving the barrier at time t is given by the following equation [76, 77]:

$$J(t) = 2 \cdot A \cdot M_{\infty} \cdot \beta \cdot \frac{D}{l^2} \sum_{i=i}^{\infty} \frac{\alpha_i^2}{\cos \alpha_i (\beta + \beta^2 + \alpha_i^2)} \exp(-\frac{\alpha_i^2 Dt}{l^2}) \qquad \textbf{Equation 1-17}$$

with

$$\beta = K \frac{l}{h_v} \qquad \textbf{Equation 1-18}$$

and the roots of the transcendental equation, αi, given by

$$\alpha_i \tan \alpha_i = \beta \qquad \textbf{Equation 1-19}$$

Here, $M\infty$ denotes the applied mass and h_v is the height of the formulation in the donor compartment. The remaining parameters keep their meaning as introduced above.

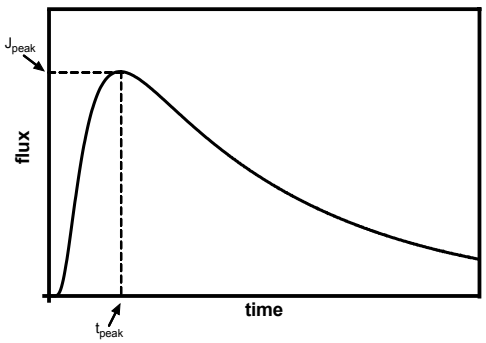

Figure 1-7 Sketch of outgoing flux across the barrier-acceptor interface over time of a finite dose experiment (solid line). The maximum of the the curve denotes the peak flux J_{max} at time to peak flux *tmax* .

Integrating Equation 1-17 yields the accumulated mass per area [78] with

$$\frac{M(t)}{M_\infty} = 1 - 2\beta \sum_{i=i}^{\infty} \frac{1}{\cos\alpha_i(\beta + \beta^2 + \alpha_i^2)} \exp\left(-\frac{\alpha_i^2 Dt}{l^2}\right) \qquad \text{Equation 1-20}$$

In comparison to Equation 1-11 for the infinite dose case solving Equation 1-20 requires a more skillful evaluation since Equation 1-20 must be solved for arbitrary values of *i*. A basic strategy to solve the transcendental equation is to use logistic regression to tabulated values of the first roots (see Figure 1-8). To find further roots a subsequent linear extrapolation from previous roots ($root_n = 2 \times root_{n-1} - root_{n-2}$) followed by a refinement step (root finding with e.g. Newton's method) [78] is key.

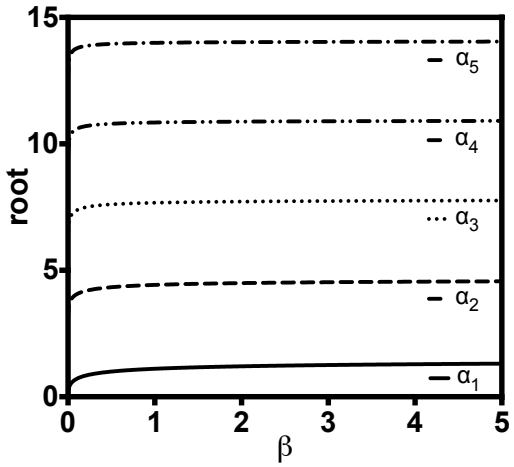

Figure 1-8 First five roots of the transcendental Equation 1-19 for continuous values of β from 0 to 5. Values fitted by logistic regression to tableted values from Crank [63].

Important parameters for evaluation of finite dose permeation experiments are the peak flux J_{peak} and time to peak flux t_{peak}.

A general strategy to easily find J_{peak} and t_{peak} is finding the root of the first derivative of $J(t)$ and hence solving the following equation for t_{peak}:

$$2 \cdot M_\infty \cdot \beta \cdot \frac{D}{l^2} \sum_{i=i}^{\infty} \frac{\alpha_i^2}{\cos\alpha_i(\beta + \beta^2 + \alpha_i^2)} \exp\left(-\frac{\alpha_i^2 Dt_{peak}}{l^2}\right) \frac{\alpha_i^2 D}{l^2} = 0 \qquad \text{Equation 1-21}$$

A reliable solution for the root finding problem is e.g. Brents method [79]. For small doses ($\beta < \sim 0.1$) J_{peak} and t_{peak} can be calculated by the following simple equations [78, 80]:

$$J_{peak} = 1.85 M_\infty \frac{D}{l^2} \qquad \text{Equation 1-22}$$

$$t_{peak} = \frac{(l^2 - h_v^2)}{6D} \qquad \text{Equation 1-23}$$

For the finite dose case, finding a parameter related to the permeability coefficient is obviously not possible since the flux changes with time. However, in 1974 Scheuplein defined the so-called transfer coefficient k_t with units of percentage of dose per time [78, 80] with:

$$k_t = \frac{\text{flux} \times 100}{\text{specific dose}} \qquad \text{Equation 1-24}$$

He used the early flux of the linear part of the curve to estimate the fraction of absorbed dose after a certain time by multiplying k_t by t. Besides the fact that this parameter depends on the applied dose, the amount will be heavily overestimated when the flux drops and leans towards zero. These two major drawbacks tremendously limit the usefulness of this parameter.

It has to be kept in mind that finite dose kinetics are also prone to variability of drug distribution in the donor, as shown in Chapter 3 and drug distribution to the non-incubated lateral parts in an Franz diffusion-cell setup (see Chapter 4) yielding a high variability in fitted parameters.

1.3.2 Mathematical analysis of skin penetration

Besides permeation profiles (accumulated mass over time) which provide valuable information about the absorption process and the transport to the blood circulation and deeper tissue, skin-concentration depth profiles supply precious data about the distribution of solute inside the barrier over time.

As for permeation experiments the kinetics clearly differ for different exposure scenarios. Figure 1-9 shows theoretical skin-concentration depth profiles for the infinite dose case (Figure 1-9 A), semi-infinite dose case (Figure 1-9 B) and finite dose case (Figure 1-9 C). These curves were produced with the help of the DSkin® soft-

ware and show the change of concentration over time and space in the *stratum corneum*. The used input parameters correspond to the simulation parameters used to produce the permeation curves in the previous section.

The infinite dose curves show the typical exponential decay for short exposure times and transition into a straight line when steady-state is reached (Figure 1-9 A). The semi-infinite case shows comparable kinetics at short times, reaches a pseudo steady-state with a straight line that will drop due to the depletion of the donor over time (Figure 1-9 B). For the finite dose scenario a straight line in the concentration over space kinetics is typically not reached and a significant drop can be recognized over time (Figure 1-9 C).

As for permeation experiments analytical solutions for the diffusion equation can be obtained to describe the change of concentration over time and space by using the appropriate initial and boundary conditions. For the infinite dose case, assuming a homogeneous membrane one can calculate the concentration inside the barrier at point x and time t [63] with

$$c(x,t) = K \times C_0 \times \left(\left(1 - \frac{x}{l}\right) - \frac{2}{\pi} \sum_{n=1}^{\infty} \frac{1}{n} \sin\left(\frac{n\pi x}{l}\right) \exp\left(-\frac{Dn^2\pi^2 t}{l^2}\right) \right) \qquad \text{Equation 1-25}$$

As for the permeation case, K denotes the barrier/vehicle partition coefficient, C_o the initial concentration in the vehicle, D the apparent diffusivity and l the macroscopic thickness of the barrier membrane with $0 \leq x \leq l$. The equation can only be applied if the donor does not deplete over time (typical infinite dose assumption), the receptor compartment is kept at a theoretical zero concentration (perfect sink conditions) and no solute is present inside the barrier at $t = 0$. Obviously, only the passive diffusion process is modeled. Hence, permeation enhancement, binding phenomena, convection effects are not part of the model.

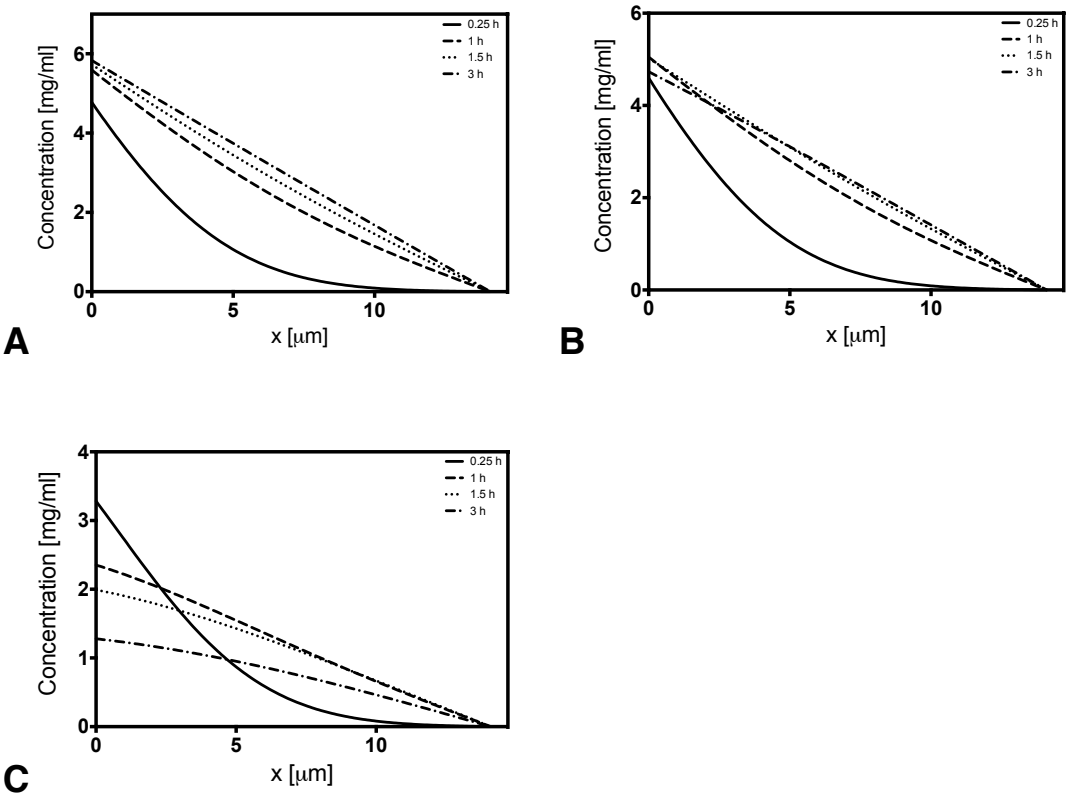

Figure 1-9 Theoretical change of concentration in the barrier over time for the infinite dose (A), semi-infinite dose (B) and finite dose (C) case. Simulations were performed using the DSkin® software.

Equation 1-25 can be of great benefit to estimate values for partition coefficient (K) and diffusion coefficient (D) and extrapolate the skin-concentration depth profile for later time points [81] or even other exposure scenarios (see Chapter 4 and [82]). For late times the skin-concentration depth profile will reach steady-state and Equation 1-25 simplifies to

$$c_{ss}(x) = K \times C_0 \left(1 - \frac{x}{l}\right) \qquad \textbf{Equation 1-26}$$

Obviously, information about diffusivity can only be obtained before the steady-state is reached. Hence, in order to obtain kinetic parameters fitting Equation 1-25 to experimental data should focus on short incubation times.

For the finite dose case an analytical solution for the diffusion equation can be obtained with α and β (as defined earlier in Equation 1-18 and Equation 1-19) [78]:

$$c(x,t) = 2 \times K \times C_0 \times \sum_{n=1}^{\infty} \frac{\beta \cos(\alpha_n x/h) - \alpha_n \sin(\alpha_n x/h)}{\beta + \beta^2 + \alpha_n^2} \exp\left(-\frac{\alpha_n^2 Dt}{l^2}\right) \qquad \text{Equation 1-27}$$

As for the infinite dose case the same limitations hold (e.g. perfect sink conditions and no solute in the barrier at $t = 0$).

1.3.3 Pharmacokinetic models in skin absorption

Compartmental or pharmacokinetic models (PK) are used since the early beginnings of mathematical description to study the fate of a substance that was applied in the systemic circulation and are also part of the history of describing transdermal drug absorption. They treat the body as a series of well-stirred compartments. The basic idea is the elimination of space dependence of the partial differential diffusion equation (Equation 1-2) to obtain a series of ordinary differential equations (ODEs) that describe the change of amount of solute in different compartments over time.

For the family of PK models a set of first-order rate constant can be assigned to denote the transfer of a compound from one compartment to another. Figure 1-10 shows two examples of skin compartment models: a one-compartment skin model and a two-compartment skin model.

The corresponding first-order ODE of the one-compartment model can be expressed by the following expression:

$$V_2 \frac{dC_2}{dt} = k_1 C_1 - k_{-1} C_2 + k_{-2} C_3 - k_2 C_2 \qquad \text{Equation 1-28}$$

For the two-compartment model the following equations hold, respectively:

$$V_2 \frac{dC_2}{dt} = k_1 C_1 - k_{-1} C_2 + k_{-2} C_3 - k_2 C_2 \qquad \text{Equation 1-29}$$

$$V_3 \frac{dC_3}{dt} = k_2 C_2 - k_{-2} C_3 + k_{-3} C_4 - k_3 C_3 \qquad \text{Equation 1-30}$$

The separation of the skin in a lipophilic part (the *stratum corneum*) and hydrophilic part (viable epidermis) is common practice to mimic the heterogeneity of the skin [83, 84].

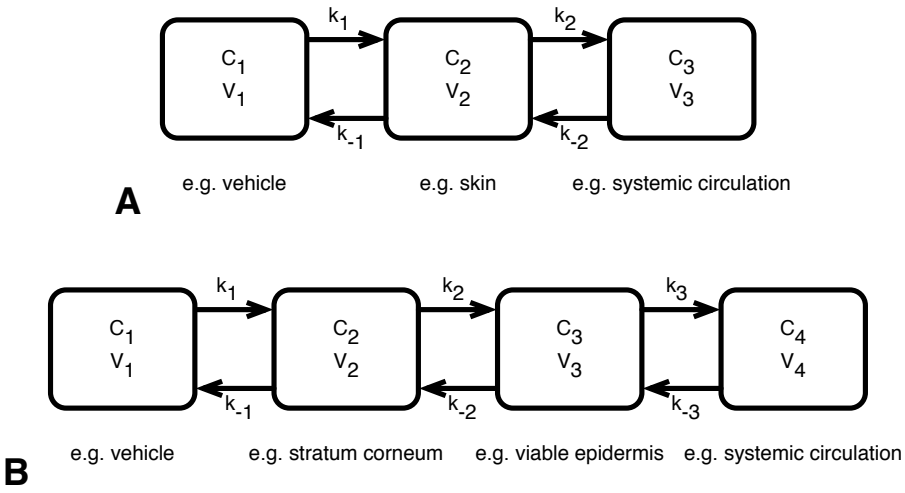

Figure 1-10 Exemplary sketch of a one-compartment (A) and two-compartment (B) skin model. Here, the number denotes the number of compartments used to describe the skin barrier, rather than the number of overall compartments. *C* denotes to the average concentration in the compartment, assuming simplified well-stirred conditions and V is the volume of the compartment that is accessible for the solute distribution.

The underlying ODEs can be solved either analytically (for the most part only for easy equations) or numerically. Numerical solvers for non-stiff equations are for example Euler's method or the fourth-order Runge-Kutta method (widely known as RK4). For stiff equations the Backward Differentiation Formula (BDF) is a well known algorithm.

In comparison to solutions of the diffusion equation, using compartmental models can have some advantages. (A) Obviously, the solution of a set of ODEs can often be derived with little hassle in comparison to complex multi-compartmental diffusion models which are more cumbersome mathematically. For simple models even analytical solutions can be derived with ease. (B) Complicated exposure scenarios with e.g. periodic application or evaporation can be implemented very easily in comparison to complex diffusion models. (C) Adding systemic PK models to a skin PK model can be achieved with little overhead. (D) Even numerical integration of the ODE is typically much faster than solving the diffusion equation numerically.

One big drawback comes with the oversimplification of having well-stirred compartments that obviously does not reflect reality. Certain kinetics, such as the transition of first-order to zero-order characteristics can only be described unsatisfactorily.

PK models were typically used in the past to analyse *in-vivo* data [85, 86]. A lot of effort was spent to relate rate constants to physicochemical parameters of the diffusant and fit experimental plasma-curves or *in-vitro* permeation profiles to PK models [87, 88] generally with less success than for the class of diffusion models [65]. Despite a growing trend towards numerical diffusion models, the class of PK models recently regained attention by the work of Davies et. al [89]. They showed that an efficient skin compartmental model can be constructed by a two-layer approach. For excellent overviews on PK models the interested reader is kindly referred to references [83, 90, 91]. Besides PK models, in 1992 Seta and coworkers presented another compartmental approach and successfully studied the transport of radiolabeled hydrocortisone through hairless guinea-pig skin using three skin layers (*stratum corneum*, viable epidermis and dermis) [84]. They divided each compartment in several hypothetical thin elements and calculated the flux between each element. This approach can be numbered among compartmental models but rather trends towards numerical finite differences approaches.

1.3.4 Numerical solutions of the diffusion equation

Numerical methods for solving the diffusion equation for various initial and boundary conditions are important techniques and allow a more flexible construction of advanced skin models (e.g. incorporation of binding effects [92], iontophoretic transdermal delivery [93], repeated applications [94], controlled release vehicles [95] and *in-vitro* lateral transport (see Chapter 4). In comparison to classical PK skin compartment models (see previous section), it is typically much more convenient to relate the necessary input parameters (for the simple diffusion problem only diffusivities and partition coefficients are needed) to physicochemical parameters of the diffusant [65]. These models can be used for descriptive and predictive tasks as well as for the theoretical investigation of the interplay among input parameters.

The basic idea consists of the discretization of time and space domain (gridding) and a numerical approximation of the partial differential diffusion equation (e.g. for the most trivial form see Equation 1-2). The discretization allows the construction of coarse-grained macroscopic and fine-grained microscopic models (a basic example is depicted in Figure 1-11).

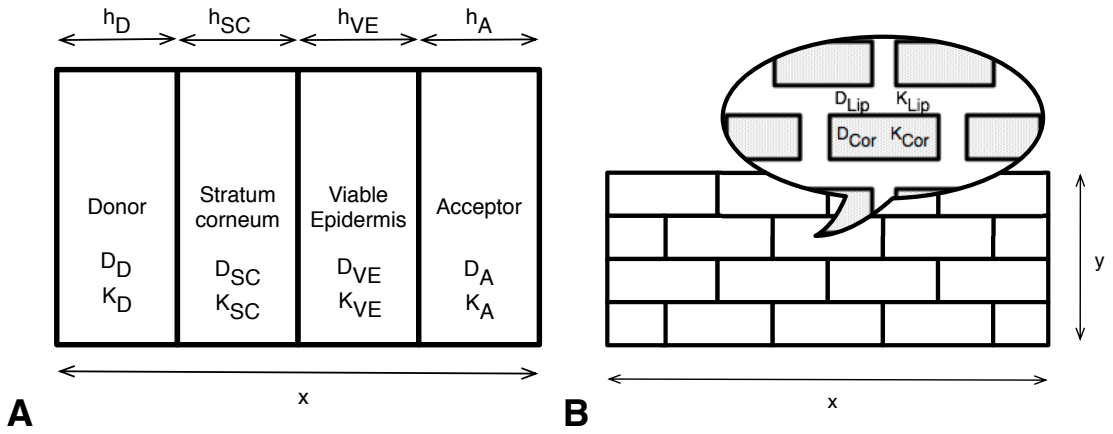

Figure 1-11 Simplified depiction of a macroscopic diffusion model with effective diffusivities and partition coefficients (A) and a microscopic representation of the brick-and-mortal structure [6] of the *stratum corneum* (B) with diffusivities and partition parameters for the lipid and the corneocyte phase. Figures are not drawn to scale.

Macroscopic models do neglect the heterogeneity of different skin layers and use effective kinetic parameters of a diffusant for each layer to describe the transport process. Usually, these kind of models are only needed for solving the underlying diffusion equation for the one-dimensional case and hence treat the skin as a series of multi-layered slabs (Figure 1-11 A). Microscopic models allow a heterogeneous representation of the *stratum corneum* [96] (lipid phase and protein phase, see Figure 1-11 B and hence yield a more in-depth analysis of the underlying transport processes. In this case, the absorption kinetics do not only rely on the definition of diffusion parameters but also on the definition of spatial geometry. Due to the high spatial resolution these models typically require much higher computational costs in comparison to coarse-grained macroscopic models. By mathematical homogenization it is possible to reduce a microscopic model to a macroscopic one with preservation of model properties (e.g. anisotropic diffusivity in the *stratum corneum*) (see Chapter 4 and [97]).

From a numerical perspective, several techniques exist to approximate the solution of the diffusion equation. For the one-dimensional case, probably the most prominent method is the finite differences approach. Assuming a constant diffusivity Equation 1-2 can be approximated by

$$\frac{C_i^{t+1} - C_i^t}{\Delta t} = D\frac{C_{i-1}^t - 2C_i^t + C_{i+1}^t}{(\Delta x)^2}$$ **Equation 1-31**

The left-hand side of the equation is approximated by first-order forward differences and the right-hand by second-order central differences that both arise from Taylor series expansions. As for every numerical method, the time and space domain is discretized. In this case C_i^t denotes the concentration at point $i \times \Delta x$ for time $t \times \Delta t$ with a system of constant space step size Δx and time step size Δt. Obviously the above mentioned equation can be easily generalized to problems in 2D and 3D space. Reformulation of Equation 1-31 yields

$$C_i^{t+1} = MC_{i-1}^t + (1 - 2M)C_i^t + MC_{i+1}^t$$ **Equation 1-32**

with

$$M = D\frac{\Delta t}{(\Delta x)^2}$$ **Equation 1-33**

Because of the fact that every point of a certain layer only depends on points from the past there is no functional relationship between different points of one time layer (it is a so-called *uncoupled problem*). This leads to the problem of numerical instabilities that depend on the value of M (Equation 1-33) and hence on the choice of Δt for a given spatial resolution Δx. It can be shown that this explicit method is only stable for values of $M \leq 0.5$ (for the one-dimensional case). A violation of this recommendation can produce noise which may result (empirically it always does for the diffusion equation) in non-smoothable rounding errors. For small diffusion coefficients (e.g. in the *stratum corneum*) this restriction can lead to extremely small time steps and therefore to high computational runtimes.

An elegant way to overcome this problem is the use of implicit methods that rely not only on data from the last time point (Figure 1-12).

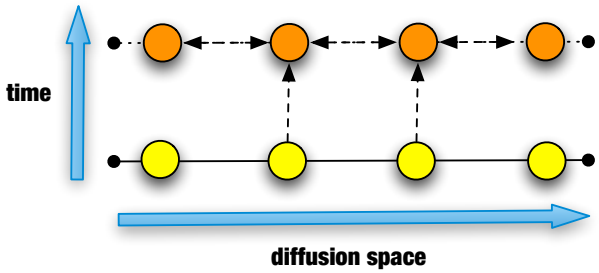

Figure 1-12 Implicit finite differences method. Orange points indicate unknown values, yellow points represent known values.

Undoubtful, the most widely used approach is the so-called Crank-Nicolson method [63] (Equation 1-34 and Figure 1-13) that is unconditionally stable and provides a better overall error than the explicit approach.

$$\frac{C_i^{t+1} - C_i^t}{\Delta t} = \frac{D}{2}\left(\frac{C_{i-1}^{t+1} - 2C_i^{t+1} + C_{i+1}^{t+1}}{(\Delta x)^2} + \frac{C_{i-1}^{t} - 2C_i^{t} + C_{i+1}^{t}}{(\Delta x)^2}\right) \qquad \textbf{Equation 1-34}$$

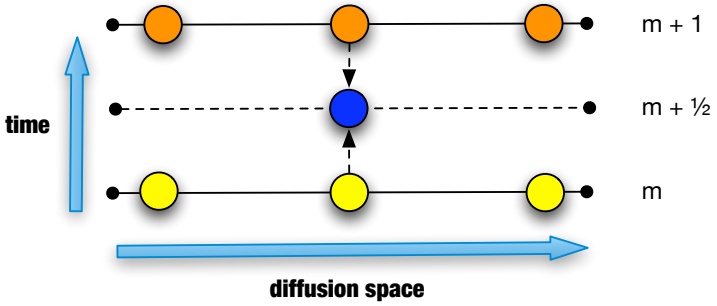

Figure 1-13 Crank-Nicolson method with the additional artificial time layer (with blue point). Orange points indicate unknown values, yellow points represent known values.

This equation yields a system of linear equations (Equation 1-37) that can be efficiently solved by e.g. the Thomas algorithm (an optimized form of Gaussian elimination that can solve tridiagonal systems of equations).

$$\mathbf{A} = \begin{bmatrix} (1+M) & -\frac{M}{2} & 0 & \cdots & 0 \\ -\frac{M}{2} & (1+M) & -\frac{M}{2} & \ddots & \vdots \\ 0 & -\frac{M}{2} & \ddots & \ddots & 0 \\ \vdots & \ddots & \ddots & \ddots & -\frac{M}{2} \\ 0 & \cdots & 0 & -\frac{M}{2} & (1+M) \end{bmatrix} \qquad \text{Equation 1-35}$$

$$\mathbf{B} = \begin{bmatrix} (1-M) & \frac{M}{2} & 0 & \cdots & 0 \\ \frac{M}{2} & (1-M) & \frac{M}{2} & \ddots & \vdots \\ 0 & \frac{M}{2} & \ddots & \ddots & 0 \\ \vdots & \ddots & \ddots & \ddots & \frac{M}{2} \\ 0 & \cdots & 0 & \frac{M}{2} & (1-M) \end{bmatrix} \qquad \text{Equation 1-36}$$

$$\mathbf{A}c^{m+1} = \mathbf{B}c^{m} \qquad \text{Equation 1-37}$$

Using this implicit methods, it is possible to choose larger time steps, which decreases the number of computational steps in spite of the fact that the solving of the system of linear equations is computationally more complex compared to the explicit method. Various work on modeling transdermal transport that are based on finite differences exist ([92, 94, 95, 98], see Chapter 5).

Finite differences are not the only mesh-based technique to find approximate solutions to partial differential equations, such as the diffusion equation. The method of finite elements that is widely used in the field of mechanical engineering and finite volume approaches that can efficiently handle unstructured girds and is often applied in the field of computational fluid dynamics are known to successfully model transdermal transport ([81, 99, 100], see Chapter 5). For excellent overviews about numerical models the interested reader is kindly referred to [101, 102].

1.3.5 Quantitative structure activity relationships (QSAR)

Quantitative structure activity relationships typically try to correlate molecular properties to some kind of biological activity. Here, an activity response variable is often related to a set of molecular descriptors or features of a chemical entity by a regression model. A typical workflow to construct a QSAR-model starts with the gathering of training and validation data of the objective. Subsequently, a set of descriptors for each entity (molecular properties or features) should be generated or collected. At this stage, a subset of the descriptor space must be chosen to train the model and compare the predicted objective value with the validation set. To avoid overtraining,

only the most significant descriptors should be incorporated into the model. Standard methods from the field of machine learning, such as cross-validation and bootstrapping can be useful to build a meaningful and robust prediction model.

Obviously, this class of models is highly restricted since these concepts typically provide only one type of static output (e.g. a number or class). Moreover, information about time-dependency of the objective cannot be provided. Another drawback is the lack of predictive confidence of most models when using input parameters beyond the feature space of the training set. Despite these limitations, QSAR models have been used successfully to predict various properties of a compound and are suggested by the European Union in the field of risk assessment [21].

In the case of skin studies, a prominent measure of interest is the normalized steady-state flux (permeability k_p). Widely used data sets that provide permeability values were published by Flynn in 1990 [103] and Wilschut et al. in 1995 [104]. One of the most famous QSAR-models to predict *stratum corneum* k_p of a compound solved in an aqueous donor solution was published by Potts and Guy in 1992 [74]:

$$log\ k_p = a + b \cdot logK_{o/w} - c \cdot MW$$

Equation 1-38

This equation is in direct correlation to the log-transform of Equation 1-13 assuming similar relationships of partition and diffusion coefficient as stated in Equation 1-7 and Equation 1-10. Here, the free parameter a denotes the characteristic of the barrier. The heterogeneity and biological complexity of the *startum corneum* were vastly simplified and subsequently treated as a black-box-like structure. The model was trained by multi-linear fitting of a, b and c to available data from the Flynn database (93 compounds) and yielded reasonable accuracy (r^2 = 0.67). Since a variation of 30% in experimental data is reasonable, Potts and Guy assumed that their model completely describes the data used for training. A revised version of the model in comparison to similar approaches can be found in [104]. Needles to say, this class of QSAR-models is not restricted to molecular weight and lipophilic character as input parameters. Incorporation of hydrogen bond activity [105, 106], retardation coefficient (RC) [107] and charge [108] yielded promising results.

In contrast to the class of linear, mechanistic QSAR-models, empirical models typically do not rely on any physical-based assumptions and treat the whole process as a black box. Prominent examples are artificial neural networks (ANN) [109, 110] and k-nearest neighbor approaches (kNN) [111]. These empirical models typically provide no information about the underlying processes but might overcome uncertainties (e.g. possible protein binding inside the skin, metabolization, different routes of substance travel, ionization) due to their fuzzy nature and provide excellent results from a practical point of view [112].

A recent overview regarding mechanistic and empirical models can be found elsewhere [112].

2 Aims of the thesis

The growing interest to address skin absorption of substances in the fields of risk assessment and drug delivery leads to serious challenges in investigating hundreds of substances in different formulations, mixtures and exposure scenarios. To overcome the ethical and financial burden *in-vivo* human or animal studies impose on scientists, *in-vitro* methods have been developed in the past (see Chapter 1). These methods showed great potential and were successfully applied to explore different exposure settings of a great number of xenobiotics. However, the investigation of skin penetration and permeation using these techniques is often a cumbersome and time-consuming process, heavily limited by restricted access to excised human skin (considered the gold standard). Animal skin and reconstructed or artificial skin technologies still face difficulties in comparability and just shift the "availability problem" to another level. Since the beginning of 1960 mathematical models concerning the underlying diffusion problem evolved quickly and gained more and more importance in the field of studying transdermal substance transport. Apart from the possibility to describe the fate of a substance in various degrees of complexity (see Chapter 1) there is a clear vision of *in-silico* approaches to predict the outcome of an exposure or application scenario *in-vivo* – either totally from scratch using only substance and system descriptors (e.g. molecular weight and lipophilic character of the target substance) or with guidance from *in-vitro* experiments. At this, it is important to note that most models and concepts highly depend on precise and carefully examined input and validation data gathered for various application scenarios to perform well.

The aims of this thesis were i) to address and explore distinct problems associated with finite and infinite dose experiments *in-vitro* with the help of mathematical models to improve data quality and offer insights into the underlying concepts of substance transport through the skin, ii) to construct a *in-silico* model to predict the *in-vivo* scenario from model input data derived from *in-vitro* experiments.

First, we studied the influence of substance coverage on drug permeation experiments using only small amounts of formulation (Chapter 3). Subsequently, the importance of the lateral skin compartment in finite dose *in-vitro* studies was investi-

gated using three different classes of computational models (Chapter 4). This work has been done in cooperation with the Goethe Center for Scientific Computing (Professor Gabriel Wittum, Frankfurt University). Chapter 5 focuses on the construction of a one-dimensional heterogeneous diffusion model that simulates and predicts *in-vitro* and *in-vivo* finite dose scenarios based on input parameters gathered from infinite dose *in-vitro* experiments - a strategy that showed promising results in the field of *in-silico* - *in-vivo* correlation using experimental guidance.

Chapter 6 (Outlook) quickly outlines work that was conducted to improve computational models on the microscopic scale (predicting keratin binding of substances to incorporate this concepts into mathematical models – see Section 6.1), to address the problem of signal damping in optical analytical methods measuring skin penetration (see Section 6.3) and to theoretically investigate the impact of skin topography on skin absorption using a GPU-accelerated 2D-diffusion model (see Section 6.2). The work last mentioned was carried out by Jan Riehm as part of his master's thesis under supervision of D. Selzer.

The thesis will be divided into the following four chapters:

Chapter 3: "Influence of the application area on finite dose permeation in relation to drug type applied"

Chapter 4: "Finite dose skin mass balance including the lateral part: Comparison between experiment, pharmacokinetic modeling and diffusion models"

Chapter 5: "A strategy for *in-silico* prediction of skin absorption in man"

Chapter 6: "Outlook"

3 Influence of the application area on finite dose permeation in relation to drug type applied

Parts of this chapter have been published in:

Hahn, T., Selzer, D., Neumann, D., Kostka, K. H., Lehr, C.-M., Schaefer, U. F. (2012). Influence of the Application Area on Finite Dose Permeation in Relation to Drug Type Applied. *Exp Dermatol,* 21(3), 233–235.

The author of the thesis made the following contributions to the publication:

Developed the mathematical model to determine formulation coverage. Performed and interpreted all calculations. Wrote parts of the manuscript.

Tsambika Hahn performed and interpreted all major experiments and wrote the manuscript.

3.1 Abstract

For finite dose skin absorption experiments, a homogeneous donor distribution over the skin surface is usually assumed. However, the influence of the surface distribution on skin absorption is still unknown. The aim of this study was to evaluate the influence of the application area on the permeation of drugs during finite dose skin absorption experiments in static Franz diffusion cells. Permeation experiments with stained aqueous drug formulations were conducted and the application area was determined by a suitable, objective, automated computational approach. In contrast to the maximum incubation area possible in the diffusion cell setup, the application area was the area actually in contact with the donor at the start of incubation. The permeation of caffeine is strongly dependent on the application area: The variability between single experiments decreased including the application area. In addition, biopsies from stained skin area contained significantly more caffeine than biopsies of non-stained skin. For the lipophilic flufenamic acid this was not the case. The variability highly increased after inclusion of the application area. In contrast to caffeine, due to lipophilicity, flufenamic acid distributes fast in the *stratum corneum* covering the maximal possible diffusion area. Thus, a correction of the area is misleading. In summary, depending on the drug's physicochemical characteristics, the real application area may influence skin absorption.

3.2 Introduction

In skin absorption studies infinite dosing is usually employed to evaluate kinetic parameters like permeation coefficient [104, 113]. However, this does not represent the *in-vivo* situation, where usually a finite dose is applied to the skin, and additional effects may influence drug absorption, e.g. the evaporation of excipients [114]. In the OECD guideline 428 [54] and the guidance document 28 [55] finite dose experiments are defined as experiments with a maximum applied donor volume of 10 μl/cm² of liquid formulations. For semisolid and solid substances, values range from 1 to 10 mg/cm² [54, 55, 115].

The ideal application should result in a homogeneous layer of the drug formulation over the whole incubation area. Otherwise, the variation between the experiments will increase [116]. However, a homogeneous drug distribution over the whole incubation area is problematic due to wrinkles of the skin.

For creams and ointments even distribution may be confirmed visually, but for uncoloured aqueous solutions and gels the distribution cannot easily be determined. To this day the distribution of a drug over the incubation area has only scarcely been analysed: In two publications, the distribution of a fluorescent model drug in sunscreens over the skin was investigated *in-vivo* [117, 118] to correlate the results with the sun protection factor. Another publication investigated the distribution of the drug formulation containing a fluorescent dye with and without microparticles over the incubation area by *in-vivo* laser scanning microscopy [119]. These publications, however, did not correlate the skin surface distribution to the absorption of the model drug into the skin.

To address this topic concerning the effect of inhomogeneous donor formulation distribution on *in-vitro* permeation results, *in-vitro* finite dose permeation experiments were performed applying a donor by two different methods, i) distribution with a punch, and ii) distribution with a disc. To distinguish between skin with and without contact to donor formulation, aqueous drug solutions were stained with a dye. The drugs employed in this study were caffeine and flufenamic acid (FFA). After incubation the application area was determined by a newly developed computer-based method to ensure objectivity and to handle high-throughput data processing.

The influence of the application area on the permeation was investigated with respect to its impact on the variability of the data. Furthermore, lateral drug distribution was analysed by quantification of skin biopsies with and without contact to the donor formulation. To quantify the skin absorption of both substances the relative peak flux, as well as the peak flux time were determined.

3.3 Materials and methods

3.3.1 Materials and instruments

All materials used were of highest analytical grade and were used as purchased. Ringer's solution was provided by Fresenius Kabi, Bad Homburg, Germany. Purified water was prepared by a Millipore Synthesis device (Millipore GmbH, Schwalbach, Germany). The following instruments were used: static Franz diffusion cells type 4G-01-00-20 (PermeGear, Riegelsville, PA, USA), incubation area 1.767 cm^2 and receptor volume 12.1 ml, dialysis membranes with MW-cut-off of 12-14 kDa (Medicell International Ltd, London, Great Britain, VWR Darmstadt, Germany), 25 mm syringe filters 0.2 μm cellulose acetate membrane (VWR International, West Chester, PA, USA).

3.3.2 Skin

Human abdominal skin was obtained from female Caucasian donors undergoing plastic reduction surgery at the Department of Plastic and Hand surgery, Caritaskrankenhaus, Lebach, Germany. The skin was prepared according to [38] and stored in the freezer at -26°C for a maximum of six months. During this time the skin's absorption properties are not changed [120-122]. For this study, skin of three donors was used. The study was approved by the Ethical Committee of the Aerztekammer des Saarlandes no. 204/08. Heat-separated epidermis (HSE) was prepared by heat separation technique according to [123].

3.3.3 Permeation experiments

Permeation experiments were performed in a static Franz diffusion cell as described elsewhere [113]. Before incubation, the epidermis was equilibrated with the receptor solution for one hour. The receptor solution consisted of PBS pH 7.4 for caffeine and Soerensen phosphate buffer pH 7.4 for FFA. To prevent microbial contamination the receptor was stabilized with 0.05% (w/v) sodium azide. Caffeine was used in a concentration of 1mg/ml in PBS without NaCl and stained with 0.1% (w/v) methylene blue (sodium chloride was omitted due to salt formation with methylene blue). Previous studies have shown that the same permeation coefficients are ob-

tained with and without NaCl. FFA was used in a concentration of 1 mg/ml in Soerensen phosphate buffer stained with 0.1% (w/v) eosin Y. All permeation experiments were performed with the donor chamber sealed by parafilm and aluminium foil to avoid water evaporation. Samples were taken from 0 h to 41 h. For each set of experiments 6 to 8 single experiments were carried out. The removed receptor solution (400 µl) was replaced immediately by fresh buffer.

3.3.4 Application of the donor

Different finite dose application schemes were applied:

- ***Punch:*** application of 17.6 µl of the donor formulation, then distribution of the formulation by 360° rotation of a Teflon punch (in-house, 14 mm diameter), removal of the punch and covering with a Teflon disc with a diameter of 14 mm. The drug amount removed with the punch was determined by extraction.

- ***Disc:*** application of 15.6 µl of the donor formulation, then distribution and covering with a Teflon disc with a diameter of 14 mm according to [124].

In all finite dose experiments, a dose less than 10 µl/cm was incubated with the skin to meet finite dose conditions.

3.3.5 Mass recovery

After incubation, all compartments were thoroughly examined for drug content: the remaining donor on the surface of the skin, drug on the parts of the Franz diffusion cell, and the skin. Caffeine was extracted from the skin with methanol 50% (v/v), sonication for 30 min and further shaking for one hour followed by filtration through a cellulose acetate filter. FFA was extracted with 0.05 N NaOH for two hours at room temperature and filtration through cotton. In all experiments, a total mass recovery of 92.4 to 99.7% for caffeine and 94.0 to 114.5% for FFA were found. The extraction power of the drug from HSE was determined with standard solutions being 97.8 ± 3.8% for FFA [38] and 87.4 ± 5.1% for caffeine [125].

3.3.6 Drug quantification

Caffeine and FFA were quantified according to [125]. For calibration, both substances were dissolved in the respective extraction medium in concentrations of 0.03 – 20 μg/ml. Stability tests were performed for both substances in all solvents used for at least 41 h at 32°C to ensure no degradation would take place during incubation. The dyes had no influence on the analytics and the permeation of the drug.

3.3.7 Analysis of the application area

For accurate determination of the application area, the donor formulation was stained with a dye. After incubation, the dye was still visible on the skin surface and the contact area of the donor formulation with the skin could be analysed. Following incubation, the skin was removed from the Franz diffusion cell and the donor distribution over the skin surface was visualized by means of a scanner with a resolution of 1200 dpi as tagged image file format (TIFF) data. The scans were analysed by a two-step approach to check for formulation coverage and homogeneity of the distribution.

First, the coverage was determined by using a hue-saturation-value (HSV) colour model [126] and by comparison to a non-stained skin sample. Second, the stained area was inspected for homogeneity by comparison to a perfectly stained skin sample from infinite dose experiments using a red-green-blue (RGB) colour model.

To obtain the fraction of formulation coverage Φ (Equation 3-1) each image file was mapped to HSV colour space using appropriate thresholds in the hue channel to separate stained and non-stained pixels (Figure 3-1 B, D).

$$\phi = \frac{\text{stained pixels of the incubation area}}{\text{number of total pixels of the incubation area}} \qquad \text{Equation 3-1}$$

To analyse the homogeneity of dye distribution the stained area of the sample skin after incubation (Figure 3-1A, C) was compared to a reference image from infinite dose application with perfect staining (Figure 3-1 E, F).

To measure the difference to perfect staining the images were mapped to RGB colour space and the absolute robust *z*-score (*z*-score) of intensities of a dye-dependent colour channel of a reference staining (infinite dose case) and the stained parts of finite dose sample image, previously identified by the HSV method, was calculated according to:

$$z = \frac{|x - ref|}{\sigma^2}$$

Equation 3-2

Here, x is the median of intensities in the separation channel of the sample image, *ref* is the median of intensities in the separation channel of the infinite dose reference image and σ_{ref} is the median absolute deviation of the intensities in the separation channel of the infinite dose reference image.

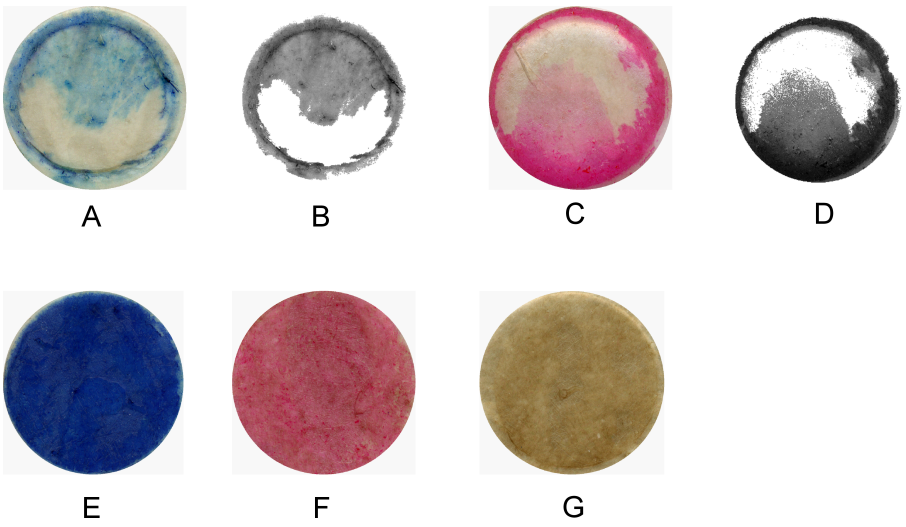

Figure 3-1 Visualization of the application area from scans. A: caffeine stained with methylene blue, finite dose, B: caffeine stained with methylene blue, finite dose, coverage; C: FFA stained with eosin Y, finite dose, D: FFA stained with eosin Y, finite dose, coverage; E: caffeine stained with methylene blue, infinite dose (reference); F: FFA stained with eosin Y, infinite dose (reference); G: incubated with unstained drug solution (blank), identical for both drugs.

For methylene blue stained skin the red channel showed a Gaussian like distribution in intensities and allowed a clear separation (peak shift) between stained and unstained areas. For eosin Y stained skin the green channel showed the best separation potential.

All methods were implemented using MATLAB 7.8.0 (The MathWorks, Natick, Massachusetts, USA) with the Image Processing Toolbox.

Coverage, expressed as percentage of the whole incubation area and the homogeneity of distribution (*z*-score) were determined for each experiment and the mean of all experiments was calculated.

3.3.8 Determination of relative peak flux and peak flux time

To characterize different finite dose experiments the relative peak flux J_{max}^{rel} and the peak flux time t_{max} were calculated. This was done by applying a three-step approach by first fitting the experimental data to obtain diffusion and partition parameters of the permeant. Secondly, the flux profile for every finite dose experiment was calculated. Finally, the relative peak flux J_{max}^{rel} and the peak flux time t_{max} were evaluated. Furthermore, the flux characteristics for every experiment using an uncorrected and corrected incubation area (using the calculated application area) were compared.

First, the cumulative amount of drug leaving the membrane at time t was fitted for every time point of an experiment (Equation 3-3 [78]). Here, M is the applied mass per area, D is the apparent diffusion coefficient, K the partitioning coefficient between donor and skin, h is the macroscopic thickness of the skin and h_v is the theoretical height of the applied volume to the skin in the Franz diffusion cell.

$$\frac{M(t)}{M_\infty} = 1 - 2\beta \sum_{n=1}^{\infty} \frac{1}{\cos\alpha_n \left(\beta + \beta^2 + \alpha_n^2\right)} \exp\left(-\frac{\alpha_n^2 Dt}{l^2}\right) \qquad \text{Equation 3-3}$$

with

$$\beta = K\frac{l}{h_v} \qquad \text{Equation 3-4}$$

and the roots of the transcendental equation, α_n, given by

$$\alpha_n \tan\alpha_n = \beta \qquad \text{Equation 3-5}$$

To avoid the use of a fixed macroscopic thickness of the skin, $p_1=D/h^2$ and $p_2=K*h$ were used as dependent variables for the fitting procedure [18, 127].

Secondly, the fitted values p_1 and p_2 as well as the corresponding values for M_t and h_v were used in the analytical solution to describe the flux J over time curve (Equation 3-6 [77, 128]). Finally, the relative peak flux J_{max}^{rel} and the corresponding peak flux time t_{max} were obtained by numerically differentiating Equation 3-6 with respect to t, setting the derivative to zero and finding of the root by using Newton's method.

$$J(t) = 2M_\infty \beta \frac{D}{l^2} \sum_{n=1}^{\infty} \frac{\alpha_n^2}{\cos\alpha_n \left(\beta + \beta^2 + \alpha_n^2\right)} \exp\left(-\frac{\alpha_n^2 Dt}{l^2}\right) \qquad \text{Equation 3-6}$$

To compare experiments with different amounts of applied substance the relative peak flux J_{max}^{rel} was calculated by normalizing the absolute peak flux J_{max} to the applied dose M :

$$J_{max}^{rel} = \frac{J_{max}}{M_\infty} \qquad \text{Equation 3-7}$$

All equations and mathematical operations were implemented using Python 2.7.1[2] and the *SciPy* package [129].

3.3.9 Analysis of lateral drug distribution

Drug distribution in stained and unstained skin parts was analysed after incubation in the permeation setup. 15.6 µl of the stained drug formulation were applied to the skin as a drop without further distribution. This setup led to inhomogeneous formulation distribution over the incubation area. Thus, not all skin available for diffusion was in contact with the donor formulation. After predetermined time intervals of incubation (after 41 h, and additionally for FFA after 2 h and 20 h), 5 mm biopsies were taken from both completely stained and from completely unstained skin

[2] http://www.python.org/

parts of the skin inside the donor area of the Franz diffusion cell and analysed for their drug content. This allowed for comparison of the biopsy with contact to the donor formulation to the one without contact.

3.3.10 Statistics

Statistical tests were performed with Sigma Stat 3 (SYSTAT Software Inc., Point Richmond, CA, USA) to determine significant differences in results. A significant difference was detected at $p < 0.05$.

3.4 Results

3.4.1 Permeation profiles, uncorrected surface distribution

The permeation profiles of caffeine are only slightly in accordance with typical finite dose profiles including an approach of the curve to a maximum (Figure 3-2, black circles). A flattening of the curve can only be assumed. For the disc application the profile is similar to infinite dose behaviour (Figure 3-2 B, black circles). In both application schemes, a similar cumulative drug amount permeated after 41 h incubation (punch: 38.4 ± 9.4 %/cm , disc: 37.7 ± 10.5 %/cm) and a high variability between the single experiments was found (Figure 3-2). The permeation profiles of FFA resembled typical finite dose permeation graphs (Figure 3-3, black circles) approaching a maximum after longer incubation times. Both application methods led to this characteristic permeation profile. With the punch, however, the maximum was statistically lower than for the disc (Figure 3-3 B), i.e. 40.5 ± 2.6 %/cm versus 48.2 ± 3.4 %/cm after 41 h incubation. The variability between the individual experiments was low.

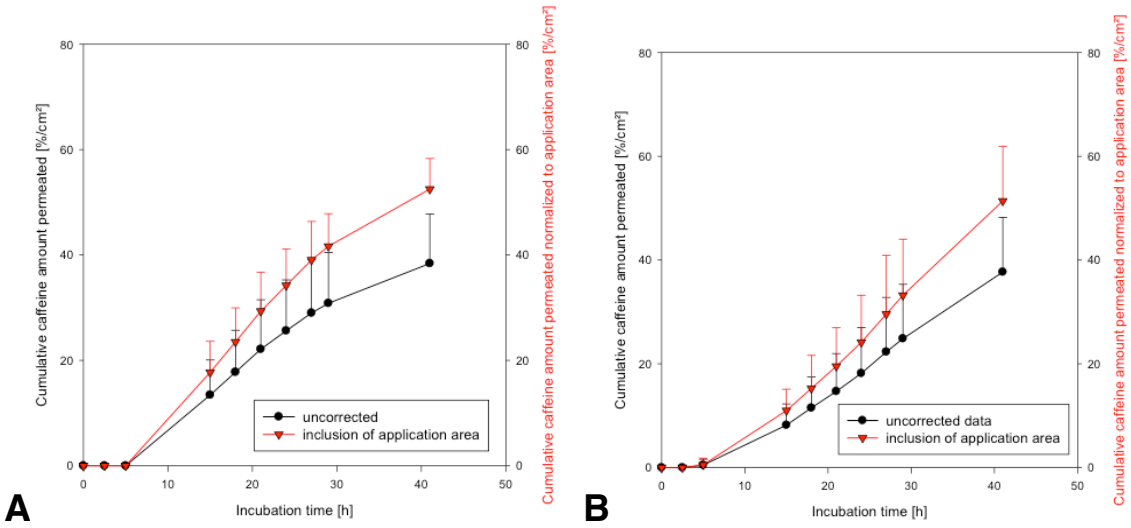

Figure 3-2 Permeation profiles of caffeine through heat-separated epidermis. Black circles: Relative cumulative caffeine amount per applied dose normalized to total incubation area (uncorrected). Red triangles: Relative cumulative caffeine amount per applied dose normalized to application area (inclusion of application area). Donor: caffeine 1 mg/ml. A: punch application, n=7. B: disc application, n=6. Mean, SD (provided only in one direction for the sake of clarity).

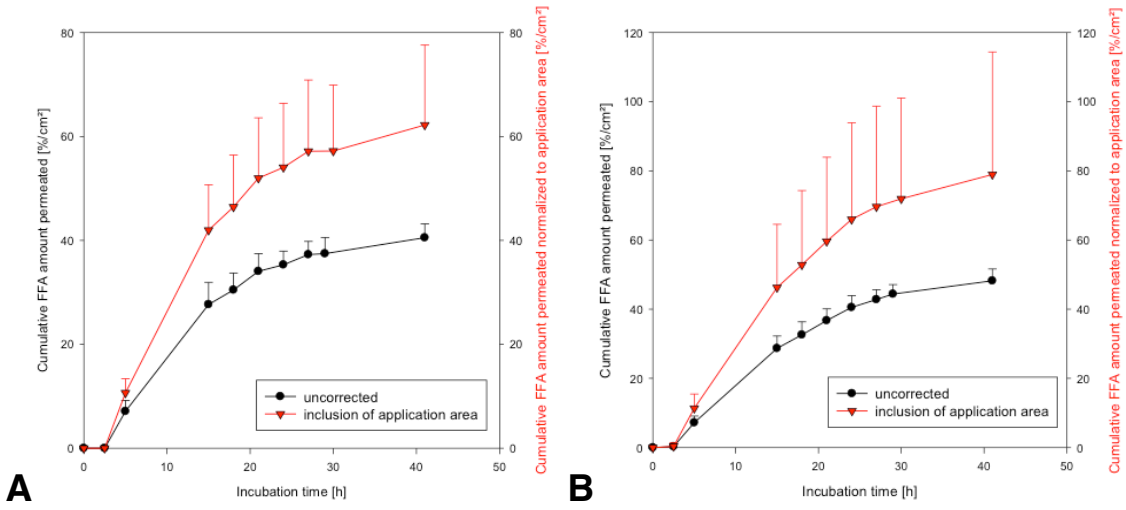

Figure 3-3 Permeation profiles of FFA through heat-separated epidermis. Black circles: Relative cumulative FFA amount per applied dose normalized to total incubation area (uncorrected). Red triangles: Relative cumulative caffeine amount per applied dose normalized to application area (inclusion of application area). Donor: FFA 1 mg/ml. A: punch application, n=8. B: disc application, n=8. Mean, SD (provided only in one direction for the sake of clarity).

3.4.2 Donor surface distribution

Coverage was similar for both dyes with high variability between the different experiments (Table 3-1). Results of this identification method for methylene blue are shown in Figure 3-1 B (compared to Figure 3-1 A), and for eosin Y in Figure 3-1 D (compared to Figure 3-1 C). *Z*-scores were dependent on the dye, however, within each group very similar (Table 3-1).

Table 3-1 Mean relative peak flux, peak flux time, and coverage of FFA and caffeine (CAF) using different application methods in comparison to the mean relative peak flux using the application area. Mean ± SD.

	FFA Disc	FFA Punch	CAF Disk	CAF Punch
Employed dye	Eosin Y	Eosin Y	Methylene blue	Methylene blue
J_{max}^{rel} **x 10^{-2} [%/cm^2 h]**	4.0 ± 0.6	3.2 ± 0.5	1.8 ± 0.7	2.3 ± 0.9
J_{max}^{rel} **x 10^{-2} (eff. incl. area) [%/cm^2 h]**	Not applicable	Not applicable	2.5 ± 0.1	3.1 ± 0.7
t_{max} **[h]**	5.6 ± 1.1	3.8 ± 0.9	16.2 ± 6.0	12.2 ± 3.6
Coverage [%]	67.9 ± 18.6	68.5 ± 16.2	74.2 ± 18.5	73.7 ± 18.1
z-score	0.7 ± 0.5	0.9 ± 0.7	4.9 ± 1.7	5.9 ± 0.4

3.4.3 Permeation data combined with calculated application area/coverage

To find out whether the application area had an effect on permeation, the previously obtained permeation profiles for caffeine and FFA were normalized to the application area of each single experiment.

Inclusion of the application area led to a decrease in variability of the permeation profiles of caffeine (Figure 3-2 red triangles). The relative standard deviation decreased strongly, too, and was slightly reduced over the incubation time (e.g. after 41 h for the punch 24% before and 11% after correction).

The permeation experiments with FFA exhibited a much lower variability between the different experiments compared to caffeine, even though the coverage was similar to the caffeine experiments. After including the application area, the variability between the experiments highly increased (Figure 3-2 red triangles), as well as the relative standard deviation (e.g. after 41 h for the punch 7% before and 25% after correction).

3.4.4 Relative peak flux and peak flux time

The relative peak flux determined for the caffeine finite dose experiments was significantly lower than the values obtained for FFA permeation for both application methods (Table 3-1). Also, the relative peak flux of FFA was significantly higher for the disc than for the punch. For caffeine this was not the case. Using the calculated application area for caffeine the relative peak flux increased considerably, whereas for FFA this inclusion was not applicable (Table 3-1). The peak flux time was significantly higher for caffeine than for FFA for both application methods. Furthermore, the peak flux time for FFA was higher for the disc application compared to the punch.

3.4.5 Lateral drug distribution

After 2 h incubation with FFA, only in the skin parts in contact with the donor formulation FFA could be detected. With increasing incubation time, the FFA amount in the stained skin parts decreased while in the non-stained parts it increased. After 20 h no significant difference between stained and non-stained skin could be detected any more (2.33 ± 2.52% of applied dose vs. 0.31 ± 0.05% of applied dose, mean ± SD), and after 41 h the amount of FFA in biopsies with or without staining was similar (0.28 ± 0.04% of applied dose vs. 0.26 ± 0.01% of applied dose, mean ± SD). For caffeine, no lateral distribution could be observed after 41 h incubation.

3.5 Discussion

The goal of this study was to evaluate the influence of drug distribution of the application area on the results of finite dose permeation experiments using aqueous donor solutions. Therefore, two different application methods were tested and an automated detection system for surface distribution based on dyes was developed. In addition, a three-step approach to calculate relative peak flux and peak flux time to characterize permeation was introduced.

3.5.1 Dye as a marker for skin contact with the donor formulation

The aqueous donor phase employed in this study shows a high contact angle on the skin surface and therefore does not spread easily. The highly water soluble dyes employed in this study can be assumed to remain in the aqueous donor solution and are not distributed laterally over the lipophilic *stratum corneum*, making them an ideal compound for marking the contact area of the hydrophilic formulation with the skin (application area).

3.5.2 Suitability of the automated computer-assisted approach for determination of coverage

Based on the analysis of hue values and *z*-scores by an automated computer-assisted method the determination of coverage and homogeneity is an objective method to characterize the formulation distribution on skin's surface. However, since the HSV colour space is a cylindrical-coordinate representation, two thresholds to define the blank skin (hue range) have to be determined. Within this range all pixels from the sample skin image will count as blank skin and all pixels outside this range will count as stained skin. Hue values between 0.02 and 0.35 were chosen empirically to identify non-stained skin pixels from a non-stained skin sample (Figure 3-1 G). These thresholds did guarantee a conservative prediction of staining since no false positive pixels were detected in a negative test set with only blank skin samples. Changing these parameters can significantly impact the definition of the coverage. Thus, for every batch of experiments a blank reference skin sample image (Figure 3-1 G) should be used to gather appropriate thresholds. The original sample images of skin

(Figure 3-1 A, C) showed excellent consistency with the determined application areas (Figure 3-1 B, D).

Calculation of the absolute robust *z*-score requires a median intensity level and the median absolute deviation of the RGB colour channel of a perfectly stained reference skin sample image (Figure 3-1 E, F). Since eosin Y showed z-scores near zero, this indicates that the dye distribution was close to a perfect staining (Table 3-1). For methylene blue, the values are reasonable.

Besides increasing the speed of the evaluation process, the great benefits from using this automated approach is objectivity and stability of coverage, and colour distribution analysis for finite dose experiments that is not possible using a manual inspection method. In addition, the transfer of this method to evaluate formulation distribution *in-vivo* is possible, if digital images made by photography were used instead of the scanned.

3.5.3 Calculation of relative peak flux

Determination of the highest flux during finite dose skin absorption experiments is quite difficult. Some approaches determine the steepest and linear part of the curve and from there calculate the flux [116, 130].

Flux values calculated from cumulative amount per time measurements without fitting the data can lead to fuzzy values, especially if only limited time points close to the flux plateau are available. By using the diffusion and partition parameters from the fitting procedure a fine-grained flux profile can be calculated by using the analytical solution. A subsequent numerical derivation of the formula guarantees a precise determination of relative peak flux and peak flux time without the limitation given by the sample intervals of the experimental setup.

The relative peak flux for caffeine calculated in this study was significantly lower than for FFA for both application methods (Table 3-1) and the peak flux time was much higher. This is in accordance with previously published data [124, 125].

Using coverage correction to obtain the application area and subsequent calculation of the relative peak flux yields a clear increase in peak flux values. These coverage

corrected relative peak flux values are more reliable. Certainly, peak flux times are not affected. These corrections should be applied carefully, since the potency of a substance for lateral distribution strongly affects the area actually available for substance absorption. This correction cannot be applied, if other phenomena like strong lateral distribution (see next paragraph) do affect the diffusion area. This is the case for FFA and therefore the relative peak flux values are not provided.

3.5.4 Permeation profiles and lateral drug distribution

The permeation profiles for caffeine do not resemble the typical finite dose characteristics (Figure 3-2). It is possible that after 41 h the effect of donor depletion is just not yet visible in the permeation profiles due to slower permeation of caffeine (Table 3-1).

The lower permeated FFA amount after application with the punch (Figure 3-3) may be explained by transfer of donor formulation to the upper part of the Franz diffusion cell during distribution over the incubation area by spreading, reducing the amount of formulation in contact with the incubation area.

The effect of the application area on the permeation profiles depends on the drug employed. For FFA, the variability between the experiments increased after including the application area, leading to the assumption that other additional effects may influence the drug absorption. These effects may be explained by lateral distribution of the lipophilic FFA (log $K_{o/w}$ ~4.8) [124, 125]. Skin biopsies taken after different incubation intervals from stained and unstained skin resulted in information about the time profile of lateral distribution of FFA, which was distributed homogenously over the whole incubation area after 20 h. As caffeine is a relatively hydrophilic compound (log $K_{o/w}$ -0.08) [124, 125] it cannot be transported into the lipid bilayers as easily as FFA.

Lateral distribution was investigated from aqueous solution. This medium was chosen to gain general data for a substance and make the data comparable to the extended Flynn database [131, 132]. Moreover, penetration enhancing effects, e.g. of oils or ethanol, were excluded.

A direct visualization of lateral drug distribution over time would be preferred. For fluorescent dyes, the fluorescent recovery after photo bleaching (FRAP) technique can be employed [133] to analyse lateral diffusion. However, quantitative results are difficult to obtain for non-fluorescent drugs due to the low amount of drug actually diffusing laterally and thus of analytics. This problem is even increased by finite dose application. Thus, lateral distribution in our study was investigated by means of skin biopsies.

3.5.5 Remarks and the clinical relevance

In-vivo experiments are quite expensive and its number will be reduced in the future. Therefore, *in-vitro* skin absorption studies are important to gain first information about the absorption kinetics of a substance. Correlations between *in-vitro* and *in-vivo* experiments have been shown previously [38, 134, 135]. Thus, for example for bioequivalence studies *in-vitro* experiments are beneficial to determine e.g. the difference between two vehicles [136].

Finite dose experiments are even closer to the real-life scenario of a patient applying a small amount of a topical formulation. Due to that similarity, finite dose experiments are of major interest to predict the drug absorption. During *in-vivo* application, differences in the homogeneity of donor formulation distribution are also possible, thus an analysis of the influence of inhomogeneous donor distribution is important, too.

3.6 Conclusion

As shown in this paper, including the application area does not automatically improve the results from skin permeation studies using aqueous solutions, leading to more consistent results. Depending on the physicochemical characteristics of the drug, especially lipophilicity, different behavior has to be considered. For the more hydrophilic substances (e.g. caffeine) the degree of contact to the skin is evident for permeation and this parameter should be included in the analysis of finite dose experiments. For lipophilic substances, e.g. FFA, however, the application area has less effect on the permeation of the drug.

It is assumed that lipophilic substances might be distributed over the whole incubation area by lateral diffusion in the lipophilic *stratum corneum*. For more hydrophilic compounds, lateral distribution over the lipophilic *stratum corneum* is unlikely.

One question that remains is whether a limit of lipophilicity exists up to where distribution has an influence on permeation. To answer this question, another study with substances covering a wide range of lipophilicity would be required.

4 Finite dose skin mass balance including the lateral part: Comparison between experiment, pharmacokinetic modeling and diffusion models

Parts of this chapter have been published in:

Selzer, D., Hahn, T., Naegel, A., Heisig, M., Kostka, K. H., Lehr, C.-M., Neumann, D., Schaefer, U. F., Wittum, G. (2013). Finite Dose Skin Mass Balance Including the Latral Part: Comparison Between Experiment, Pharmacokinetic Modeling and Diffusion Models. *J Control Release,* 165(2), 119–128.

The author of the thesis made the following contributions to the publication:

Developed the pharmacokinetic model and the data correction with stretching factor. Wrote parts of the manuscript. Interpreted the data. Developed the QSAR model to predict donor diffusivity.

Tsambika Hahn performed and interpreted all major experiments and wrote the manuscript.

The Wittum group in Frankfurt made the following contributions to this chapter: Developed the detailed/homogenized diffusion model and adapted it to finite dose, and performed the diffusion model simulations.

4.1 Abstract

In-vitro finite dose skin absorption of flufenamic acid and caffeine was investigated experimentally and mathematically. Mass balance over time in the different compartments of skin in the Franz-diffusion cell experiments (donor, *stratum corneum* (SC), deeper skin layers (DSL), lateral skin parts and acceptor) was analyzed. Especially the mass inside the lateral, compressed skin part was considered. Three mathematical models, a pharmacokinetic model (PK), a detailed two-dimensional diffusion model (DIFF) and a homogenized diffusion model (HOM) were applied to the experimental data. The PK model and HOM model were able to determine substance mass in the lateral skin compartment. The DIFF and the HOM models employed input parameters derived from infinite dose studies to predict the underlying diffusion process and the PK model was fitted to the experimental data. For both drugs high amounts of substance could be found in the lateral skin compartment after 6 hours of incubation, which emphasizes not to elide the lateral parts in the modeling during finite dose skin absorption studies. All models could satisfyingly predict or describe the experimental data.

4.2 Introduction

As delivery of drug to the skin is gaining more relevance nowadays, the pharmaceutical industry is interested in evaluating the absorption of active entities to the skin. Moreover, the cosmetic industry is also interested in a risk assessment, since the systemic availability of topically applied cosmetic substances, is usually desired to be avoided.

To achieve this, usually infinite dose skin absorption experiments are performed. In these experiments, the dose on the application site and the amount of substance in the donor are large and effectively do not vary with time. Unfortunately, one obvious drawback of these experiments is that they have often little in common with realistic *in-vivo* exposure scenarios, when only a small amount of a topical formulation is evenly distributed on the skin surface. Correspondingly, the OECD guideline 428 [54] and the guidance document 28 [55], define finite dose experiments by an applied dose of 10 μl/cm or less to the skin. Due to the limited amount of substance, the transient character may lead to a substantial deviation from the steady-state situation that is characteristic for an infinite dose setting. In this context, in particular the role of the lateral compartment in experimental studies, has recently gained some attention [137-139].

As skin absorption experiments are generally time consuming, the development of suitable mathematical tools and descriptions is equally important (i) to investigate the absorption behaviour and (ii) to offer predictions of substance absorption, in order to reduce the number of experiments significantly. For the finite dose situation, different models have been developed. Most of them solely focus on the permeation profiles of a drug through a skin membrane [30, 140]. However, these do not consider the drug amount in each skin layer. The effect of lateral diffusion has to the best of our knowledge not yet been investigated before.

The aim of the present work is to investigate *in-vitro* skin absorption for the transient case and under finite dose conditions both experimentally and from a modeling perspective. We applied three different mathematical models (pharmacokinetic model, detailed diffusion model and homogenized diffusion model) and in particu-

lar shed some light on the influence of a lateral compartment on mass balance profiles

Thus, as a first step, mass balance profiles for the different skin layers were established experimentally. After incubation with one of the two model drugs flufenamic acid (FFA) or caffeine (CAF), the skin compartments were separated carefully by a highly standardized method for tape-stripping the *stratum corneum* (SC) *[38, 39]* and subsequent separation of the DSL compartment from the lateral compartment (see supplementary information). From quantification of the drug amount in each compartment, information about the absorption behaviour of the substance to the skin can be gained, e.g., the formation of a drug depot in the upper skin layers [35, 141]. Depots in skin layers may play an important role for controlled release systems applied to the skin such as application of nano-sized systems [142, 143].

On the modeling side, a pharmacokinetic model (PK) was developed describing the mass profiles of the drug in each skin compartment over time. The novelty of this model was the separation of the skin into not only the SC and the deeper skin layers (DSL), but also into an additional lateral skin part. This compartment is usually neglected during mathematical descriptions of experimental data. To simulate mass profiles in the different compartments, a microscopic detailed diffusion model (DIFF) previously developed for infinite dose [81] was adapted to the finite dose scenario. The input parameters for this model were previously derived from infinite dose experiments [125], and the same parameters were used for the finite dose case. Finally, a homogenized diffusion model (HOM) was used to predict the mass profiles on a larger scale than the detailed diffusion model, including the lateral compartment into the model.

4.3 Materials and Methods

4.3.1 Materials and instruments

The following chemicals were used: potassium dihydrogen phosphate, citric acid x H_2O (Merck, Darmstadt, Germany), caffeine, flufenamic acid, acetonitrile, methanol (Sigma-Aldrich, Steinheim, Germany), orthophosphoric acid, sodium hydrogen phosphate dihydrate (Riedel-de Haën, Sigma-Aldrich, Seelze, Germany). Purified water was prepared by a Millipore Synthesis device (Millipore GmbH, Schwalbach, Germany).

Static Franz diffusion cells type 6G-01-00-15-12 with a receptor volume of 12.1 ml and an incubation area of 1.767 cm^2 were provided by Perme Gear, Riegelsville, PA, USA; tesa® Film kristall-klar, (t-tape, 33 m x 19 mm, #57330-00000-02, cut to pieces of 16 x 19 mm) was provided by tesa AG, Hamburg, Germany; cryomicrotome (MEV) was provided by SLEE, Mainz, Germany; centrifuge (Rotina 420R) was provided by Hettich Zentrifugen, Tuttlingen, Germany.

4.3.2 Skin

Excised human full-thickness skin was obtained from three female Caucasian donors undergoing abdominal plastic surgery. The study was approved by the Ethical Committee of the Aerztekammer des Saarlandes no. 204/08.

The skin was treated according to [38] and stored in the freezer at -26°C for a maximum of six months. Care was taken to strictly avoid repeated freezing and thawing of the skin. It has been shown that this treatment does not impair the barrier function of the skin [120-122, 144].

4.3.3 Skin absorption experiments

A 25 mm punch of the frozen skin was taken on the day of the experiment and allowed to thaw. After cleaning the skin with distilled water and drying it with cotton balls, the skin was mounted in a Franz diffusion cell (FD-C) with the epidermis side up. The skin was equilibrated with the receptor solution (Soerensen phosphate

buffer pH 7.4) for one hour. Previous studies have shown that after this time the skin hydration is in equilibrium state.

Afterwards, 25 μl of the donor solution was applied to the skin. The donor formulation was spread evenly over the incubation area by means of a teflon punch with a diameter of 14 mm [145]. After removal of the punch, a teflon disc with a diameter of 14 mm was placed onto the donor to prevent evaporation during incubation. The punch was later rinsed off and the actual amount of donor formulation remaining on the skin was determined. In all experiments, a finite dose was achieved according to [54, 55]. After application of the donor, the donor compartment was sealed with parafilm and aluminum foil. The whole setup was incubated at 32 ± 1 °C.

The donor consisted of the respective drug dissolved in Soerensen phosphate buffer pH 7.4 in concentrations of 1 mg/ml for flufenamic acid (FFA), and 1 mg/ml and 12.5 mg/ml for caffeine (CAF). For all experiments sink conditions have been maintained.

4.3.4 Isolation of the different skin compartments and determination of the stretching factor for data correction

After incubation, the skin was cleaned of remaining donor formulation by cotton balls. Then, tape-stripping was performed *in-vitro* with tesa® Film kristall-klar under highly standardized conditions according to [37, 39].

After complete removal of the SC by tape-stripping, the rest of the skin was frozen using expanding carbon dioxide. Then, a punch of 13 mm diameter was taken from the stripped area of the frozen skin and cut by cryo-sectioning.

The experimental methodology (skin stretching before tape-stripping and the usage of a smaller punch to separate the *DSL*) does promote the formation of a "pseudo-lateral" skin part in addition to an actual lateral skin part (Figure 4-1).

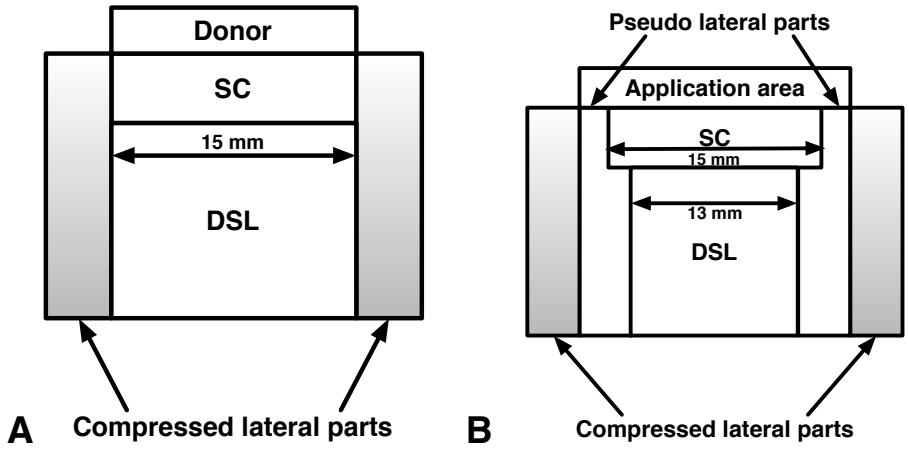

Figure 4-1 Schematic visualization of the geometric problems associated with stretching the skin before tape-stripping. A: skin during incubation. B: skin stretched after incubation.

Since this effect does falsify mass recovery results and the degree of stretching of the skin is typically unknown, the stretching factor *f* was introduced to scale mass recovery data from the experiment with

$$f = \frac{A_{Stretched} - A_{Incubated}}{A_{Incubated}} \qquad \text{Equation 4-1}$$

We assumed a horizontal uniform drug distribution within each model compartment (Donor, *SC*, *DSL*, Lateral, and Acceptor) and used a first order mass balance model (Figure 4-2) to estimate the stretching factor *f*.

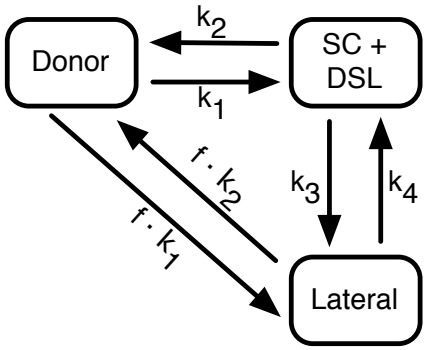

Figure 4-2 Mass balance model to estimate the stretching factor *f*.

f is the ratio of the difference between stretched area $A_{\text{Stretched}}$ and incubated area $A_{\text{Incubated}}$ normalized to $A_{Incubated}$. We assumed an artificial flux from the donor compartment directly to the lateral compartment via the »pseudo-lateral« compartment that corresponds to skin stretching induced by the used tape-stripping procedure (Fig. S1a B). In this mass balance model the rate constants of the flux through the stretched skin part outside of the stripped area to the lateral skin part should commensurate with the rate constants to the skin parts of the incubated area. The proportionality factor should correspond to the scaling factor f. The set of ordinary differential equations (ODEs) of the model was solved numerically and the rate equations as well as the stretching factor f were fitted to the mass over time curves by minimizing the root mean square deviation (RMSD) of the fitted results and experimental data points. The procedure was implemented using Python 2.7.1 and the *SciPy* package [129].

The amount of drug in the SC, DSL and the lateral skin part was scaled according to the ratio of surface area of the stretched skin and the area of incubation.

The extension of the increase of incubation area was calculated by:

$$s = \frac{d_i \cdot (\sqrt{f + 1} - 1)}{2} \qquad \text{Equation 4-2}$$

Here, d_i is the inner diameter of the Franz diffusion cell.

4.3.5 Validation of the stretching factor

To validate the stretching factor, full-thickness skin was incubated in a Franz diffusion cell with the donor formulation as before. After incubation, the skin was not stretched in preparation for tape stripping. Instead, a 16 mm biopsy was taken to remove all incubated skin parts. The remaining skin rest was regarded as compressed, lateral parts without any contact to the donor formulation. All skin compartments (Donor, Incubated skin (SC+DSL), Lateral skin parts, Acceptor) were quantified for their drug content. For each drug the longest incubation time of the experimental range was chosen, for FFA and for CAF (12.5 mg/ml) at 6 h and for CAF (1 mg/ml) at 12 h.

4.3.6 Mass balance

After incubation, all compartments of the setup were thoroughly examined for drug content, namely the donor solution remaining on the skin surface (donor), the tape-strips (SC), the cryo-cuts (DSL), and the lateral skin parts. FFA was extracted using 0.05 N sodium hydroxide solution and CAF with phosphate buffer pH 2.6 for 2 h. The samples from the acceptor were measured without further dilution steps. FFA and CAF were quantified by HPLC according to [125] at the wavelength of 262 nm for CAF. For all experiments, the obtained total recovery for FFA (LLOQ of 50 ng/ml) ranged from 83.8% to 96.8% and for CAF (LLOQ of 30 ng/ml) from 87.9% to 107.3%.

4.3.7 Pharmacokinetic modeling

Pharmacokinetic (PK) modeling was applied to analyze mass profiles in the different compartments for FFA and CAF finite dose experiments. The model treats the different skin layers as well stirred compartments. First-order kinetics were assumed to describe the substance mass flux for every compartment which yielded a set of ordinary differential equations (ODEs). As an extension of the classical models, a lateral compartment was added explicitly, into which the drug can enter (Figure 4-3). The transport constants k_5 and k_6 in this model represent an averaged transport via the *SC* and *DSL* to the lateral compartment.

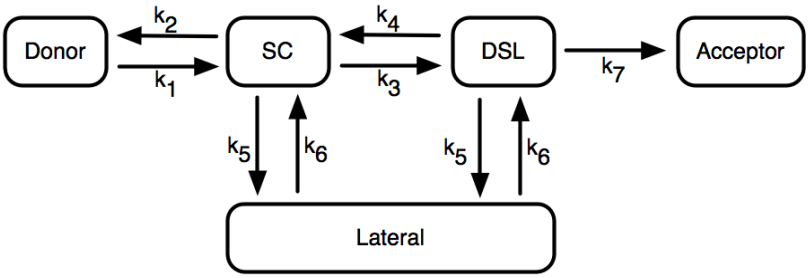

Figure 4-3 Pharmacokinetic model developed to analyze drug distribution between various relevant compartments in the skin. Here, k_1 to k_7 are first-order rate constants.

The set of ODEs was numerically integrated and fitted (nonlinear least squares regression) to experimental data using Python 2.7.2 with the *SciPy* package [129]. The root mean square deviation (RMSD) was used as an indicator for accuracy. A grid search was applied to find appropriate starting values in order to avoid sticking in a local minimum.

4.3.8 Detailed diffusion model

An alternative transport model is a diffusion process in an idealized, two-dimensional model membrane. This has previously been described for an infinite dose setting [81, 125], and is now extended to a finite dose scenario. The core part of the model is a brick-and-mortar like structure, which represents the SC. On the top and bottom side of this structure two additional compartments have been added, (c.f. Figure 4-4).

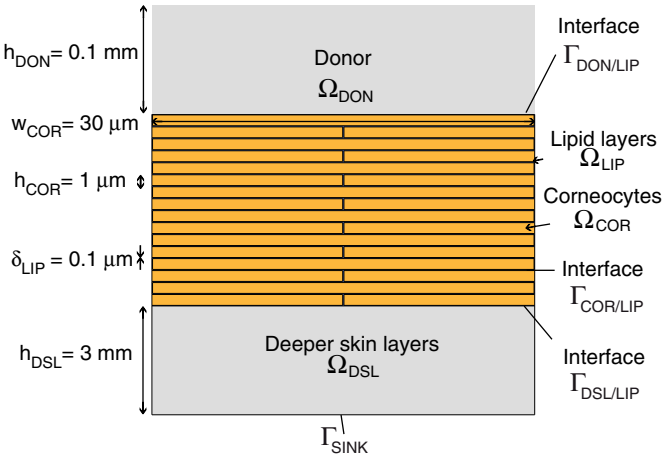

Figure 4-4 Microscopic diffusion model (modified from [81]): dimensions (left) and domains and interfaces (right). The bottom boundary Γ_{SINK} provides a perfect sink. Diffusion and partition coefficients are listed in Table 4-1.

These model the donor chamber (DON) of the diffusion cell and the deeper skin layers (DSL) respectively. The heights for DON and DSL compartments are h_{DON} = 0.1 mm and h_{DSL} = 3 mm, respectively. The substance mass in the acceptor compartment is defined as the mass that is leaving the system at h_{DSL} = 3mm. Initially, no substance is present in SC and DSL, and a defined concentration, which matches the experimental setup, is provided in the donor.

The model equation is given by [62]

$$\partial_t(ku) + \partial_x[-kD\,\partial_x u] + \partial_y\big[-kD\,\partial_y u\big] = 0 \qquad \text{Equation 4-3}$$

where the solution u is defined by a set of diffusion and partition coefficients, which are assumed to be piecewise constant for any phase $A \in \{DON, COR, LIP, DSL\}$. With the concentration $c \coloneqq ku$, the functions k are uniquely defined up to a constant by the interface condition $K_{A/B}c_B = c_A$, if u is continuous on the interface between two phases $A, B \in \{DON, SC, DSL\}, A \neq B$. By definition, fluxes are preserved.

Several other models have been discussed in the literature, e.g. [78, 128]. However, the finite dose model employed in this work is to the best of our knowledge the first model considering the microscopic structure of the *stratum corneum*. A lateral compartment is not included in the model, as modeling a diffusion cell with a diameter of 15 mm in a full resolution model with a corneocyte width of 30 μm is not viable within a reasonable timescale. The model relies on a variety of diffusion and partition coefficients, which are provided in Table 4-1. Except for the diffusion coefficient in the donor, D_{DON} , all parameters were taken from infinite dose experiments performed previously [65, 81]. A relationship to predict the diffusion coefficient D_{DON} in an aqueous solution from the solute molecular weight was proposed by Anderson et al. [64] with

$$D_{DON} = D^0_{DON} \cdot MW^{-n} \qquad \text{Equation 4-4}$$

where D_{DON} is the diffusion coefficient in a certain medium, n and D^0_{Don} are constants associated with the medium at a defined temperature, and MW the molecular weight in Da. Using 37 substances and their corresponding molecular weight (gathered from the PubChem database [146]) and diffusion coefficient in water at 27°C [147] the previous equation was fitted to the log-transformed data using a linear model, resulting in $D^{CAF}_{Don} = 2.92E-02\ cm^2/h$ with a 95% CI of [2.77E-02, 3.08E-02] and $D^{FFA}_{Don} = 2.47E-02\ cm^2/h$ with a 95% CI of [2.31E-02, 2.65E-02].

Table 4-1 Input parameters for simulation of skin absorption with 2D diffusion model [81, 125].

Parameter		FFA	CAF
D_{DON}	[cm^2/h]	2.47E-02	2.92E-02
D_{LIP}	[cm^2/h]	1.10E-04	2.10E-04
D_{COR}	[cm^2/h]	5.10E-07	1.40E-07
D_{DSL}	[cm^2/h]	4.90E-03	2.30E-03
$K_{LIP/DON}$		20.32	2.15
$K_{COR/LIP}$		0.21	2.22
$K_{DSL/LIP}$		0.1	0.08

4.3.9 Homogenized diffusion model

The above mentioned diffusion model does not consider lateral. As an alternative, we consider the following *homogenized diffusion model (HOM)*: In this case the microscopic heterogeneous structure of the SC is not resolved explicitly, but is treated as a macroscopic homogeneous compartment. A sketch of the underlying model geometry is depicted in Figure 4-5. On this geometry, we solve the model equation in cylindrical coordinates:

$$\partial_t(\mathrm{rkc}) + \partial_r[-\mathrm{rD_{rr}}\,\partial_r c] + \partial_z[-\mathrm{rD_{zz}}\,\partial_z c] = 0 \qquad \text{Equation 4-5}$$

with a continuous solution $u = u(r, z, t)$. Now the diffusion coefficients D_{rr}, D_{zz} are the diagonal entries of an anisotropic diffusion tensor. This tensor represents the structure of the corneocytes implicitly in terms of different diffusion coefficients in lateral (r) and transversal (z) direction. This approach is similar to [148, 149], but in addition, r is used as scaling factor. Thus, it reflects the increase in volume in the outer parts of the diffusion cell.

Diffusion in the donor (DON) and in the deeper skin layers (DSL), is undirected, i.e., $D_{DON,rr} = D_{DON,zz} = D_{DON}$ and $D_{DSL,rr} = D_{DSL,zz} = D_{DSL}$. Diffusion in the SC is modeled by coefficients

$$D_{SC,ii} := D_{LIP}\,\alpha_{ii}(\xi) \qquad \text{Equation 4-6}$$

where the non-dimensional factor

$$\alpha_{ii}(\xi) = \alpha_{ii}^{0} + \frac{(\alpha_{ii}^{\infty} - \alpha_{ii}^{0})(1 - \alpha_{ii}^{0})\xi}{(\alpha_{ii}^{\infty} - 1) + (1 - \alpha_{ii}^{0})\xi} \qquad \text{Equation 4-7}$$

represents the anisotropy as a function of the effective corneocyte diffusivity

$$\xi = \frac{D_{COR}}{D_{LIP}} K_{\frac{COR}{LIP}} \qquad \text{Equation 4-8}$$

and of two geometry dependent constants α_{ii}^{0} and α_{ii}^{∞}. The theoretical foundations can be found in [97].

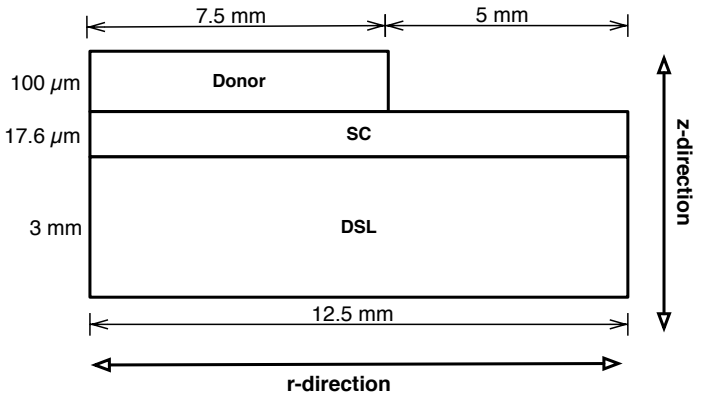

Figure 4-5 Homogenized diffusion model: The model geometry is a cross section through half a diffusion cell (not drawn to scale).

For this model, two different approaches were applied: In the HOM1 model, all parameters except for the diffusion coefficients in the SC, $D_{SC,rr}$ and $D_{SC,zz}$, are taken from [81]. This basic data is provided in Table A-1 A. The coefficients are determined

from Equation 4-6 by a least squares regression analysis for the diffusivity $\xi := \exp(\theta_1)$. In order to improve on this further, a model with three regression parameters, θ_1, θ_2 and θ_3, referred to as HOM3, was applied. In addition to the previously mentioned parameter ξ, DSL diffusivity and partition coefficients were parameterized by:

$$D^*_{DSL} := D_{DSL} \exp(\theta_2) \qquad \text{Equation 4-9}$$

$$K^*_{SC/DON} := K_{SC/DON} \exp(\theta_3) \qquad \text{Equation 4-10}$$

$$K^*_{SC/DSL} := K_{SC/DSL} / K_{SC/DON} \, K^*_{SC/DON} \qquad \text{Equation 4-11}$$

In this model all parameters except for D_{DON} were determined by regression.

4.3.10 Model overview and parameter estimates

A comparison of the above mentioned models is provided in Table A-1 A. For the PK and both HOM models some parameters were optimized using a non-linear regression analysis to obtain a better fit to the experimental data. In these parameter estimations, which were performed by a Gauss-Newton solver, the standard deviation (sum of squared residuals / number of degrees of freedom) was used as the objective.

4.3.11 Statistics

Graph Pad Prism 6.0 for Macintosh (GraphPad Software, La Jolla, California, USA) was used for calculating student t-test. Significant differences were found at $p < 0.05$.

4.4 Results

4.4.1 Experimental data

FFA finite dose experiments resulted in a relatively fast decrease of drug in the donor. Already after 15 min the drug amount in the donor was reduced to around 60% of the applied dose (Figure 4-6 A). After this quick donor reduction, the donor continued to deplete more slowly, reaching around 20% remaining in the donor compartment after 6 h incubation. In the SC around 30% of the applied dose was found after 15 min and a plateau was reached and maintained until 2 h after application (Figure 4-6 B). Afterwards, the FFA amount decreased to 10-20% with high variability at the 4 h and 6 h data points. The drug amount in the DSL increased constantly, reaching a plateau at approximately 50% after 4 h of incubation (Figure 4-6 C). No FFA could be quantified in the acceptor compartment until 6 h of incubation due to analytical reasons (Figure 4-6 D). The drug amount determined in the lateral skin part appeared to increase after longer incubation (Figure 4-6 E). However, data is affected by high variability, especially for later time points, a tendency comparable to the other compartments.

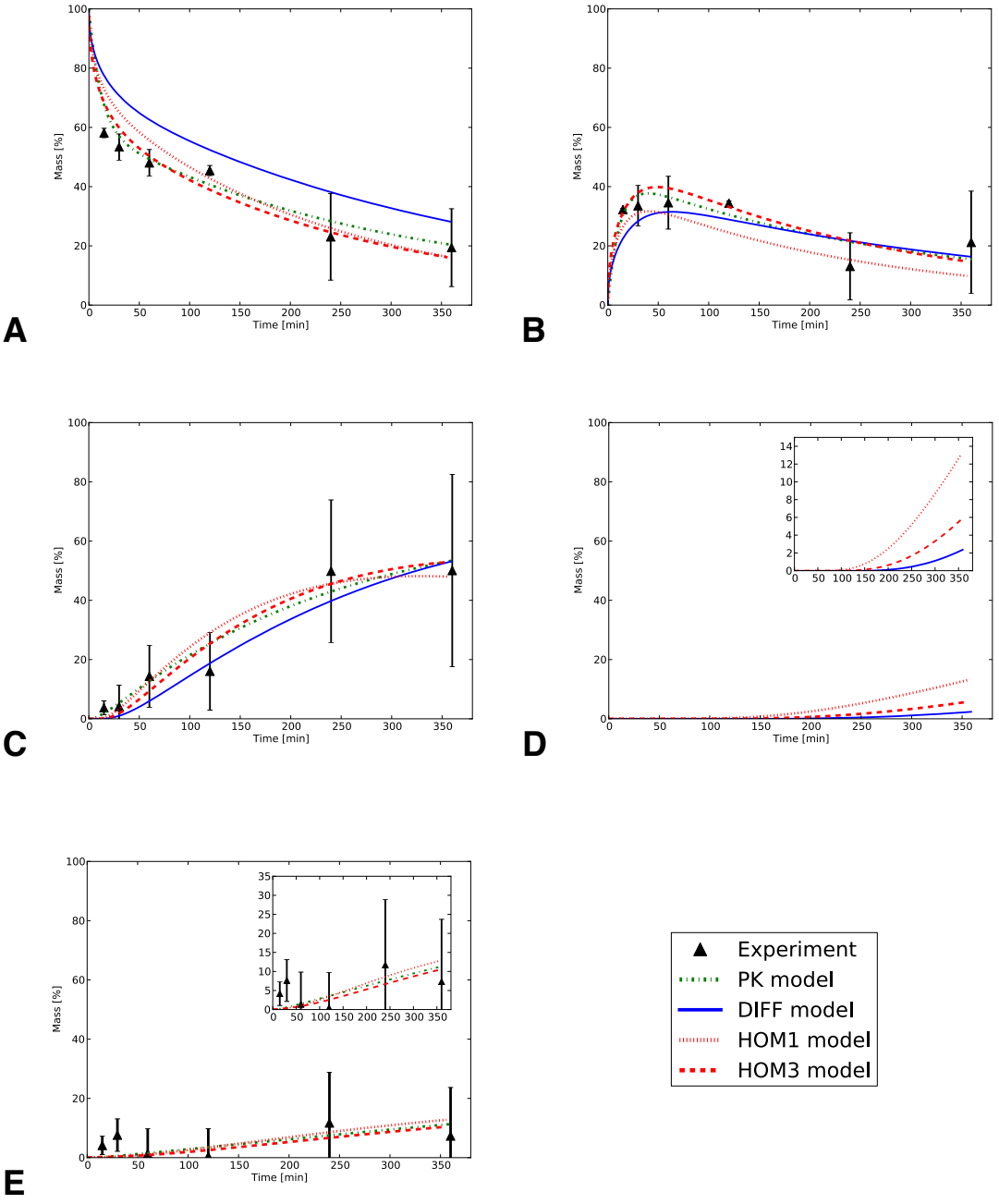

Figure 4-6 FFA mass profiles over time: experimental data, PK fitting, detailed diffusion simulation and homogenized diffusion models. A: Mass profile of the Donor compartment. B: Mass profile of the SC compartment. C: Mass profile of the DSL compartment. D: Mass profile of the Acceptor compartment (diffusion model with mass leaving the system). E: Mass profile of the lateral compartment (diffusion model data not available).

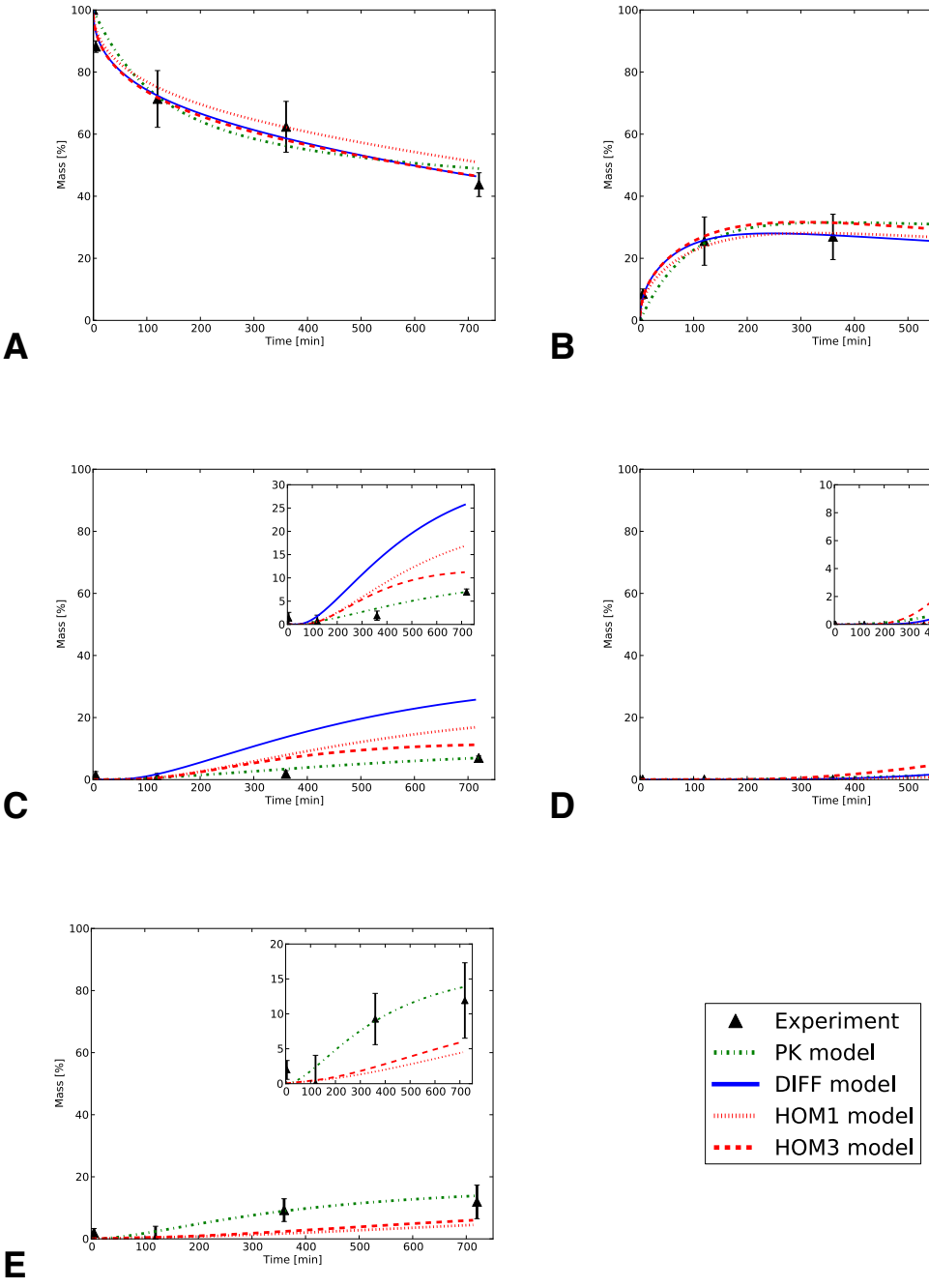

Figure 4-7 CAF (1 mg/ml) mass profiles over time: experimental data, PK fitting, detailed diffusion simulation and homogenized diffusion models. A: Mass profile of the Donor compartment. B: Mass profile of the SC compartment. C: Mass profile of the DSL compartment. D: Mass profile of the Acceptor compartment (diffusion model with mass leaving the system). E: Mass profile of the lateral compartment (diffusion model data not available).

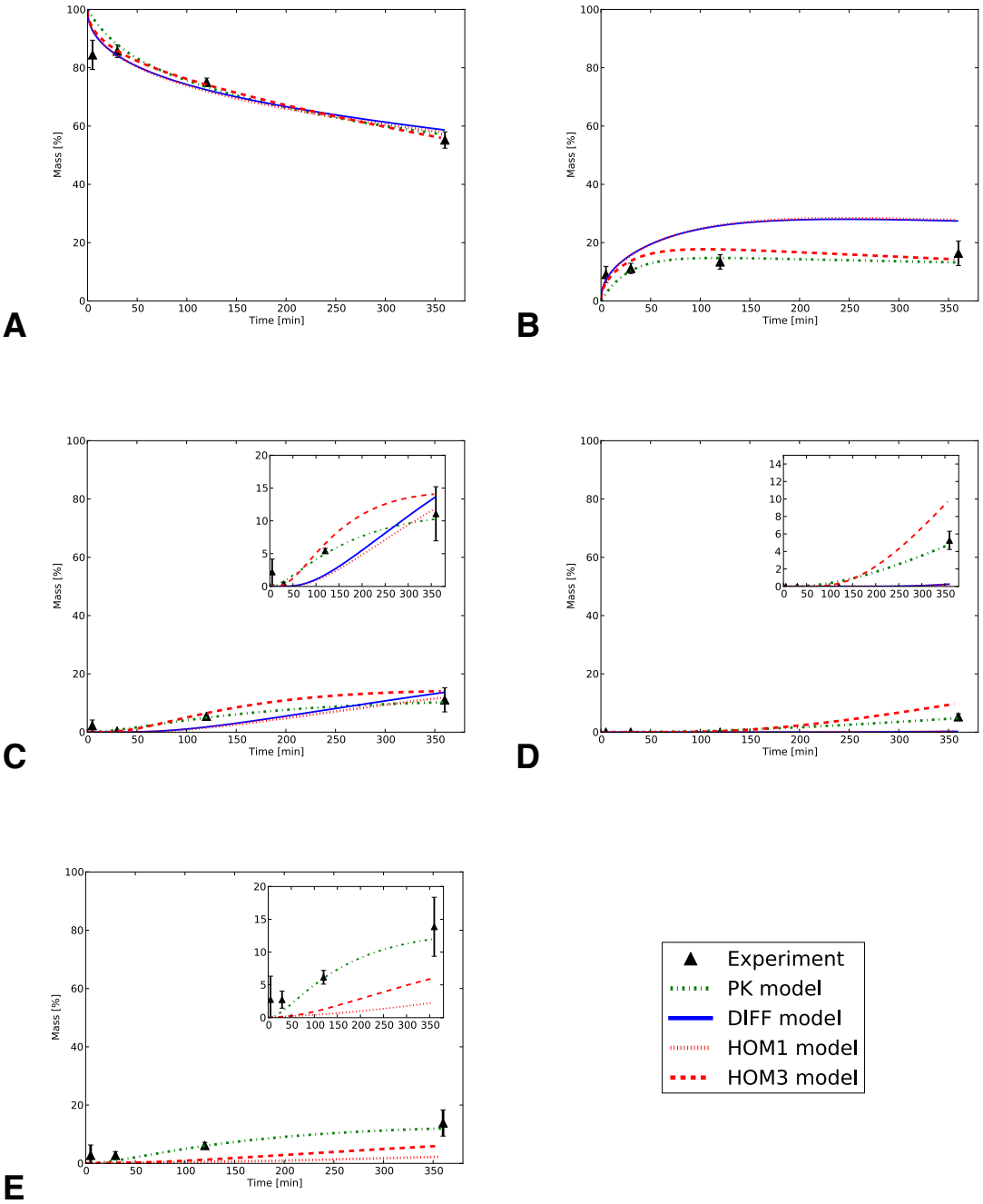

Figure 4-8 CAF (12.5 mg/ml) mass profiles over time: experimental data, PK fitting, detailed diffusion simulation and homogenized diffusion models. A: Mass profile of the Donor compartment. B: Mass profile of the SC compartment. C: Mass profile of the DSL compartment. D: Mass profile of the Acceptor compartment (diffusion model with mass leaving the system). E: Mass profile of the lateral compartment (diffusion model data not available).

In the 1 mg/ml CAF experiments, the drug in the donor did not decrease as fast as for FFA. After 5 min, still more than 85% of the initial dose could be found, decreasing slowly and reaching around 60% remaining on the skin after 6 h (Figure 4-7 A). At the last measuring time point (12 h), still more than 40% of the drug was found in the donor.

In the SC, a plateau at around 25% was reached after 2 h and maintained until 6 h, then slowly increasing to around 35% at the end of incubation after 12 h (Figure 4-7 B).

The amount of drug in the DSL remained very low until 6 h due to values close to the lower limit of quantification and then increased to around 10% at 12 h (Figure 4-7 C). Only after the longest incubation at 12 h, CAF was found in the acceptor (Figure 4-7 D).

However, the variation was quite high due to concentration values close to the LLOQ. The CAF amount in the lateral compartment slowly increased, reaching around 10% of the applied dose after 12 h incubation (Figure 4-7 E).
For the 12.5 mg/ml experiments, the course of relative drug amount in the donor was similar to the 1 mg/ml data (Figure 4-8 A). In the SC, a plateau was reached very fast between 10% and 15% and maintained until 6 h after application (Figure 4-8 B). The amount of CAF in the DSL increased slowly, reaching around 10% after 6 h (Figure 4-8 C). After 6 h incubation, around 5% of the applied CAF was found in the acceptor phase (Figure 4-8 D). No CAF was found at earlier time points. In the lateral compartment the CAF amount increased to around 15% after 6 h (Figure 4-8 E).

For the 12.5 mg/ml and 1 mg/ml CAF data differences in relative amount in the SC (Figure 4-7 B and Figure 4-8 B) and DSL (Figure 4-7 C and Figure 4-8 C) were observed. 6 hours after application SC levels at 1mg/ml were approximately 1.5 times the relative amount of the 12.5 mg/ml experiments and DSL levels at 12.5 mg/ml approximately 6 times the relative amount of the 1 mg/ml experiments. The donor depleted roughly 10 percent faster in the 1 mg/ml CAF experiments.

4.4.2 Results for different models

The outcome of all three models for FFA and CAF is depicted in Figure 4-6 to Figure 4-8. A summary of standard deviations for all models is additionally provided in Table 4-2 B. The deviations of the objective are found to be reasonably small in all cases.

The DIFF and HOM models slightly overpredict the amount in the SC for the 12.5 mg/ml CAF experiments and slightly overpredict the amount in the DSL for the 1mg/ml CAF experiments. For the PK model the rate constants found by regression and the corresponding standard errors are reported in Table A-2. For FFA it was obviously not possible to fit the efflux rate constant k_7, which was thus set to zero. The optimized diffusivities for the HOM1 model are shown in Table A-1 A. The optimized parameters for the HOM3 model, indicated by a *, are listed in Table A-1 B. The corresponding regression coefficients are reported in Tables A-3 A and A-3 B respectively.

Table 4-2 Overview of models features and comparison of goodness of fit.

	PK	HOM(3)	HOM(1)	DIFF
A **General information**				
Primary Purpose	Fit			Prediction
Type of input parameters	Rate constants	Diffusion and partition coeff.	Diffusion and partition coeff.	Diffusion and partition coeff.
Number of input parameters	6 for FFA/ 7 for CAF	6 +geometry	6 +geometry	7 + geometry
Number of regression parameters	6 for FFA/ 7 for CAF	3	1	none
Time dependence	yes	yes	yes	yes
Spatial resolution	No, only compartment	intermediate	intermediate	Up to cellular structures
Lateral compartment	modeled	separate for SC and DSL	separate for SC and DSL	not modeled
Computational cost	Low	intermediate	intermediate	High
B **Regression results** **Standard deviation and number of independent variables (in parentheses)**				
FFA	4.82 (24)	5.23 (27)	6.61 (29)	8.47 (24)*
CAF (1mg/ml)	3.26 (13)	4.32 (17)	5.03 (19)	5.76 (16)*
CAF (12.5 mg/ml)	3.56 (13)	3.99 (17)	5.94 (19)	5.27 (16)*

4.5 Discussion

Based on the experimental design and the anatomical conditions, we investigated mass balance profiles for *in-vitro* finite dose skin diffusion experiments. Full thickness skin was separated and analysed in different compartments (Donor, SC, DSL, lateral compartment, Acceptor) for two substances in aqueous solution: FFA (1 mg/ml) and CAF (1 mg/ml and 12.5 mg/ml).

This experimental setup was then represented in different mathematical models.

4.5.1 Data correction and validation of the stretching factor

By scaling of the experimental data the drug amount in the lateral skin parts decreased and in the SC+DSL compartments it increased. Experiments with unstretched skin resulted in similar drug amounts in the SC+DSL and in the lateral skin compartments as the scaled experimental data set (Figure 4-9).

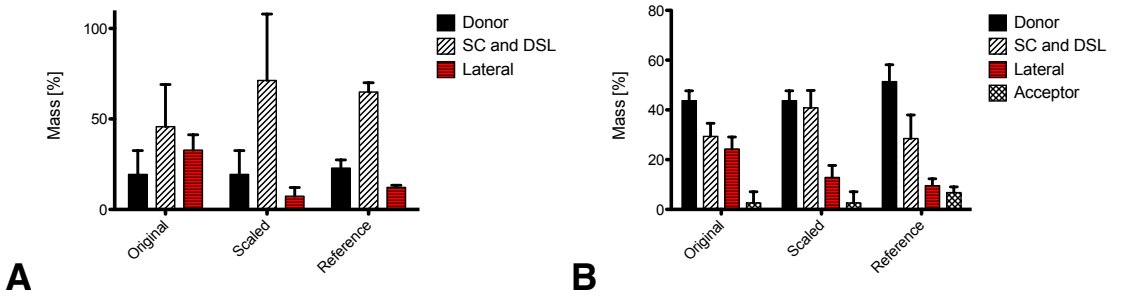

Figure 4-9 Relative drug amount recovered from the different compartments. Donor: Formulation recovered from the skin surface and surface of donor compartment. SC and DSL: skin punch of incubated area. Lateral: Skin outside of the incubated area. Acceptor: drug in acceptor compartment. Original: data from tape-stripping experiments. Scaled: data from tape-stripping experiments scaled with stretching factor. Reference: data from experiments without stretching. A: FFA 1 mg/ml: n=5. B: CAF 1 mg/ml: n=4

No significant differences (t-test, $p > 0.05$) could be found between the scaled experimental data and the data obtained from the experiments with unstretched skin (Reference) both for FFA and CAF. The difference between Reference and Original in the lateral part was significant for both drugs. This showed that estimation of a

stretching term is a suitable method to correct the experimental data for the conditions during incubation and tape-stripping for this setup

4.5.2 Experimental data

Experimental mass profiles for FFA show clearly a finite dose behavior with a strong depletion of the donor and a depletion of mass in the SC after reaching a plateau in the course of the experiment (Figure 4-6 A,B). In contrast, CAF experiments show more infinite dose-like properties with a significantly slower depletion of the donor and a constant mass plateau in the SC over sample time (Figure 4-7 A,B and Figure 4-8 A,B). This is in agreement with experiments from the infinite dose scenario, showing a slower penetration of CAF in comparison to FFA [81]. Mass profiles of CAF in the SC are clearly different for the different concentrations: For CAF at 1 mg/ml around 25 to 35% of the drug can be found in the SC, whereas for the higher concentration at 12.5 mg/ml the values reach only up to 15%. One explanation for the different profiles is a saturation effect in the SC, allowing only a certain CAF amount to be taken up by the SC, e.g. reversible protein binding to keratin. Binding in SC was shown recently for theophylline, which has a very similar structure to CAF [58, 98, 150].

This effect has consequences for the amount of substance in the DSL over time, showing a much higher amount for 12.5 mg/ml (11%) in comparison to 1 mg/ml (2%) after 6 h of incubation. Surprisingly, for both concentrations nearly the same relative amount was found in the lateral compartment.

4.5.3 Drug transport to the lateral parts

Speaking of the lateral skin parts, a high amount of drug can be found (e.g. more than 10% for CAF at 12.5 mg/ml after 6 h of incubation, Figure 4-8 E). Thus, there is evidence not to elide the lateral parts in the modeling during finite dose skin absorption studies. Most studies investigating finite dose experiments do not discuss the lateral drug amount found in their studies but lateral diffusion of e.g. benzyl alcohol into the clamped parts of the diffusion cell has been assumed previously [151]. In agreement with results from Gee et al. [137], which determined the lateral

transport of CAF, hydrocortisone, and ibuprofen, the lipophilic FFA exhibited a lower tendency to move laterally than the hydrophilic CAF. From microscopic pictures (Figure 4-10) taken both from untreated skin and from skin squeezed in a FD-C for 20 h, no significant difference was found for the SC thickness (p=0.218). The dermis, however, appeared much denser than before. The geometry and physiology of the skin is clearly changed and it is assumed that this altered configuration may reduce the possibility of using measured diffusivity and partition behavior from fully hydrated skin experiments.

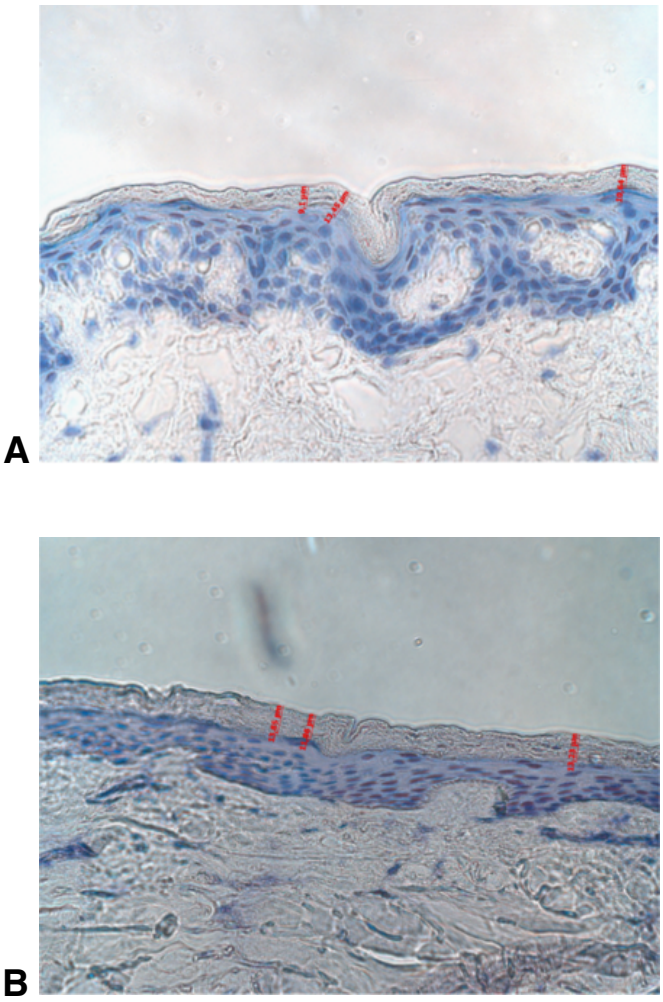

Figure 4-10 Cross sections of skin biopsies from untreated skin (A), and from the lateral, compressed part of a skin sample squeezed in a Franz diffusion cell during incubation with buffer for 20 h (B). Stained with haematoxylin. Magnification is 200 x.

4.5.4 Model comparison and evaluation

With the PK, DIFF and HOM models this study employed three different computational models serving very different purposes to describe and predict the experimental setup.

In contrast to Seta and coworkers [84], the experimental resolution of the epidermis is divided in lipophilic (SC) and hydrophilic parts (viable epidermis), which is more reasonable from a physiological point of view in our opinion. The same holds true for the works by Kasting and coworkers [78, 151] which focused on volatile compounds and thus did only supply mass balance information about skin as a whole tissue [140, 152] and, in a further study, about epidermis and dermis [153]. For the modeling part, the aforementioned works belong to the class of one-dimensional diffusion models, e.g., [76], [86, 154, 155], [128]. The primary focus in these works was on absorption, i.e., mass accumulation in the acceptor, however. None of the above cited models do consider lateral diffusion to parts of the skin outside the incubated application area.

To explain the mass transport between different compartments and to evaluate this influence of the lateral compartment further, an easy to use extended pharmacokinetic model (PK) was constructed. In this approach the whole experimental setup is described in terms of compartments. Interestingly enough, the class of PK models recently gained some attention again: The work by Davies and coworkers [89], e.g., showed to be efficient with two skin compartments already. Overview articles relating to one or two compartment PK models can be found in the literature [83, 90, 91]. PK models using first-order rate constants were typically used to monitor the *in-vivo* situation [85, 86] and a lot of effort was spent trying to relate rate constants to physicochemical properties of the diffusant and to fit a model to plasma-level curves or *in-vitro* permeation profiles [87, 88]. In contrast to the previous mentioned work, a lateral compartment was added to fully describe the experimental setting.

Although, when compared to the DIFF model, this approach does only provide a very limited spatial resolution, the model features a low computational complexity. In order to provide additional insight of all effects occurring during incubation, model parameters were determined by parameter fitting with respect to the experi-

mental data. To reduce the number of constants an averaged transport (rate constants k_5 and k_6) between SC and lateral compartment as well as between DSL and lateral compartment, was assumed. Unsurprisingly this yields excellent agreement to the experimental data. For the CAF experiments the ratio of rate constants k_3 and k_4 (SC and DSL) and k_5 and k_6 (SC/DSL and lateral compartment) are in agreement with the experimental findings, showing a faster transport from the SC to the DSL for the 12.5 mg/ml experiments and a faster transport from the SC/DSL to the lateral compartment for the 1 mg/ml experiments.

After successful description of the experimental setup a detailed diffusion model (DIFF) driven by input parameters gathered from infinite dose experiments was applied. It has been shown, that this is reasonable even for finite dose kinetics [30, 84], whereas estimation from finite dose experiments may show great intra-individual variability [155]. In contrast to one-dimensional models cited above, the work at hand relies on a microscopic two-dimensional geometry. This model is thus meant to be predictive, as all parameters are in principle directly related to physicochemical properties of the substance.

An out of the box use of the DIFF model provided good predictions of the mass profiles in each compartment for both drugs over the incubation times of 6 h or 12 h: While the agreements with the experiment are excellent for FFA, some minor differences are found for CAF. At low donor CAF concentration, e.g., the model produces an overestimate of DSL concentration, whereas at high donor CAF concentration, an overestimate of SC concentration is obtained. Due to the differing experimental results, this finding could be expected. Explanations for the overestimation could be lateral diffusion in the DSL and a saturation effect in the SC. Furthermore, some minor differences in the acceptor compartment can easily be explained by analytical reasons, e.g. concentration below the LLOQ.

The general drawback of the model is however the absence of a lateral compartment. As explained above, this is due to the very high resolution. Also note, that although a parameter optimization is possible in principle, it was not applied here, because of the high computational complexity.

As some authors suggest, high resolution PK models, e.g., [30], provide an improved spatial resolution in z-direction. In this case, each compartment represents a single layer of tissue in SC and DSL respectively. As this corresponds to a set of discretized partial differential equations, we pursue a different approach with the class of HOM models.

The homogenized HOM models serve as a compromise between the previously mentioned models: In contrast to the DIFF model the cells in the SC membrane are not resolved in full detail, but sophisticatedly represented in an averaged (homogenized) way. This allows representing a diffusion cell with realistic dimensions on a 1 cm scale (cf. Figure 4-4). Like in the PK model it is thus possible to study the influence of lateral diffusion with the HOM models as well. In addition, these models inherit the desirable features of prediction and interpretation of parameters from the DIFF model. Note however, that the yet unknown variation in physiology and the involved alteration of the diffusion and partition parameters at the boundary to the lateral compartment were not included in the computational model.

Due to the reduced computational complexity of the HOM models, these models are also suitable for optimization of parameters on a reasonable computational timescale. When it comes to accuracy, not surprisingly, the HOM models range between the PK model, which was optimized by parameter fitting, and the DIFF model, which has a predictive character. The HOM1 model being optimized based on a single parameter produces slightly weaker results than the HOM3 model, which is obtained by optimizing three parameters. As indicated in Table A-1, the absolute values of the corresponding diffusion and partition coefficients are quite comparable between both models however.

The apparent diffusion coefficients in transversal direction, $D_{SC,zz}$, is three orders of magnitude smaller than the coefficients for lipid diffusion D_{LIP}. For CAF, the resulting values for $D_{SC,zz}$ are in the range reported in [81]. Similarly, the lateral coefficients $D_{SC,rr}$ are one order of magnitude smaller than D_{LIP}. For the interpretation of D_{DSL} it is important that this value may be afflicted with some error, as a constant thickness of 3 mm was assumed.

As shown in Equation 4-6, the SC diffusion coefficients $D_{SC,zz}$ and $D_{SC,rr}$ are coupled. This has another important consequence for the interpretation of the contribution of lateral diffusion. In particular when considering CAF at 1 mg/ml, overshooting occurs for the amount in DSL (Figure 4-7 C), whereas undershooting occurs for the amount in LAT (Figure 4-7 E). Less pronounced, the same phenomenon also occurs for CAF at 12.5 mg/ml (Figure 4-8 C and Figure 4-8 E).

Thus, it is not possible to accelerate diffusion into the lateral part of the SC and to slow down diffusion into the DSL at the same time. Controversially, for the PK model, an appropriate choice of rate constants k_5 and k_6 may have a compensating effect. This completely allows for reflecting the experimentally observed lateral diffusion. In contrast to the PK model, both HOM models distinguish between the lateral part of the SC and of the DSL compartment. More precisely, both HOM models indeed support the hypothesis that lateral diffusion in the SC is subordinate and mainly occurs in the DSL (Figure 4-11 A-C). Due to the larger cross-sectional area of the DSL compared to the SC this seems reasonable.

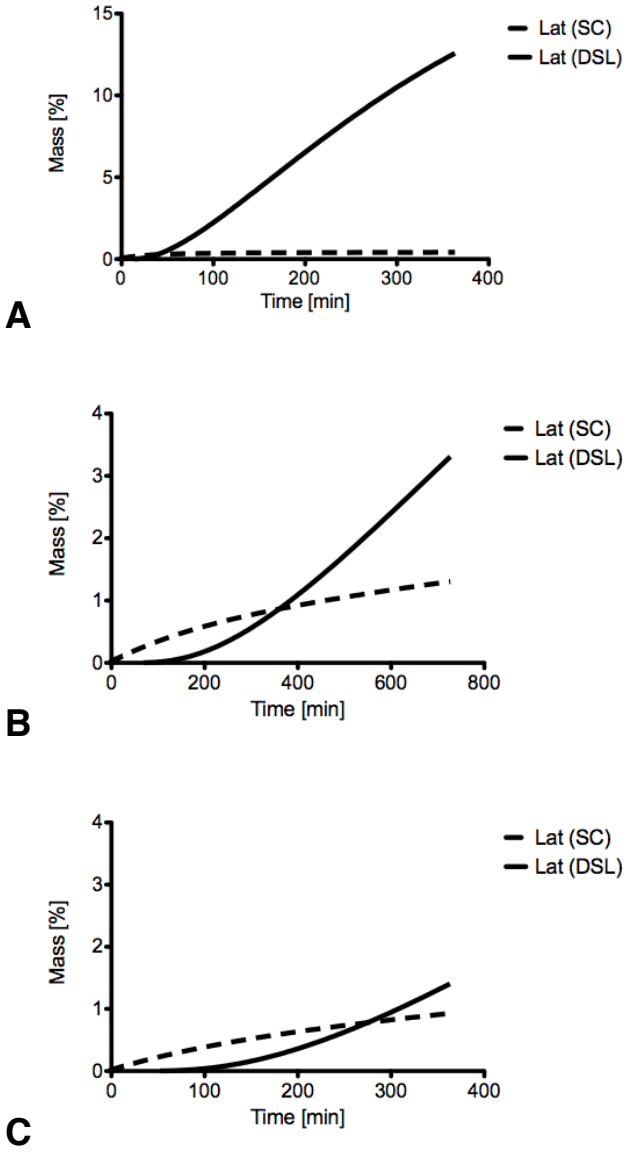

Figure 4-11 Homogenized modeling of FFA (1 mg/ml) (A), CAF (1 mg/ml) (B) and CAF (12.5 mg/ml) (C) mass profiles over time. Relative mass distribution inside the lateral compartments of SC and DSL

4.6 Conclusion

With the help of the presented mathematical models the experimental setup of finite dose skin absorption experiments in a Franz diffusion cell can be thoroughly investigated. All models explain and, to a certain extent, also predict the experimental data. *In-vitro* mass transport to the lateral parts for the transient case should be considered to get optimal recovery experimentally and proper mass balance for mathematical models.

The PK model is suitable for describing the whole setup and gives information about the diffusion process also into the lateral skin parts. It includes some structural information, but is primarily based on fitted parameters (rate constants) that are difficult to interpret. This approach may expand the knowledge about the whole absorption process in a Franz diffusion cell.

Reflecting a different philosophy, the detailed diffusion model predicts the diffusion of FFA and CAF into the different skin compartments in a finite dose setup reasonably. It is a transfer of an infinite dose model to the finite dose scenario and does not rely on fitted parameters. Due to the computational complexity it currently does not include a lateral compartment however.

In between the homogenized diffusion model has the advantage of describing the experimental setup more accurately while keeping the advantages of a diffusion model except for domain separation in the SC (corneocytes and lipid channel). Thus, simulation of the drug transport into the different compartments including the lateral part is possible.

5 A strategy for *in-silico* prediction of skin absorption in man

Parts of this chapter have been submitted as an original research article:

Selzer, D., Neumann, D., Wagner, H., Kostka, K. H., Lehr, C.-M., Schaefer, U. F. (2013). A Strategy for *In-Silico* Prediction of Skin Absorption in Man. *J Control Release* (submitted)

The author of the thesis made the following contributions to the publication:

Developed the mathematical model. Performed all calculations and interpreted all experiments. Wrote the manuscript.

Heike Wagner performed the experiments.

5.1 Abstract

Some for time, *in-silico* models to address substance transport into and through the skin are gaining more and more importance in different fields of science and industry. Especially, the mathematical prediction of *in-vivo* skin absorption is of great interest to overcome ethical and economical issues.

The presented work outlines a strategy to address this problem and in particular, investigates *in-vitro* and *in-vivo* skin penetration experiments of the model compound flufenamic acid solved in an ointment by means of a mathematical model. Experimental *stratum corneum* concentration-depth profiles (SC-CDP) for various time intervals using two different *in-vitro* systems (Franz diffusion cell, Saarbruecken penetration model) were examined and simulated with the help of a highly optimized three compartment numerical diffusion model and compared to findings of SC-CDPs of the *in-vivo* scenario.

Fitted model input parameters (diffusion coefficient and partition coefficient with respect to the *stratum corneum*) for the *in-vitro* infinite dose case could be used to predict in-use conditions *in-vitro*. Despite apparent differences in calculated partition coefficients between *in-vivo* and *in-vitro* studies, prediction of *in-vivo* scenarios from input parameters calculated from the *in-vitro* case yielded reasonable results.

5.2 Introduction

The importance of substance transport into and trough the skin has grown consistently in different fields of science and industry over the past decade. Not only pharmaceutical applications for the local or systemic administration of drugs or applications in the cosmetic industries rely on carefully investigations of the underlying transport kinetics, especially regulation authorities such as REACH (Regulation, Evaluation, Authorization and Restriction of Chemicals) [21] request information about characteristics of potential harmful xenobiotic exposure to the human skin [156, 157].

In-vivo experiments in the field of skin absorption are considered the gold standard but are difficult to perform and evaluate due to the complexity of processes involved and obviously face ethical concerns [19, 20]. Hence, experiments with regard to *in-vitro* test systems are used frequently to overcome these issues [22, 23, 158]. In the past, it has been shown repeatedly that these test systems are capable of mimicking the *in-vivo* situation reasonably [38, 44, 134]. Many investigations on dermal research were performed under infinite dose conditions, which were done by applying a sufficiently large amount of the test formulation to the surface of the skin, so that neither the drug nor any of the vehicular components were appreciably reduced during the course of the experiment. The advantage of this procedure is that a very reproducible way of application can be performed, quasi steady-state conditions might be reached in the *stratum corneum* (SC) [159] and effects caused by rubbing are avoided. On the other hand, this procedure is very distant from in-use applications, where typically small amounts of drug preparation are applied on a relatively large area of the skin by massaging.

Until now, abundant information about drug distribution within the skin are available concerning infinite dosing. In contrast, the amount of data for finite dosing is rather limited [160], and much sparser, if experiments with semisolid drug preparations and other objectives than permeation data are of interest.

Based on available data [161] it was decided to carry out a study gathering input parameters (SC diffusivity and partition coefficient) with respect to a mathematical model based on experimental results of two different *in-vitro* test systems, the Saar-

bruecken penetration model (SB-M) and the Franz diffusion cell (FD-C), using the tape stripping technique [39]. With the help of an *in-silico* model these input parameters were used to predict the situation *in-vivo*. Experimental data was examined under infinite dose and finite dose conditions for the aforementioned test systems and *in-vivo* studies. Finite dosing was carried out on the basis of different guidance documents, which state that finite dosing is given when the amount of ointment applied to the skin is between 1-10 mg/cm [54-56]. Consequently, infinite dose conditions were implemented by application of more than 10 mg/cm of formulation. These procedures were performed with a semisolid drug preparation.

For some time past, mathematical models predicting skin absorption are considered alternatives to experimental investigations by different regulatory agencies [162-164]. For complex mechanistic models it could be shown that *in-vitro* infinite and finite dose concentration-depth profiles could be predicted reasonably but require a complex set of input parameters [81, 82, 125]. In contrast, in this work a sparse parameter one-dimensional diffusion model was used to not only investigate and predict the *in-vitro* situation but to predict the *in-vivo* situation with help of *in-vitro* based model input parameters as well. For this purpose, the underlying diffusion equation was solved numerically. First of all, the model was fitted to *in-vitro* concentration-depth profiles to obtain information about diffusivity and partition coefficient with respect to the SC. Subsequently, *in-vitro* infinite dose fitting results were used to predict the *in-vitro* finite dose scenario as conducted successfully before for aqueous formulations [82, 165]. Finally, *in-vivo* concentration-depth profiles for the finite and infinite dose case were predicted from data obtained from *in-vitro* studies. A schematic overview about the used strategy is provided in Figure 5-1.

Predictions for the *in-vitro* finite dose setup as well as predictions of *in-vivo* scenarios showed promising results. A positive outcome of the presented study should not only give a better hint on the theory of the drug's diffusion into the SC but most likely be a starting point to reduce experimental work *in-vitro* and *in-vivo*. It will therefore reduce costs and time within the development of semisolid drug formulations and other dermally applied formulations.

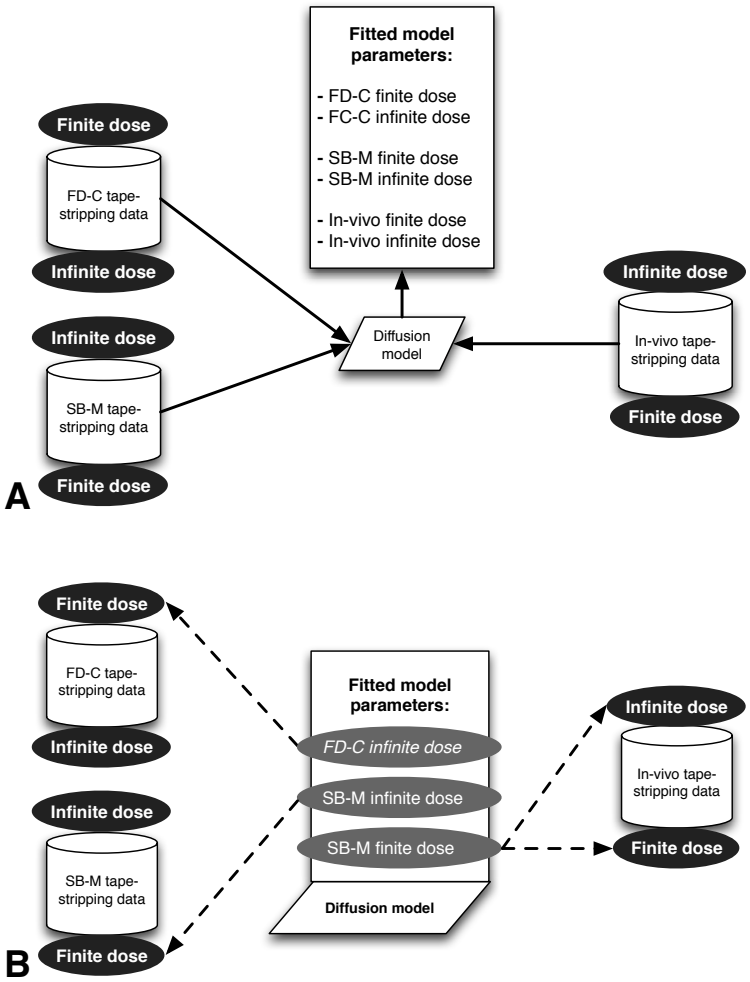

Figure 5-1 Two-step strategy to analyze and predict *in-vivo* and *in-vitro* concentration-depth profiles. First, model input parameters (partition coefficient and diffusion coefficient) were fitted to experimental data (A). In a second step, the *in-vitro* finite dose scenario is predicted by using model input parameters taken from *in-vitro* infinite dose fittings (first step). Furthermore, the *in-vivo* setup is predicted from fitted *in-vitro* model input parameters (first step).

5.3 Materials and methods

The following materials and equipment were used: Flufenamic acid (Kali-Chemie Pharma, Hannover, D); wool alcohols ointment and Multifilm kristall-klar (Beiersdorf, Hamburg, D); Ringer solution, McIlvaine citric acid-phosphate buffer pH 2.2, NaOH (Merck, Darmstadt, D); Plastibase® (Heyden GmbH, Muenchen, D); methanol (Baker, Deventer, NL); Franz diffusion cells type 4G-01-00-20-15, area = 3.142 cm^2 , acceptor volume = 15 ml (PermeGear, Riegelsville, PA, USA) teflon filter Minisart - pore size 0.2 μm (Sartorius, Goettingen, D); isocratic HPLC consisting of a 655 A 40 autosampler, L 4250 detector, L 6220 pump, 6000 K data interface and 5 μm LiChrospher® 100 / RP-18 column / 12.5 cm x 4 mm (Merck-Hitachi, Darmstadt, D); Dialysis membrane, cut off 10,000 (Dianorm GmbH, Munich, Germany); Cellulose membrane, cut off 10,000 (Medicell International LTD, London, GB).

The non-steroidal drug flufenamic acid (FFA), solved in a concentration of 0.9% in wool alcohols ointment (German Pharmacopoeia 1999), was used as drug preparation under infinite and finite dose conditions. Prior to the application, the drug preparation was stored at 32°C for one week to allow complete dissolution of the drug in the ointment base. This was checked by light microscopic investigations.

5.3.1 Skin samples for *in-vitro* experiments

Skin samples were taken from Caucasian female donors undergoing abdominal surgery with the approval of the ethic committee of the Caritas-Hospital Lebach, Germany. Immediately after excision the subcutaneous fatty tissue was removed using a scalpel. The skin was cut into 10 x 10 cm pieces, wrapped in aluminium foil and stored in polyethylene bags at -26°C until use. The maximum storage time was three months.

5.3.2 Saarbruecken penetration model (SB-M) experiments

Details of the experiments are given in [161]. Briefly, for infinite dosing an ointment layer of at least 2 mm was applied whereas for finite dosing 4-6 mg ointment per cm^2 was evenly spread on the skin surface. All experiments were carried out at a

skin surface temperature of 32 ± 1°C for different time intervals (0.5, 1, 3 and 6 hours) at occlusive conditions.

5.3.3 Franz diffusion cell (FD-C) experiments

Details of the experiments are given in [161]. In short, application of the ointment was conducted similar to the procedure described previously (SB-M). As receptor fluid Soerensen phosphate buffer pH 7.4 was used and mixed with a magnetic stirring bar at 500 rpm. The skin specimen was prehydrated for 30 minutes prior to the application of the formulation. All experiments were carried out as described in the previous section (SB-M).

5.3.4 Horizontal segmentation of the *stratum corneum* (SC)

To compare the results of both models, the skin was always treated in exactly the same manner at the end of all experiments [38]. First, the remaining ointment was removed by wiping the skin with cotton. Second, the skin was successively stripped with 20 pieces of adhesive tape. In a standardized procedure (pressure: 2 kg for 10 sec), tapes were removed rapidly and combined in 6 pools of 1, 1, 3, 4, 5 and 6 strips for analytical purposes. Due to this procedure, each of the removed cell layers had nearly the same thickness, which had been shown in previous studies in different laboratories [33, 166, 167]. The first tape strip was always discarded because of potential contamination.

5.3.5 *In-vivo* experiments

6 human volunteers (3 male, 3 female), aged 23 - 29 years, from whom informed consent was obtained, participated in the study [38]. They were in good health and had no history of any dermatological disease.

A template of Fixomull® with 4 holes was fixed on the volar left and right forearm of each volunteer. Each hole released an area of 15 mm in diameter and represented one experimental area. The drug preparation was applied according to the *in-vitro* experiments. The administration areas were not covered during the incubation time

(0.25, 0.5, 1 and 3 h), but the volunteers were asked to reduce their movements to avoid any loss of drug preparation.

The tape-stripping procedure was performed by exerting the pressure just with the forefinger. To increase reproducibility, the procedure was carried out by the same person according to the AAPS/FDA Workshop report [34] and the Guidance for Industry [168].

5.3.6 *In-vitro* release experiments

The release of FFA from the ointment was examined for different concentrations (0.225%, 0.45%, 0.675% and 0.9%) using an infinite dose setup (approximately 0.3 g of applied formulation). For that reason, by means of a FD-C setup, released mass over time across a dialysis membrane (0-6 h, 5 time points) and cellulose membrane (0-53 h, 11-18 time points) was determined, respectively.

5.3.7 Assay method and HPLC-procedure

For a detailed description of the extraction procedure and the HPLC analysis [detection limit 20 ng/ml] see Wagner et al. [38]. The linearity of the HPLC method was checked over a quantification range from 50 to 10,000 ng/ml, providing a good linearity between the area of the UV-absorption peak and the respective concentration with r = 0.999 and an accuracy of 97.8 ± 3.8%.

5.3.8 Determination of diffusivity of FFA in the ointment

As stated before, the release of FFA for different concentrations (0.225%, 0.45%, 0.675% and 0.9%) was examined using a dialysis membrane and a cellulose membrane. To estimate diffusivity D of FFA inside the vehicle the amount released per area Q over time t for initial concentration C_0 (assuming a uniform distribution of FFA within the ointment at t=0) was fitted for every single experiment using a non-linear least squares approach (Equation 5-1) [169].

$$Q = 2C_0\left(\frac{Dt}{\pi}\right)^{\frac{1}{2}} \qquad \text{Equation 5-1}$$

Since equation 1 only holds true for a loss of initial concentration of approximately up to 30% over time, the general solution (Equation 5-2) with thickness of applied ointment layer h (h=2mm) was applied to analyze the impact of a potential loss of initial concentration and ensure valid results with respect to the diffusion coefficient [169].

$$Q = hC_0\left[1 - \frac{8}{\pi^2}\sum_{m=0}^{\infty}\frac{1}{(2m+1)^2}e^{\left(-\frac{D(2m+1)^2\pi^2 t}{4h^2}\right)}\right] \qquad \text{Equation 5-2}$$

Here, the underlying infinite sum was calculated until maximum possible machine accuracy was reached (comparison to the machine epsilon) [125] .

5.3.9 Diffusion model

The diffusion of FFA from the ointment through the *SC* was simulated using a one-dimensional diffusion model. Three compartments (vehicle, *SC*, deeper skin layers) were implemented to address different diffusion kinetics of the heterogeneous system for the *in-vitro* and *in-vivo* scenario. For every compartment a set of diffusion coefficients and partition coefficients with respect to adjacent compartments was assigned. The underlying diffusion equation (Equation 5-3) was solved numerically using an implicit Crank-Nicolson finite differences solver [63].

$$\frac{\delta c(x,t)}{\delta t} = \frac{\delta}{\delta x}\left(D\frac{\delta}{\delta x}c(x,t)\right) \qquad \text{Equation 5-3}$$

Phase transitions were modeled in two steps. First the change of diffusivity at compartment boundaries was addressed by decomposing the Crank-Nicolson scheme into in- and outgoing fluxes and by a subsequent substitution of every diffusion coefficient in the Crank-Nicolson scheme for a given cell (position in the discretized spatial domain) with the harmonic mean of the diffusion coefficients of its adjacent cells according to work of Seta et al. (Equation 5 in [84]). Partitioning was incorporated into the Crank-Nicolson scheme by reducing back diffusion (multiplication of assigned diffusivity in a cell with partition coefficient K) for the direction of a "negative jump" (K < 1).

A sufficient spatial resolution at phase transitions is crucial to achieve stable and reasonable results in simulation but can largely slow down the speed of computation. To overcome this problem while gaining maximum speed of computations a non-uniform grid approach according to [170] was applied. Here, a base space step size of 1 μm was used within every compartment. Towards phase transitions the step size was exponentially decreased to at least 1/10 μm. A test grid simulating a heterogeneous system with a change in diffusivity is depicted in Figure 5-2. Dirichlet boundary conditions and reflecting boundary conditions were implemented to model infinite dosing and finite dosing, respectively.

At the start of the calculation, the concentration in the donor was set to the concentration of the drug in the ointment base as employed in the experiment. The concentration in all other elements was zero.

As basis for calculations of infinite dosing the following assumptions were made: The thickness of the SC was assumed to be 15 μm for *in-vitro* simulations and 17 μm for *in-vivo* simulations that matches the findings from the tape-stripping procedure. The thickness of the deeper skin layers was assumed to be 2000 μm.

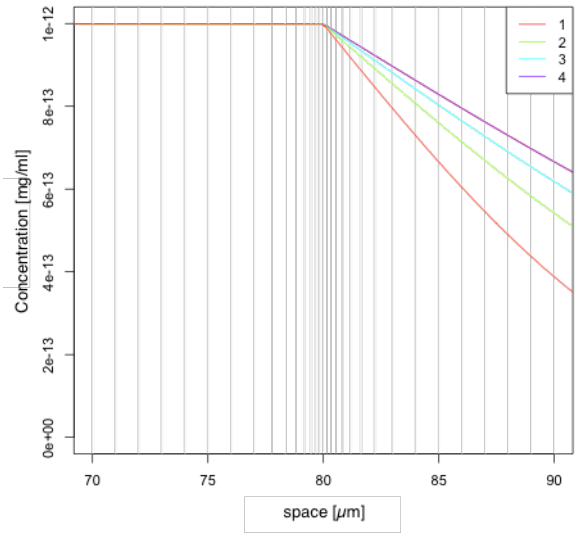

Figure 5-2 Test simulation for different times (1 h, 2h, 3h, 4h) given a heterogeneous system with a change of diffusivity at 80 μm using a non-uniform grid. Grey vertical lines denote to the one-dimensional grid and resolution increases exponentially towards the compartment boundary at 80 μm.

The thickness of the donor was calculated from the amount of ointment base applied and the specific density of the ointment base (= 0.836 g/cm). While the donor could be depleted of the drug, the tissue following the deeper skin layers was assumed to be a perfect sink (the concentration at the end of the deeper skin layers was always zero).

5.3.10 Model input parameters, fitting and prediction

Determination of diffusivity in the ointment was performed as mentioned previously. Diffusivity in the deeper skin layers was computed as the harmonic mean of values taken from the literature [125, 165] (D_{DSL} = 8166.67 $\mu m^2/h$). Partition coefficient $K_{SC/DSL}$ was taken from [165] ($K_{SC/DSL}$ = 4.36).

$K_{SC/Vehicle}$ (henceforth referred to as K_{SC}) and D_{SC} were fitted using a non-linear least squares approach according to the following protocol:

1. The concentration-depth profiles for every time point were fitted separately (approach 1).
2. The total set of concentration-depth profiles for all times was fitted in one step (approach 2).

This procedure was applied to infinite and finite dose data from FD-C and SB-M systems separately. For the *in-vivo* scenario, only approach 2 was applied.

After comparison of the findings, in a first step the kinetic parameters from the *in-vitro* infinite dose case were used to predict the *in-vitro* finite dose scenario – a procedure that could be successfully applied before with the help of complex 2D diffusion models for the simulation of drug release from an aqueous formulation [82, 165].

In a second step the potential to predict the *in-vivo* scenario from parameters fitted from the *in-vitro* case was examined.

5.3.11 Software and programming

The diffusion model was implemented in C++ and compiled using the Apple LLVM version 5.0. Fitting was performed with the R programming language version 2.15.1 [171]. For statistical evaluation GraphPad Prism version 6.0 for Macintosh (GraphPad Software, La Jolla, California, USA) was used.

5.4 Results

5.4.1 Estimation of ointment diffusivity of FFA

Distribution of fitting results (Figure 5-3) of the diffusion coefficient of FFA in the ointment released over two different membrane systems (dialysis membrane and cellulose membrane) showed significant differences between the two groups (dialysis vs. cellulose membrane) with p=0.02 (Wilcoxon-Mann-Whitney test).

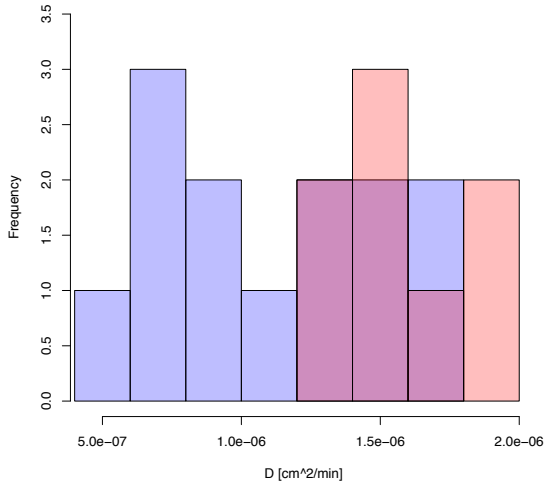

Figure 5-3 Distribution of FFA diffusivity in the ointment determined by fittings to data from release experiments over a dialysis membrane (red bars) and a cellulose membrane (blue bars).

All single fits could be considered highly significant ($p < 0.01$). In comparison to results from the cellulose membrane, release over the dialysis membrane is accelerated by a factor of approximately 1.6.

Since variation of vehicle diffusivity in the given range did not alter concentration-depth profiles of the SC significantly for various test simulations (e.g. maximum differences in concentration of < 0.01% for late times in the more error prone finite dose scenario), for the subsequent simulations the harmonic mean of all estimated diffusion coefficients with $D_{Vehicle} = 6583.19\ \mu m^2/h$ was used as a model input parameter.

5.4.2 Fitting of *in-vitro* infinite dose profiles

Experimental results for both FD-C and SB-M showed a characteristic jump in concentration at the Vehicle/SC boundary given a vehicle initial concentration of 7.55 mg/ml (Figure 5-4). Here, concentrations in the upper segment of the SC are slightly higher for the SB-M setup in comparison to the FD-C. Both sets of experiments approach towards steady state, whereas SB-M experiments tend to reach steady-state slower. Average relative standard deviation of experimental data is slightly higher for the FD-C setup (45%) in comparison to the SB-M (38%).

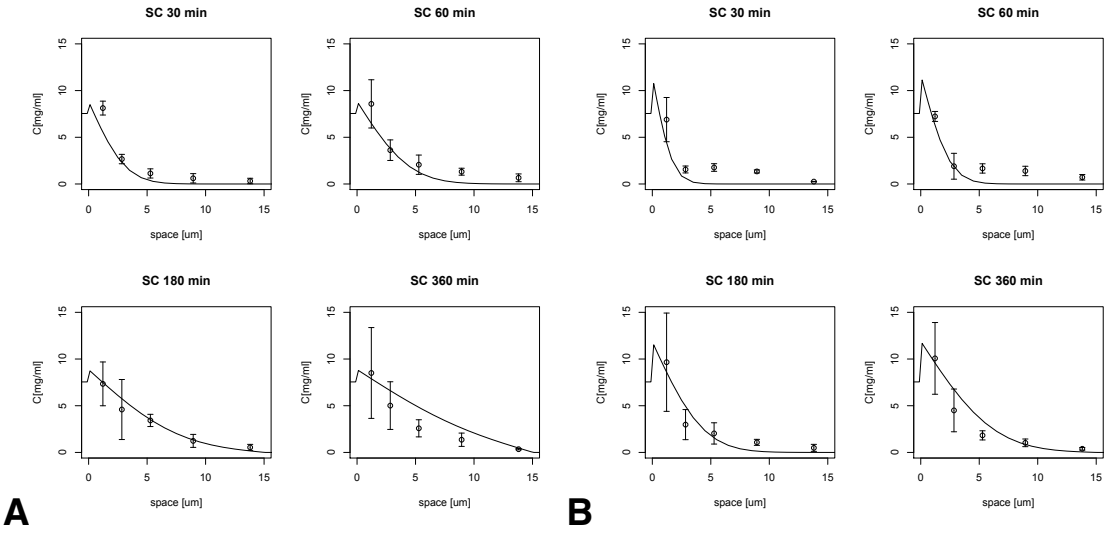

Figure 5-4 Overall fitted *stratum corneum* concentration-depth profiles of the infinite dose FD-C setup (A) and infinite dose SB-M setup (B) for various time points. Open circles denote experimental findings and solid lines denote the fitted model output. Data variation is given as standard deviation.

Fitting of SC diffusivity and partition coefficient showed reasonable results with low residual standard errors (Table 5-1). Figure 5-4 shows results from fitting every data point of all times in total (All times, Table 5-1). For both setups individual fittings show higher theoretical permeabilities k_p ($k_p = \frac{D \times K}{h}$) for early times in comparison to late times with a higher average permeability for the FD-C setup (factor of 2.33 Table 5-1).

Table 5-1 Infinite dose fitting results (D_{SC}, K_{SC}) of FFA concentration-depth profiles for FD-C experiments (A) and SB-M experiments (B) for different time points separately and total fit of all times points (All times). Theoretical permeability k_p was calculated from D_{SC}, K_{SC} and SC thickness. The residual standard error (RSE) is given for each fit separately.

	Times [min]	D_{SC} ± SE [$\mu m^2/h$]	K_{SC} ± SE	k_p [$\mu m/h$] ± SE	RSE
A	30	5.24 ± 1.55	1.93 ± 0.29	6.75E-01 ± 2.24E-01	0.63
	60	5.71 ± 2.66	1.56 ± 0.30	5.99E-01 ± 3.01E-01	1.07
	180	6.36 ± 1.46	1.10 ± 0.08	4.67E-01 ± 1.13E-01	0.51
	360	1.84 ± 0.47	1.37 ± 0.12	1.68E-01 ± 4.57E-02	0.62
	All times	6.53 ± 1.98	1.17 ± 0.11	5.09E-01 ± 1.62E-01	1.19
B	30	3.67 ± 2.59	1.93 ± 0.92	4.74E-01 ± 4.03E-01	1.25
	60	2.23 ± 1.48	1.83 ± 0.74	2.71E-01 ± 2.10E-01	1.26
	180	0.95 ± 0.44	2.24 ± 0.60	1.42E-01 ± 7.63E-02	1.21
	360	0.80 ± 0.22	1.97 ± 0.25	1.05E-01 ± 3.21E-02	0.77
	All times	2.06 ± 0.57	1.59 ± 0.20	2.18E-01 ± 6.64E-02	1.33

5.4.3 Fitting of *in-vitro* finite dose profiles

As for the infinite dose scenario, experimental results for FD-C and SB-M showed a characteristic jump in concentration at the Vehicle/SC boundary (Figure 5-5). SB-M experiments tend to reach towards a pseudo steady-state for late times. Average relative standard deviation of experimental data is slightly higher for the SB-M setup (41%) in comparison to the FD-C (36%).

Fitting of SC diffusivity and partition coefficient for finite dose experiments using a FD-C and SB-M setup showed very reasonable results with low residual standard errors (Figure 5-5, Table 5-2). Simulation results (fitted model) showed a decline of 11 % (FD-C) and 17 % (SB-M) after 6 h of simulations for the vehicle concentrations indicating the transient nature of the underlying process. High permeability values could be detected for single fittings of short incubation times for both FD-C and SB-M (Table 5-2).

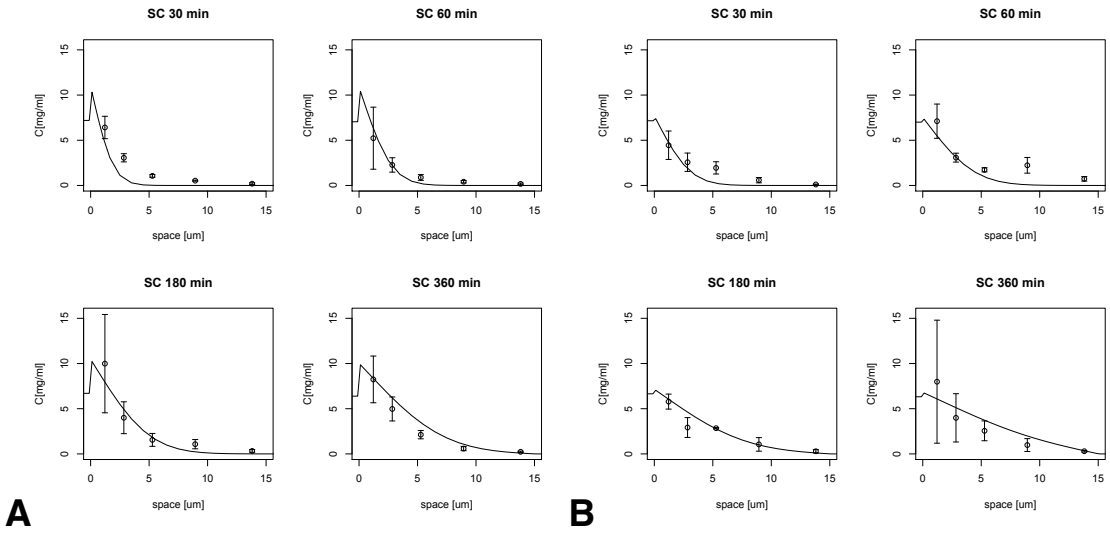

Figure 5-5 Overall fitted *stratum corneum* concentration-depth profiles of the finite dose FD-C setup (A) and finite dose SB-M setup for various time points. Open circles denote experimental findings and solid lines denote the fitted model output. Data variation is given as standard deviation.

Fitting of SC diffusivity and partition coefficient showed reasonable results with low residual standard errors (Table 5-2). Figure 5-5 shows results from fitting every data point of all times in total (All times, Table 5-2).

Table 5-2 Finite dose fitting results (D_{SC}, K_{SC}) of FFA concentration-depth profiles for FD-C experiments (A) and SB-M experiments (B) for different time points separately and total fit of all times points (All times). Theoretical permeability k_p was calculated from D_{SC}, K_{SC} and SC thickness. The residual standard error (RSE) is given for each fit separately.

	Times [min]	D_{SC} ± SE [$\mu m^2/h$]	K_{SC} ± SE	k_p [$\mu m/h$] ± SE	RSE
A	30	9.65 ± 1.96	1.29 ± 0.11	8.28E-01 ± 1.84E-01	0.36
	60	4.23 ± 1.04	1.05 ± 0.11	2.95E-01 ± 7.95E-02	0.35
	180	1.24 ± 0.37	2.25 ± 0.35	1.86E-01 ± 6.18E-02	0.82
	360	1.36 ± 0.14	1.54 ± 0.06	1.39E-01 ± 1.56E-02	0.25
	All times	2.45 ± 0.57	1.58 ± 0.17	2.58E-01 ± 6.61E-02	1.07
B	30	29.55 ± 8.29	0.71 ± 0.07	1.41E+00 ± 4.17E-01	0.36
	60	8.55 ± 6.29	1.21 ± 0.34	6.91E-01 ± 5.44E-01	1.41
	180	6.28 ± 2.78	0.88 ± 0.13	3.69E-01 ± 1.73E-01	0.75
	360	1.53 ± 0.53	1.41 ± 0.18	1.44E-01 ± 5.28E-02	0.77
	All times	5.85 ± 1.93	1.08 ± 0.12	4.22E-01 ± 1.47E-01	1.12

For both *in-vitro* setups fittings for every time point separately show higher theoretical permeabilities for early times in comparison to late times with an higher average permeability for the SB-M setup (factor of 1.64 Table 5-2). Overall, finite dose permeabilities showed similar values in comparison to infinite dose experiments. (All times, Table 5-1, Table 5-2).

5.4.4 Prediction of *in-vitro* finite dose profiles from infinite dose input parameters

Given this evidence, prediction of the *in-vitro* finite dose scenario from input values gathered from the infinite dose case was carried out and showed reasonable results (Figure 5-6) with low relative absolute errors of the fit (0.63 for FD-C and 0.61 for SB-M).

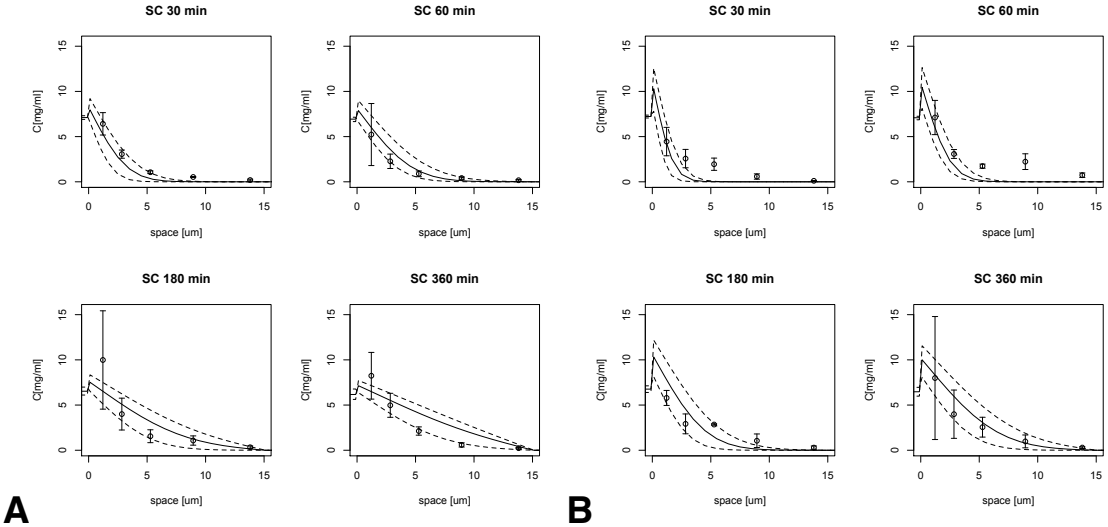

Figure 5-6 Predicted *in-vitro* finite dose experiments for the FD-C setup (A) and SB-M setup (B). Open circles denote experimental findings and solid lines denote the simulation results (prediction). Dashed lines indicate the 95% confidence interval. Data variation is given as standard deviation.

5.4.5 Drug concentration – SC depth – profiles: *In-vivo*

In-vivo experimental data showed a characteristic jump of concentration below the initial concentration of the vehicle for all time points (Figure 5-7). Concentration-depth profiles for the infinite and finite dose tend to establish a (pseudo) steady-state after 180 min. Fittings of SC diffusivity and partition coefficient using the dif-

fusion model could describe the fate of the substance excellently (Figure 5-7, dashed lines). However, fitted diffusivities showed extremely high values in comparison to *in-vitro* studies leading to high theoretical permeability values (Table 5-3 A). Partition coefficients showed a reduction of factor 4-5 in comparison to *in-vitro* studies (Table 5-1 All times, Table 5-2 All times, Table 5-3 A).

Table 5-3 Overall fitting results (D_{SC}, K_{SC}) of FFA concentration-depth profiles for *in-vivo* infinite dose and finite dose scenarios (A). Lower part of the table (B) shows fitting results for K_{SC} with fixed values D_{SC}^{*} for *stratum corneum* diffusivity (taken from *in-vitro* fittings).

	Experiment	D_{SC} ± SE [$\mu m^2/h$]	K_{SC} ± SE	k_p ± SE [$\mu m/h$]	RSE
A	Infinite dose	54.53 ± 17.16	0.35 ± 0.03	1.12E+00 ± 3.66E-01	0.37
	Finite dose	36.60 ± 10.04	0.26 ± 0.02	5.60E-01 ± 1.59E-01	0.24
B	Infinite dose	5.85 ± 1.93 *(SB-M finite dose)	0.55 ± 0.06	1.89E-01 ± 6.58E-02	0.62
	Finite dose	5.85 ± 1.93 *(SB-M finite dose)	0.38 ± 0.04	1.31E-01 ± 4.53E-02	0.37

Due to the steady-state-like curve shape of both finite and infinite dose *in-vivo* studies (Figure 5-7, dashed lines) fitting of diffusivity can obviously lead to problems since the variation of D_{SC} does not alter the curve shape when approaching steady-state. To overcome this problem D_{SC} was set to a fixed value (taken from *in-vitro* finite dose SB-M fittings of all time points to account for an average best description of all time points) and only the partition coefficient was varied by the fitting routine. Results of this approach are depicted in Figure 5-7 (solid lines). In comparison to the first approach the fitting error did only slightly increase (Table 5-3 B). Fitted partition coefficients showed only minor differences and hence, permeability values decreased by a factor of approximately 4-6 (Table 5-3 A vs. Table 5-3 B).

In-vivo permeability values (Table 5-3 B) showed a decrease of factor 1.2-2.7 in comparison to the *in-vitro* infinite dose case (Table 5-1) and a decrease of factor 2.0-3.2 in comparison to the *in-vitro* finite dose fittings (Table 5-2). The modeled finite dose scenario reveals a FFA vehicle depletion of only 5%.

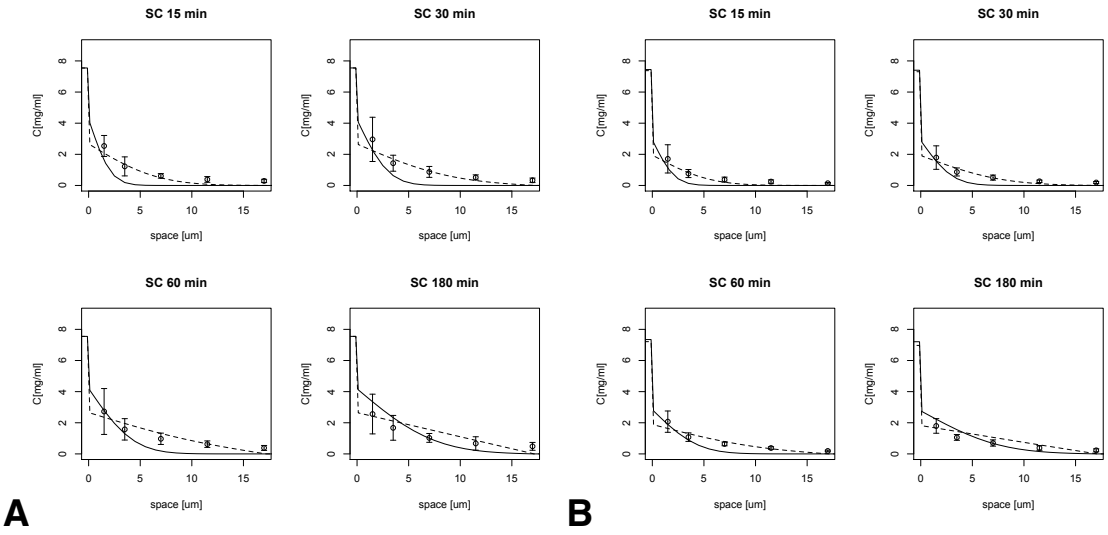

Figure 5-7 Fitted *stratum corneum* concentration-depth profiles of the *in-vivo* infinite dose case (A) and finite dose case (B) for various times with fixed D_{SC} (solid line, values taken from *in-vitro* fittings) and free D_{SC} (dashed line). Open circles denote experimental findings and solid lines denote the fitted model output. Data variation is given as standard deviation.

5.4.6 Prediction of *in-vivo* profiles from *in-vitro* input parameters

In second step, model input parameters taken from the *in-vitro* infinite dose and finite dose case (All times, Table 5-1, Table 5-2) were used to predict the *in-vivo* scenario yielding reasonable average relative errors of the fit (Table 5-4).

Table 5-4 Prediction errors (average relative error) of FFA concentration-depth profiles for *in-vivo* infinite dose and finite dose scenarios.

K_{SC} and D_{SC} taken from	*In-vivo* infinite dose prediction error	*In-vivo* finite dose prediction error
FD-C Infinite	9.18E-01	1.21E+00
FD-C Finite	9.19E-01	1.08E+00
SB-M Infinite	9.15E-01	1.06E+00
SB-M Finite	8.58E-01	1.03E+00

For both application scenarios (finite and infinite dose) input values from the SB-M finite dose fittings led to the smallest fitting error (prediction results depicted in

Figure 5-8). Simulations (Figure 5-8) lead to reasonable results, especially for short times and concentrations below stratum disjunctum [172].

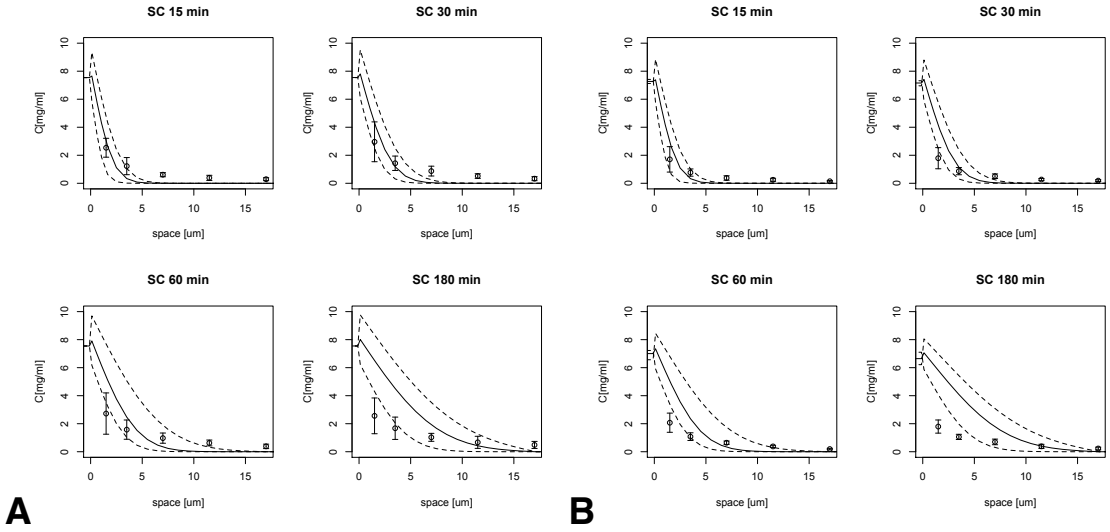

Figure 5-8 Predicted *in-vivo* experiments for the infinite dose case (A) and finite dose case (B). Open circles denote experimental findings and solid lines denote the simulation results (prediction). Dashed lines indicate the 95% confidence interval. Data variation is given as standard deviation.

5.5 Discussion

5.5.1 Fitting results and differences in *in-vitro* and *in-vivo* setups

Model fitting results for infinite and finite dose *in-vitro* studies are in very reasonable agreement with the experimental findings (Figure 5-4, Figure 5-5). Variation in diffusivity and partition coefficient (All times) can be explained by intra-individual variability in determined parameters from different experiments [173]. Average relative standard deviations of *in-vitro* and *in-vivo* concentrations over depth and time do show insignificant differences in variability (32–42% for *in-vivo* and 36-45% for *in-vitro*). These observations are in reasonable agreement with findings from literature [173]. As stated before, finite dose experiments show a more semi-infinite nature during the time of application due to the rather low donor depletion (11-17%).

The observed decrease of diffusion coefficient over time for finite and infinite scenarios is in reasonable agreement with *in-vivo* findings of Herkenne et al. [174]. These findings may be the result of the prolonged incubation time which can make fitting the curves more difficult. In addition, the resistance of the epidermis may have an impact on the curve shape after longer incubation times [160]. In contrast to the addressed diffusivity, variability of the fitted partition coefficient over time did not show a clear trend for both *in-vitro* systems (Table 5-1, Table 5-2).

In-vivo fittings of diffusivity and partition coefficient showed lower partition coefficients with values below 1 and high diffusivity and subsequently high theoretical permeabilities. In comparison to experimental data an excellent correlation could be found (Figure 5-7, dashed lines).

Due to the steady-state nature of the concentration-depth profiles after short times fitting results for D_{SC} are prone to error. Therefore, SC diffusivity was set to constant values gathered from *in-vitro* studies. Fitting results were in good agreement with experimental data (Figure 5-7, solid lines) for all time points. Partition coefficients were still lower in comparison to *in-vitro* experiments. Due to low partitioning, an even lower donor depletion was calculated, explaining the similar shapes of finite and infinite dose *in-vivo* experiments.

Speaking of theoretical permeabilities, lower calculated permeabilies for *in-vivo* experiments (Table 5-3 B) in comparison to SB-M fitting results (Table 5-1 B, Table 5-2 B, All times) could be observed.

However, student's t-test of SB-M *in-vitro* setup versus *in-vivo* setup did not indicate significant differences for the infinite dose (p=0.76) and finite dose scenario (p=0.06).

The found differences in partition coefficient between *in-vitro* and *in-vivo* studies could be attributed to a potential contamination of skin slabs with subcutaneous fatty tissue during the process of preparation of *ex-vivo* skin samples (solubility of FFA in triglycerides: 7%; solubility of FFA in wool wax ointment: 0.9%) [175].

5.5.2 Prediction of the *in-vitro* finite dose scenario from model input parameters from the infinite dose case

In 2013 it could be shown that parameters obtained from the *in-vitro* infinite dose case are suitable parameters to predict the *in-vitro* finite dose scenario for an aqueous vehicle [82, 165]. The investigations cited employ more complex two-dimensional diffusion models that need a larger set of input parameters (e.g. SC lipid diffusivities, corneocyte diffusivities, SC lipid/corneocyte partition coefficients) in comparison to the model presented. We could confirm the findings of the aforementioned works by applying a one-dimensional sparse-parameter model for a semi-solid donor formulation. Excellent agreement with experimental data for the prediction of *in-vitro* finite dosing of the two model systems (FD-C and SB-M) was found (Figure 5-6).

5.5.3 Prediction of the *in-vivo* scenario from model input parameters from the *in-vitro* case

We presented an *in-silico* model to analyse and predict *in-vivo* concentration-depth profiles of a drug for release from a semi-solid formulation. Work on predictions of *in-vivo* permeation is still scare. Pirot et al. could predict the *in-vivo* permeability of 4-cyanophenol for 60 min of application from values fitted from tape-stripping data obtained after 15 min [176]. Variability of permeability of *in-vivo* fittings of FFA re-

ported here is in reasonable agreement with results of Pirot and coworkers. Permeabilities for the *in-vitro* setups over time do show slightly larger variations (2-fold to 6-fold between highest and lowest permeability of individual setups). Therefore, fitting of all data points from all measured times in total seems to be the most reasonable option to capture the whole kinetic process over time.

Using a simple analytical solution of the diffusion equation, Herkenne et al. could show the potential of *in-vitro* tape-stripping data to predict the situation in man [177]. Parameters from the *in-vitro* and *in-vivo* case were in reasonable agreement, but also some significant differences were observed. In contrast to the study presented here, only the infinite dose scenario was examined, vehicle diffusivity and resistance of the deeper skin layers were not taken into account and porcine skin was used for *in-vitro* studies.

In this study, predicted human *in-vivo* concentration-depth profiles from data obtained from *in-vitro* cases using human skin showed promising results (Figure 5-8). Short times (15-30 min) could be described excellently but concentrations in superficial SC depths are considerably overpredicted for later times (60-180 min). Obviously, differences in partition coefficients between *in-vitro* and *in-vivo* experimental findings yield to the aforementioned discrepancies. Hence, possible alterations of solubility due to preparation of *ex-vivo* skin samples (e.g. contamination with subcutaneous fatty tissue) should be taken into account when gathering kinetic descriptors from *in-vitro* settings to describe the transdermal transport of substances in man.

5.5.4 Mathematical diffusion model

In contrast to analytical solutions of the diffusion equation, numerical approaches can be considered more versatile due to generalization (infinite vs. transient scenario), extendibility (e.g. protein binding, evaporation, blood flow) and complexity (e.g. microscopic models of the SC, multi compartment approaches). The interested reader is kindly referred to overview articles about analytical solutions and numerical approaches in the field of modeling skin transport [58, 101, 160]. However, one major drawback of numerical solutions is often the speed of computation. Due to the high level of optimization (implicit finite differences, non-uniform gridding) the

presented model is capable to be incorporated in complex operations, like fitting routines, but still run in high spatial resolution on consumer hardware for reasonable computational times.

Considering the complex nature of the human skin and the underlying transport kinetics, one has to bear in mind the following facts:

- In this study the morphological structure of the SC was simplified as a pseudo-homogenous membrane. This obviously, does not reflect the microscopic structure of the SC. This limitation can be overcome by building more complex microscopic models of the SC [96] but this would increase the number of unknown parameters [81] as well as greatly increase computational complexity, making the model less generally applicable.
- Additional mechanisms, such as binding were not considered but might influence parameters determined from *in-vitro* parameters as well as the underlying kinetic assumptions [58, 62, 178].
- *In-vivo* blood flow was not modeled and might influence *in-vitro in-vivo* correlation.

5.5.5 Comparison of FD-C and SB-M to gather input parameters to predict *in-vivo* skin penetration

Comparison of the two *in-vitro* systems for the determination of model input parameters to predict the *in-vivo* scenario shows a tendency to prefer the SB-M setup that typically describes the *in-vivo* case in a more natural way due to lower hydration states in comparison to the FD-C setup. However, the differences in average relative errors (Table 5-4) are small. Fitting errors (residual standard errors) for the *in-vitro* setups indicate slightly better results for the SB-M (Table 5-1, Table 5-2). This indicates that SB-M concentration-depth profiles could be described better with the applied mathematical model and this subsequently might influence the slightly better prediction results.

5.6 Conclusion

The application of an one-dimensional numerical *in-silico* model to simulate skin penetration turns out to be useful to describe *in-vitro* experiments for different systems (FD-C and SB-M), as well as *in-vivo* experiments for the infinite and finite dose scenario. Input parameters gathered from the *in-vitro* infinite dose case can be used to describe the *in-vitro* finite dose scenario for both model systems. Despite apparent differences in calculated partition coefficients between *in-vivo* and *in-vitro* studies, prediction of *in-vivo* scenarios from input parameters calculated from the *in-vitro* case seems to be a reasonable option. There is evidence to prefer the more *in-vivo* like SB-M as an ethical inoffensive model to predict the fate of a substance in man but certainly, a careful evaluation for a wide range of different xenobiotics is necessary and should be addressed in future works.

The application of *in-silico* models and the concepts presented in this study, will hopefully lead to an improved prediction of the *in-vivo* situation and a better understanding of the underlying physicochemical processes.

6 Outlook

The following oulook provides contributions of the author to published and unpublished work in the field of modeling and measurement of skin absorption. The methods and results are presented in a condensed fashion to comply with the scope limitations associated with this thesis.

6.1 Inclusion of binding kinetics into mathematical models to simulate transdermal absorption

Parts of this section have been published in:

Hansen, S., Selzer, D., Schaefer, U. F., Kasting, G. B. (2010). An Extended Database of Keratin Binding. *J Pharmaceut Sci*, 100(5), 1712–1726

The author of the thesis made the following contributions to the publication:

Performed the mathematical analysis of the data (fittings of the non-isotherm data, SMARTS analysis), investigated the data manually, produced the figures and wrote parts of the manuscript.

Steffi Hansen performed the experiments, fitted the isotherm data and wrote the manuscript.

6.1.1 Note

This section shortly summarizes the contributions of the author on analyzing the extended database of keratin binding. The full published article on this topic can be found elsewhere [178].

6.1.2 Introduction

Diffusion modeling is a powerful tool for predicting skin absorption. However, current advances in predicting absorption from finite doses usually fall short of expectations [30]. Often skin levels are seriously under-predicted by current models, hampering their usefulness for regulatory purposes [151]. Transient exposure is relevant to the majority of pharmaceutical and cosmetic dermal applications and often also to unintentional exposure to hazardous compounds. Predicting transient absorption of finite doses requires the understanding of processes that may only play a minor role in steady-state absorption. A major factor that will influence the kinetics of absorption is reversible binding of permeants to the tissue. Binding leads to differences in the effective and true diffusion and partition coefficients, a retardation of the absorption process, and a sustained presence of the bound compound in the tissue. Therefore, accurate estimates of binding coefficients are essential to improve finite dose skin absorption models. The present work focuses on predicting binding coefficients to the major *stratum corneum* (SC) protein keratin. Keratin intermediate filaments account for over 90% of the weight of the proteins in the stratum corneum and form the body of the cellular phase of the *stratum corneum*. Therefore, binding coefficients to keratin should be a good predictor of binding to the *stratum corneum* proteins, if the keratin is accessible to the permeant.

The current state of the art of evaluating the affinity to corneocyte proteins is to measure the partition coefficient into delipidized SC (DSC). It has earlier been recognized that the logarithmic protein/water partition coefficient $logK_{pro/w}$ is related to the logarithmic octanol/water partition coefficient $logK_{o/w}$ in terms of a linear energy relationship [64, 179]. However this relationship was developed for a rather small and largely homogeneous dataset of 16 hydrocortisone esters and methyl substituted p-cresols. Meanwhile a number of authors have published further partitioning data into DSC so that it seems worthwhile to update and extend the original dataset. In addition, the method of delipidisation has been criticized in the past as treatment with organic solvents may denature proteins and furthermore does not remove lipids covalently bound to the cornified envelope [180]. In consequence DSC might not be representative of the affinity to the corneocytes in the context of intact SC. Therefore, the current analysis will focus not only on partitioning data into DSC but broaden the analysis to integrate further keratinous substrates from human as well

as animal origins, i.e., delipidized human callus (CAL), human nail (NAI), human hair (HAI), bovine hoof and horn (BHH), and sheep wool (WOO). Their suitability for predicting keratin binding will be evaluated. CAL, DSC, and BHH have been used for such a purpose before (e.g. by Hagedorn-Leweke et al. [181]). Human nail is closely related in composition and function to these keratinous substrates. Sheep wool keratin has been used extensively for analyzing the thermodynamics of water binding to keratin and the diffusion of water through keratin matrices [182, 183]. Human hair being the equivalent to animal wool this matrix was also included in the analysis.

For this purpose we collected and, if necessary, re-analyzed binding data from the literature. Keratin affinity was expressed as a Nernst binding coefficient, i.e., in terms of a linear binding isotherm which is also equivalent to a partition coefficient. This approach is appropriate for bound concentrations that are far away from saturation of binding sites. When possible, the binding coefficient was extrapolated to the temperature of the human skin surface, 32°C. As data for hydrophilic compounds were sparse, binding to BHH and/or DSC was measured for five additional hydrophilic substances (glucose, mannitol, nicotinamide, nicotine, and sucrose).

Furthermore, if lipophilicity is indeed the main factor determining binding as suggested elsewhere [64, 179], then pH-induced changes should be compensated for by correcting *logK* for pH and using *logD* in the regression analysis. By this means the correlation would be broadened to also predict protein binding of ionizable compounds. In the meantime binding to BHH or DSC has been published for other ionizable compounds (namely flufenamic acid) however, without looking at the influence of pH on the binding coefficient [125].

Therefore, in the present work we present binding data to BHH for one more weak acid (diclofenac) and one weak base (nortriptyline) at different pH-values and degrees of ionization. Least squares regression analysis of the logarithm of the Nernst binding coefficient ($logK_{Nernst}$) was performed using descriptors for molecular size (molecular weight, MW), lipophilicity (logarithmic octanol water partition coefficient corrected fro pH, *logD*) and number of H-bond donor- and acceptor-groups in a molecule (Hbd, Hba). Furthermore a SMARTS-search was performed looking for aromatic rings, acid and basic groups as additional descriptors for keratin binding.

6.1.3 Data gathering and data treatment

Data that was measured and gathered is summarized in [178]. The procedure of data measurement is not shown in this thesis but can be found elsewhere [178]. A Nernst isotherm assumes that the relationship between bound (q) and free concentration (c_{free}) at equilibrium is linear with the factor of proportionality being the Nernst binding coefficient K_{Nernst}

$$q = K_{Nernst} \cdot c_{free} \qquad \text{Equation 6-1}$$

This is true as well for the low concentration limit of the Langmuir and the BET isotherm

$$q = \frac{k_{Langm.} \cdot \hat{q} \cdot c_{free}}{1 + k_{Langm.} \cdot c_{free}} \qquad \text{Equation 6-2}$$

$$q = \frac{k_{BET} \cdot \hat{q} \cdot c_{free}}{\left(c_{sat} - c_{free}\right) \cdot \left(1 + \frac{\left(k_{BET} - 1\right) \cdot c_{free}}{c_{sat}}\right)} \qquad \text{Equation 6-3}$$

Here $k_{Langm.}$ and $\hat{q}$ are the Langmuir binding coefficient and the maximum adsorption capacity of the monolayer while k_{BET} is the BET binding coefficient. The BET isotherm is further limited by the saturation concentration of the compound c_{sat}. Therefore, as $c_{free} \rightarrow 0$, the product of $k_{Langm.}$ and $\hat{q}$ as well as the product of $k_{BET.}$, $\hat{q}$, and c_{sat} become equivalent to K_{Nernst}. If Langmuir or BET binding coefficients were provided in the original literature these were converted to $k_{Langm.}$ and k_{BET} expressed as ml/mmol and $\hat{q}$ as mmol/g. If the data was presented graphically with no binding coefficients provided in the original literature we estimated the data from the plots to the best of our ability, re-plotted them expressing the amount adsorbed per gram protein (q) as mmol/g and the free concentration at equilibrium (c_{free}) as mmol/ml and fitted them to the appropriate model according to the former equations.

For those compounds where the influence of temperature on binding had been investigated $\log K_{Nernst}$ was extrapolated to 32 °C according to the Arrhenius relationship

$$\ln K_{Nernst} \propto 1/T \qquad \text{Equation 6-4}$$

6.1.4 Data analysis of the extended database

The extended database contains 75 chemically diverse substances (MW 32 to 1373; *logD* -4.78 to 5.70; sum of H-bond acceptor and donor groups 0 to 41) [178]. Values for MW, *logD*, and numbers of H-bond donor and acceptor groups were retrieved from ACD/PhysChem 10.02 software. For *logD,* experimental values were preferred if available. Raykar and coworkers had reported a direct relationship between the logarithmic partition coefficient into DSC (which is the equivalent to the Nernst binding coefficient) and the logarithmic octanol-water partition coefficient $logK_{O/w}$ indicating that partitioning is governed by the lipophilicity of the compound [64, 179]. We have now widely broadened the spectrum of keratinous substrates and substances that have been investigated. Figure 6-1 shows the relationship between $logK_{Nernst}$ and *logD* with the individual keratinous substrates indicated as symbols. The original linear regression done by the Anderson group is shown together with a novel linear regression analysis performed for BHH, CAL, and DSC. Binding to HAI, and WOO is markedly different from the other keratinous substrates and will therefore be analyzed separately. Figure 6-1 confirms for a much larger database that for keratinous substrates such as BHH, CAL, and DSC the Nernst binding coefficient is directly related to the octanol-water partition coefficient as had been proposed by the Anderson group. This relationship was further evaluated by defining subsets of the individual keratinous substrates and performing a linear regression analysis for these subsets as well as for the complete dataset assuming a linear energy relationship between binding to the respective keratins and octanol–water partitioning (Figure 6-2). The slopes were not significantly different for subset 1 (BHH), subset 2 (combines CAL and DSC) these are morphologically closely related), and the combination of subset 1 and 2 [one-way analysis of variance (ANOVA), not shown here] In comparison to the earlier results reported by the Anderson group the present correlation is slightly steeper due to the broadening of the data-

base (although not significantly so, according to a one-way ANOVA).

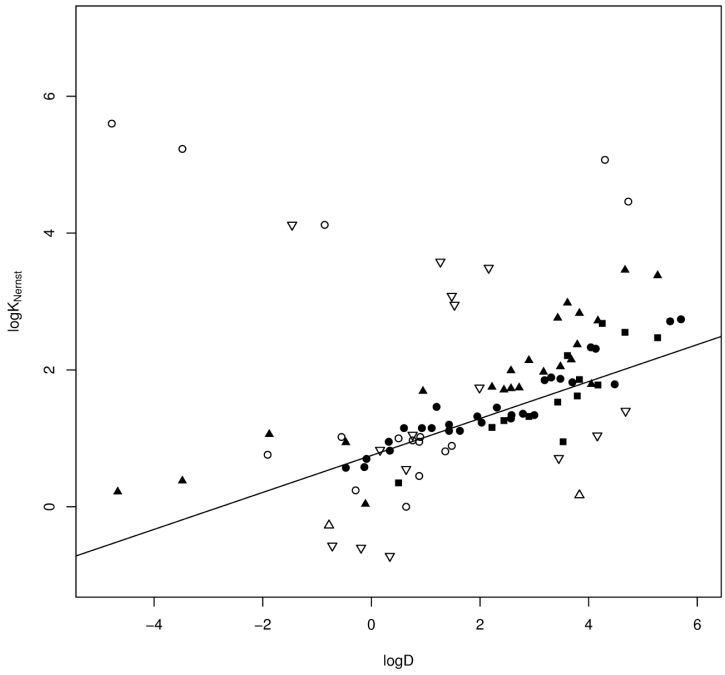

Figure 6-1 The logarithmic Nernst coefficient is shown as a function of lipophilicity for binding to BHH (filled triangle), CAL (filled square), DSC (filled circle), HAI (open inverted triangle), NAI (open triangle), WOO (open circle). The original regression analysis by the Anderson group (solid line) is shown.

While the slope of two subsets (BHH and CAL/DSC) are comparable the offset of subset BHH is twice as high as the offset of subset CAL/DSC. Therefore the goodness of fit for the combination of subset BHH and CAL/DSC is noticeably decreased compared to the individual fits (not shown here). Due to the similar slope found for the subsets it is easily possible to correct the experimental values measured for one of the two for the difference in offset between the subsets. Specifically, we subtracted the difference of the offsets determined for the subsets from experimental values measured for BHH. Subsequently a linear regression analysis was performed for the unified dataset (Figure 6-3).

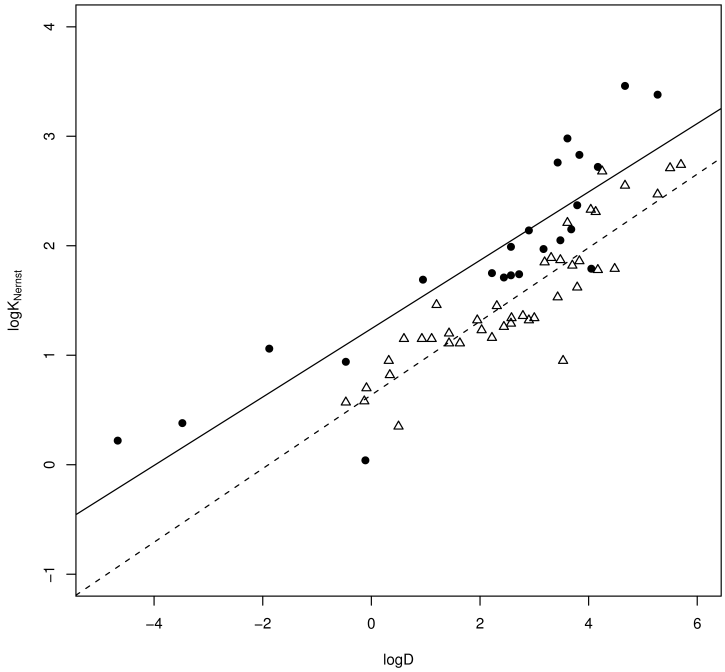

Figure 6-2 The logarithmic Nernst coefficient is shown as a function of lipophilicity together with the results of a linear regression analysis for binding to BHH (filled circle, solid line) and CAL and DSC (open triange, dashed line).

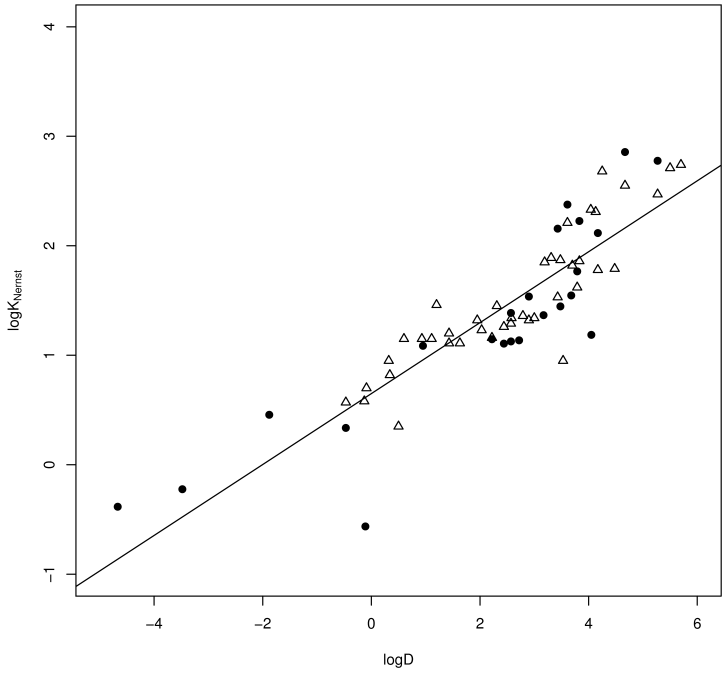

Figure 6-3 The logarithmic Nernst coefficient is shown as a function of lipophilicity for the unified dataset, i.e. binding coefficients to BHH corrected for difference in offset (filled circles), CAL, and DSC (open triangles). A linear regression analysis of the complete dataset is performed (so lid line).

6.1.5 Binding to bovine hoof and horn and human delipidized stratum corneum, ionizable compounds

Figure 6-4 highlights subset BHH/DSC among the complete dataset which encompasses only acidic and basic compounds. The purpose of analyzing this subset separately is to evaluate whether binding of ionizable compounds answers to the same principles as neutral compounds or whether additional aspects such as the charge play a role. The experimental conditions for the acids and bases considered here were such that the degree of ionization varied largely between these compounds spanning a range between 0.99 and 99.98%. Obviously, for acids and bases as well the main determinant for binding is lipophilicity. In consequence $logK_{Nernst}$ can be predicted from *logD* for ionizable compounds. It is not surprising that due to the limited number of data in this subset the slope is slightly different from the com-

plete dataset. Upon visual inspection of Figure 6-4 it becomes however clear that there are no fundamental differences between this subset and the remaining data.

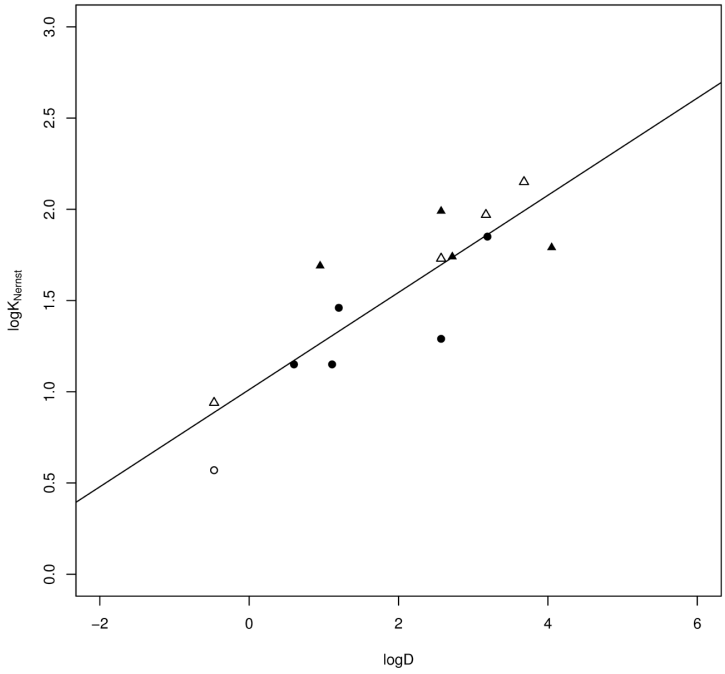

Figure 6-4 The logarithmic Nernst coefficient is shown as a function of lipophilicity together with the results of a linear regression analysis for binding to BHH (triangles), CAL (squares), DSC (circles). Only acids and bases are considered.

6.1.6 Binding to human hair and sheep wool keratin

Binding to HAI and WOO seems to be governed by distinctly different principles compared to the other keratinous substrates (Figure 6-1). Regression analyses show that *logD* is no significant determinant for $\log K_{\text{Nernst}}$ [178]. The best prediction is achieved based on the molecular weight, closely followed by the number of H-bond acceptor and H-bond donor groups in the molecule. However, in all cases the correlations are poor. A multiple linear regression analysis based on the four determinants is not feasible as MW, Hba, Hbd are collinear and *logD* is neither a significant descriptor in itself nor in combination with any of the other descriptors. The results of the regression analysis confirm that lipophilicity is not a major factor determining binding to HAI and WOO. It may be that changes in pH led to structural

changes in the protein entailing changes in the binding affinity or number of available binding sites, phenomonena which cannot be accounted for by using l*ogD*.

6.1.7 SMARTS analysis

To investigate the correlation between the occurrence of certain chemical groups or structures and the protein binding affinity in different keratin matrices we gathered the corresponding SMILES from www.chemspider.com [184]. Accordingly, we searched for compounds with no ring system, compounds with alkaline groups and compounds with acidic groups using the *obgrep* tool from the Open Babel Package , version 2.0.1 and used the assistant SMARTS search suggestions from iBabel [185]. Figure 6-5 shows the chemical profile for binding to HAI and WOO respectively, generated in a SMARTS search.

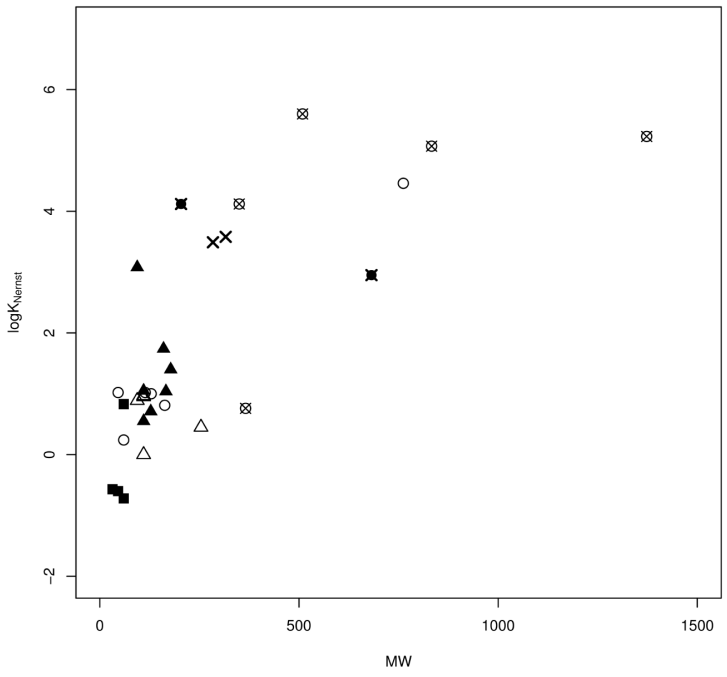

Figure 6-5 The logarithmic Nernst coefficient is shown as a function of lipophilicity for binding to HAI (solid/bold symbols) and WOO (open/light symbols) and a SMARTS analysis is performed. The following structural/chemical properties are indicated: No ring system (square), acidic group (circle), basic group (cross) and remainder (triangle). Combinations of symbols are possible (e.g. cross and filled circle for a compound binding to HAI having acidic and basic groups).

The question that can be answered with a SMARTS search is whether the remaining scatter of the data can be explained by the presences or absence of chemical structural features. For HAI and WOO the presence of aromatic rings seems to notably improve the binding affinity. Substances missing this feature are grouped at the bottom of the plot exhibiting logarithmic binding coefficients in the negative range or not greater than 1. Compounds that have acidic or basic groups tend to have higher $logK_{Nernst}$ values. Especially those compounds having both acidic and basic groups tend to have the highest $logK_{Nernst}$ values in the set of compounds that was investigated.

6.1.8 Conclusion

BHH, CAL, DSC and possibly also NAI are adequate surrogates for binding to SC keratins. This is not the case for HAI and WOO. Binding to SC keratins can be predicted from the lipophilicity of the solute according to a linear free energy relationship to $logK_{O/w}$. Ionizable compounds can be integrated into this relationship by using $logD$ instead. This result suggests that binding to SC keratins is mainly a lipophilicity driven process. An earlier relationship developed for a much smaller dataset was confirmed and refined. Based on the extended dataset we could show that the relationship between $logK_{Nernst}$ and $logK_{O/w}$ is steeper than originally assumed. This finding has consequences for the estimates of SC partition and diffusion coefficients.

6.2 Adressing skin topograhy by means of a 2D diffusion model

Images provided in this section have been taken from the master's thesis of Jan Riehm ("JSkin – A real-geometry based transdermal 2D skin diffusion model" (2013), Saarland University). Parts were taken from a manuscript in preparation for publication (written by J. Riehm and D.Selzer).

The author of the thesis made the following contributions:

Developed the concepts and provided advice and supervision to Jan Riehm during the work on his master's thesis at the Institute for Biopharmaceutics and Pharmaceutical Technology at Saarland University.

Jan Riehm developed the mathematics, implemented the software, did the analysis and produced the images.

6.2.1 Note

This section briefly summarizes the preliminary results of the study. Details on the implementation of the algorithms and in-depth analysis of the data is not presented in this thesis.

6.2.2 Introduction

Substance skin absorption is gaining enhanced interest in the field of pharmaceutics, cosmetics and risk assessment. To overcome ethical concerns regarding animal studies and human *in-vivo* investigations *in-silico* approaches are considered an alternative approach. These mathematical based models typically assume a simplified flat skin surface – a situation that is not consistent with the wrinkled topography of

native human skin. Here, we present the preliminary results of *in-silico* simulations to investigate the influence of a wrinkled skin topography on substance absorption kinetics.

6.2.3 2D-Diffusion model

To simulate substance transport with respect to a non-trivial skin surface a two-dimensional diffusion model was developed. The underlying diffusion equation (Equation 1-3) was solved numerically with the help of an explicit finite differences approach. The solver was implemented in C++ and CUDA-C to parallelize the computations on the GPU-level. Periodicity in the horizontal direction of our test geometry was implemented by applying periodic boundary conditions. Hindered diffusion (inaccessible areas) was modeled using reflecting boundary conditions. Change of diffusivity and partition effects with respect to the different skin layers was modeled similar to the 1D-approach presented in Chapter 5. The spatial domain was discretized using a uniform grid with a resolution of 1 μm.

6.2.4 Test geometries and test set library

Two test systems were created that are both 60 µm in width and 195 µm in height. Starting with the naive system (smooth SC), we have a donor compartment with a depth of 80 µm, a SC with 15 µm in thickness and a VE compartment with a height of 100 µm. All these compartments are rectangular in shape (Figure 6-6 A). The wrinkled geometry is more complex and shown in Figure 6-6 B. Integration of a pan that represents a wrinkle was accomplished by using a sine function in combination with a horizontal line at the borders that mimics a typical wrinkle formation. To preserve the thickness of the SC over the whole width of the system, we applied the normal of the function at each point and plotted a line with a distance of 15 µm along it. This symmetrical function was chosen to apply periodic boundary conditions on the sides. For infinite dosing we chose Dirichlet boundary conditions at the top and perfect sink conditions on the bottom to measure the accumulated mass in the sink. The depth of the pan was chosen to be 30 µm and has a width of 20 µm (on the upper end).

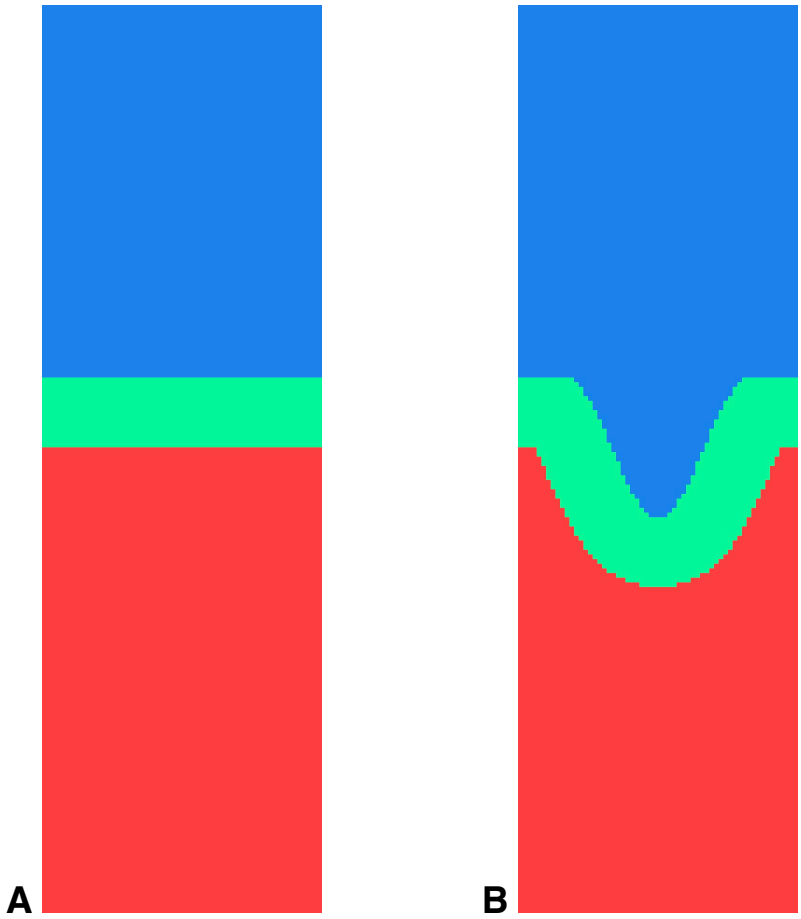

Figure 6-6 Snapshots of the naive (A) and wrinkled (B) model geometry. 10 pixels correspond to 1µm. Grid size was 10x10 pixels. The blue compartment denotes the donor, the aquamarine one the SC with a thickness of 15 µm and the red compartment denotes the VE. The depth of the wrinkle was chosen to be 30 µm.

Due to the wrinkled structure and the simultaneously unchanged width and height of the whole system, we had to normalize the computed values according to the volume fractions of each domain within the system. Both systems have a depth of 1 µm and subsequently the surface area of the SC exposed to the donor was 60 μm^2 for the naive case and 120 μm^2 for the wrinkled one. This also affected the size of the VE compartment.

After construction of geometries we created a test set of 9 combinations of different diffusion and partition coefficients (see Table 6-1). This was accomplished to investigate diffusion kinetics under different standardized conditions. A model substance of approximately 194 Da (comparable to e.g. caffeine (CAF)) was used to generate and gather basis values for diffusivities. An aqueous donor was modeled with a dif-

fusion coefficient D_{DON} of 1.00E-06 cm²/s that was approximated according to [186]. D_{DON} was never changed in the set since the effect of one magnitude in diffusivity did not affect permeability and t_{lag}. The diffusivity inside the SC and VE was assumed to be equal to CAF [125] for the basic tests (T1.1 - T1.3). Partitioning was varied (T1.1 - T1.3, T1.4 -T1.6 and T1.7 - T1.9) in a physically sound fashion (e.g. substances that solve better in the lipophilic SC than in water should mimic the same distribution characteristics at the boundary of the hydrophilic VE and lipophilic SC). D_{SC} and D_{VE} were varied within one magnitude (slower for T1.7 - T1.9 and faster for T1.4 - T1.6). The test set includes parameters that resemble small, medium sized and heavy molecules that are hydrophilic or lipophilic in character (good or poor solubility in the SC).

Table 6-1 Test set to investigate influence of different partition and diffusion coefficients on wrinkled and naive geometry.

Test ID	D_{DON} [cm²/s]	D_{SC} [cm²/s]	D_{VE} [cm²/s]	$K_{SC/DON}$	$K_{VE/SC}$
T1.1	1.00E-06	9.00E-11	6.00E-07	1.00	1.00E-01
T1.2	1.00E-06	9.00E-11	6.00E-07	10.00	1.00E-03
T1.3	1.00E-06	9.00E-11	6.00E-07	1.00E-01	10.00
T1.4	1.00E-06	9.00E-10	6.00E-06	1.00	1.00E-01
T1.5	1.00E-06	9.00E-10	6.00E-06	10.00	1.00E-03
T1.6	1.00E-06	9.00E-10	6.00E-06	1.00E-01	10.00
T1.7	1.00E-06	9.00E-12	6.00E-08	1.00	1.00E-01
T1.8	1.00E-06	9.00E-12	6.00E-08	10.00	1.00E-03
T1.9	1.00E-06	9.00E-12	6.00E-08	1.00E-01	10.00

6.2.5 Influence of wrinkles on infinite dose absorption kinetics

The human skin is not smooth but it is wrinkled and full of surface irregularities. Therefore, we investigated the influence of a wrinkled structure on diffusion kinetics in contrast to a smoothed structure (flat skin surface). For this and the following sections we denote the wrinkled case as "wrinkled" (W) and the smooth case as "naive" (N). The results from our measurements are presented in terms of the permeation k_p and the lag-time t_{lag}. We investigated an infinite dose application scenario with the aforementioned geometries and 9 different combinations of different combinations of diffusion and partition coefficients. The results for permeability values are presented in Table 6-2.

Table 6-2 k_p values calculated with the help of the 2D diffusion model for the wrinkled and naive geometries and the ratio of both.

Test ID	k_p wrinkle [cm/h]	k_p naive [cm/h]	k_p ratio (W/N)
T1.1	2.43E-04	1.65E-04	1.48
T1.2	1.16E-04	6.00E-05	1.93
T1.3	3.10E-05	2.16E-05	1.44
T1.4	2.42E-03	1.64E-03	1.47
T1.5	1.16E-03	6.06E-04	1.91
T1.6	3.09E-04	2.16E-04	1.43
T1.7	2.33E-05	1.57E-05	1.48
T1.8	5.46E-05	2.98E-06	1.83
T1.9	3.07E-06	2.14E-06	1.43

The k_p values of the wrinkled geometry are always larger than their counterparts from the naive geometry (see column ratio of Table 6-2). The ratio did not change much with changing diffusion coefficients but changed with altering partition coefficients. The bigger the difference in partition coefficients ($K_{VE/SC}$, $K_{SC/DON}$) the stronger the influence of geometry.

Table 6-3 t_{lag} values calculated with the help of the 2D diffusion model for the wrinkled and naive geometries and the ratio of both.

Test ID	t_{lag} wrinkle [h]	t_{lag} naive [h]	t_{lag} ratio (W/N)
T1.1	1.68	1.72	0.974
T1.2	5,76	5.16	1.11
T1.3	1.21	1.18	1.02
T1.4	0.17	0.17	1.00
T1.5	0.63	0.58	1.10
T1.6	0.09	0.13	0.71
T1.7	15.23	15.56	0.98
T1.8	22.32	22.36	0.99
T1.9	11.73	11.52	1.01

Next we computed the lag-time with the help of the diffusion model. The lag-time describes the point in time when the system overcomes the exponential increase in mass inside the acceptor compartment and reaches towards steady-state.

An overview of the computed values is given in Table 6-3. For the faster diffusion coefficients in T1.4–T1.6 the lag-times are lowest and for the slowest diffusion coefficient in T1.7-T1.9 the lag-times are highest. As expected, the ratios are close to one assuming no huge influence of geometry on lag-time. We only saw a large difference in test case T1.6 with a ratio of 0.71. If a substance does not have to establish a jump in concentration (K_{SC} = 1) and moves extremely quick inside the SC (high diffusivity) the fill-up of the SC with a higher volume (wrinkled case) does influence the time needed to reach steady-state significantly. As seen in Table 6-3 this literally only holds true for this special case with this extremely low lag-times (between 5.4 and 7.8 minutes to overcome the SC and VE).

There is strong evidence that the reason for higher permeabilities observed in the case of wrinkled geometries originates from the higher surface area of the SC that is exposed to the VE. As depicted in Figure 6-7 (exemplary from T1.2) the differences of average concentrations within the SC for the wrinkled and naive case are extremely small while there are high differences within the VE.

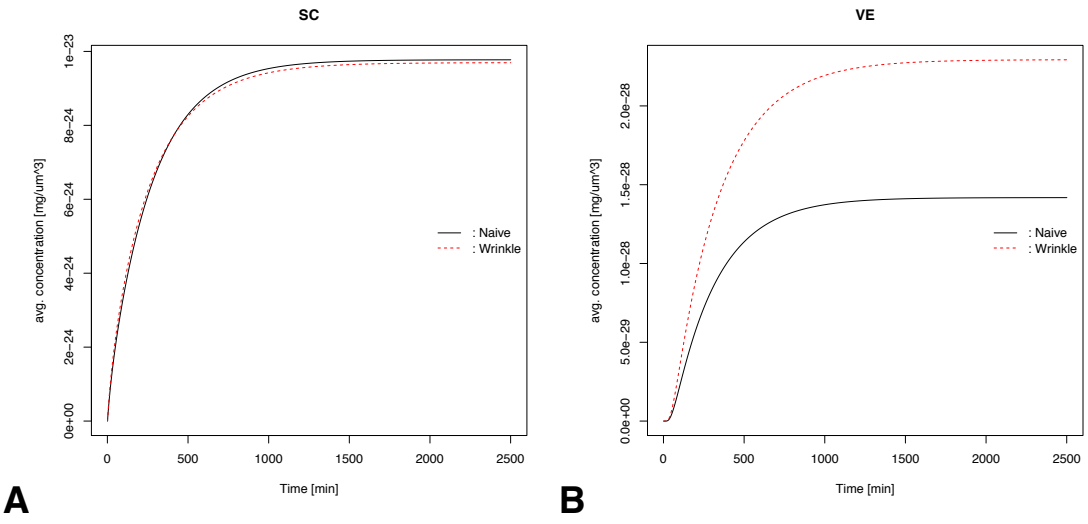

Figure 6-7 Average concentrations from T1.2 in the different compartments over time for the wrinkled and naive geometry (A: SC, B: VE).

Here, the average concentration is approximately two times higher for the wrinkled case in contrast to the naive case. This effect explains higher permeabilities for the wrinkled case since a higher concentration gradient inside the VE towards the sink can be established resulting in a stronger outgoing flux.

In summary, the created wrinkled geometry clearly leads to a higher permeability in comparison to flat skin surface and the effect is independent of change of partition coefficients and diffusion coefficients within the range of investigation. The influence on lag-time is typically negligible for risk assessment and pharmaceutical application since differences were only detected for a test candidate with a lag-time within the minute range.

6.2.6 Hindered diffusion

With our next application scenario we intended to investigate the influence of air bubbles on top of the skin surface. For example, when a transdermal patch is applied to the skin, it might not lay rigid on the skin surface. Since the skin is wrinkled and irregular on the surface it might happen that air bubbles occur under the patch (between donor and SC). In our model, air bubbles are designed as inaccessible parts of the system. Due to that fact, diffusion must occur along the boundaries of those air bubbles. To have a standard and to study the behavior for the wrinkled and non-wrinkled case we chose the presented standard geometries. The parameters of T1.2 were chosen for the modeling approach. Hindered diffusion was simulated by placing an air bubble into the mould of the wrinkle as well as on the flat SC of the naive geometry. Assuming infinite dose conditions, periodic boundaries on the left and right side and perfect sink conditions on the bottom, we performed three different runs over 2500 minutes on the two geometries under the following conditions:

1. Wrinkled geometry:

1.1 No air bubble

1.2 Air bubble covering 23.3% of the surface of the SC (23IS)

1.3 Air bubble covering 43.3% of the surface of the SC (43IS)

2. Naive geometry:

2.1 No air bubble

2.2 Air bubble covering 23.3% of the surface of the SC (23IS)

2.3 Air bubble covering 43.3% of the surface of the SC (43IS)

As stated before, the depth of the wrinkle was fixed at 30 µm. We placed air bubbles with a height of 8 µm and 15 µm (starting from the bottom) into the wrinkle. Hence the area that was occupied by the air bubbles corresponds to 23.3% and 43.3% of the surface of the wrinkled SC. Starting from the wrinkled case, we adapted the values of the inaccessible surface and applied it to the naive geometry (equal surface covering and equal bubble volume in comparison to the wrinkled case).

We computed the k_p values and lag-times. The computed values are displayed in Tables 6-4 and 6-5. As expected, the diffusant needs more time to reach the steady-state for the non-hindered counterparts (between 65% and 100% more time for the wrinkled case and between 32% and 69 % more time for the naive case). Additionally, the k_p values are smaller as for the non-hindered geometries (between 16% and 25% for the wrinkled case and between 9% and 10 % for the naive case). When comparing the ratios of the k_p values and lag times between the hindered and non-hindered geometries, on can observe an increase for t_{lag} and a decrease for k_p for the hindered geometries. With increasing size of the inaccessible surface area the permeation gets worse and the ratio between wrinkled and naive geometry decreases. The larger the inaccessible surface the larger the lag-time. As for the fully accessible case the wrinkled structure shows a higher permeability but needs more time to establish the steady-state. Besides the same surface coverage the effect on permeability and lag-time is much higher in case of the wrinkled geometry in comparison to the naive case.

Table 6-4 t_{lag} values calculated with the help of the 2D diffusion model for the wrinkled and naive geometries and the ratio of both (hindered diffusion)

Geometry	t_{lag} wrinkle [h]	t_{lag} naive [h]	tl_{ag} ratio (W/N)
23IS	9.48	6.79	1.39
43IS	11.59	8.71	1.33

Table 6-5 k_p values calculated with the help of the 2D diffusion model for the wrinkled and naive geometries and the ratio of both (hindered diffusion)

Geometry	k_p wrinkle [cm/h]	k_p naive [cm/h]	k_p ratio (W/N)
23IS	9.70E-05	5.45E-05	1.78
43IS	8.70E-05	5.37E-05	1.61

In summary we could show that besides the same surface coverage of inaccessible parts the influence on wrinkled geometry is much higher (higher factor of k_p reduction) as for the naive case.

6.2.7 Conclusion

Simulation of infinite dosing using a two-dimensional numerical diffusion model clearly showed the theoretical influence of skin topography on skin absorption. In comparison to a wrinkled geometry permeability was lower for an idealized flat skin surface. These findings were independent of any combination of tested partition and diffusion coefficients addressing the SC and viable epidermis. In comparison to the idealized case, the increased SC surface area seems to be responsible for this effect. Simulations with incomplete formulation coverage on the surface of the skin revealed a delayed and reduced skin absorption process in dependence of the degree of coverage for an idealized flat skin surface and a wrinkled geometry. However, this effect was expressed much stronger for incomplete filled wrinkles. The differences in lag-time seem to be negligible for risk assessment and pharmaceutical application.

In conclusion, the simulation of different application scenarios provides evidence that the distribution of formulation on the skin as well as the *in-vivo* skin topography should be considered when investigating skin absorption processes. The importance of these findings in regard to therapeutic formulation application should be investigated experimentally in future studies. Data on formulation distribution on the skin surface is still scarce. A potential technique to obtain this information could be MS-Imaging that has the potential to visualize and quantify the compound with respect to the spatial compound distribution [187].

6.3 Mathematical assistance to address the problem of confocal Raman microscopy signal attenuation in measuring transdermal drug transport

Parts of this section have been published in:

Franzen, L., Selzer, D., Fluhr, J., Schaefer, U. F., Windbergs, M. (2013). Towards drug quantification in human skin with confocal Raman microscopy. *Eur J Pharmaceut Biopharmaceut*, 84(2), 437–444

The author of the thesis made the following contributions to the publication:

Performed the mathematical analysis of the data (fitting of the data and profile correction) and wrote parts of the manuscript.

Lutz Franzen performed the experiments and wrote the manuscript.

6.3.1 Note

This section shortly summarizes the contributions of the author on the correction of the Raman intensity depth profiles for signal attenuation within a skin surrogate to allow concentration-depth profiling of the skin using Raman microscopy. The full article on this topic can be found elsewhere [188].

6.3.2 Introduction

Investigation of substance penetration thought human skin is an important part for rational drug development addressing the delivery via the skin route. Information of substance distribution inside the distinct skin layers is of special interest since it provides a clearer picture about the absorption mechanism. The analysis of penetration processes in the different layers is a complex and laborious procedure which requires destructive segmentation as well as extraction [189]. Furthermore, the analytical determination lacks spatial resolution. Recently, biophysical techniques like

confocal laser scanning microscopy [190] or two photon microscopy [191] have been proven to be of value by providing spatially resolved information about kinetics and depth of dermal penetration and molecular interaction with the skin. In this context, Raman spectroscopy as a complementary analytical technique to IR spectroscopy bears a lot of potential for the analysis of skin. In contrast to IR, Raman spectroscopy is not constraint by the presence of water. By detecting the frequency shift of scattered laser light after irradiating a sample, chemically selective information of the sample composition is acquired. Furthermore, combining Raman spectroscopy with a confocal microscope provides spatially resolved analysis of the sample. Thus, confocal Raman microscopy is a promising analytical approach for label free and non destructive follow-up of substances within human skin.

Confocal Raman spectroscopy has already been applied for analysis of skin hydration status [192], the effect of penetration enhancers [193] and the epidermal antioxidative potential [194, 195] of skin. However, for rational development and in vitro testing of novel dermal drug delivery systems quantitative analysis of drug penetration processes is mandatory. Unfortunately, so far drug quantification within skin based on Raman microscopy is exacerbated by Raman signal attenuation, as with increasing depth a decrease in Raman signal intensity distorts reliable drug quantification. One approach to overcome the influence of Raman signal attenuation in skin was already performed by relating the intensity of a drug Raman peak to the intensity of a skin derived Raman peak [52]. Unfortunately, as skin is a complex and inhomogeneous biological tissue, the intensity changes of a skin derived peak are due to Raman signal attenuation as well as unpredictable concentration changes of individual compounds within the tissue. For reliable quantification of substances inside human skin by Raman microscopy the exact extent of Raman signal attenuation has to be determined.

Here, we present a novel approach to quantify Raman signal attenuation in human skin. A simplified and reproducible surrogate system mimicking the optical properties of human skin was developed. Caffeine was homogeneously incorporated within the skin surrogate and Raman depth profiles of caffeine were acquired. To address the issue of Raman signal attenuation, these profiles were mathematically fitted and a correction algorithm was derived. Furthermore, excised human skin samples (heat-separated epidermis HSE) were incubated with caffeine and Raman

intensity depth profiles were acquired. Using the surrogate algorithm, these human skin intensity depth profiles were successfully corrected for Raman signal attenuation. Information about the development and characterization of the skin surrogate as well as Raman measurements can be found in [188].

6.3.3 Correction of Raman signal attenuation

One aim of the study is to develop a mathematical procedure which allows to correct Raman intensity depth profiles for signal attenuation within the surrogate. Based on this algorithm, drug concentration profiles with a direct correlation of Raman intensity changes and drug concentration changes shall be realised. In a further step, this procedure is meant to be transferred to skin samples for correction of Raman depth profiles. Based on the drug intensity depth profiles of three different skin surrogates, a mean curve is calculated. In a next step, the decrease in this curve is fitted by an exponential function (Equation 6-5). Exponential fitting is chosen because it is well known that the intensity of electromagnetic waves undergo an exponential decay while penetrating an opaque medium. To avoid overfitting, a simple exponential relationship as presented in Equation 6-5 is applied.

$$D(x) = a\, e^{-\frac{x}{b}} + (1\text{-}a) \qquad \text{Equation 6-5}$$

Least-square regression with constraint $D(0) = 1$ is applied to mathematically describe the decrease of the curve, with x being the depth along the z-axis and x = 0 being the skin surrogate surface (Equation 6-6).

$$D(x) = 0.9997\, e^{-\frac{x}{15.7581}} + (1\text{-}0.9997) \qquad \text{Equation 6-6}$$

The residual standard error is 0.04848, and the variables a and b are significantly different from zero with $p < 0.001$. Equation 6-6 exhibits a representative mathematical description of the drug Raman signal intensity attenuation within the skin surrogate. Figure 6-8 displays the mean drug intensity depth profile and the corresponding fit (Equation 6-6).

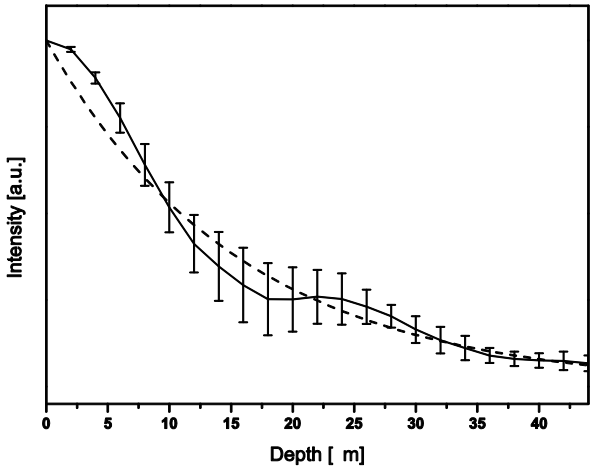

Figure 6-8 Raman mean intensity-depth profile for three skin surrogates after caffeine incorporation fitted by an exponential function (dashed line); mean +/- SD; n = 3

Apart from three single data points within the steepest decrease of the profile, the fit accurately describes the recorded data points. To obtain caffeine intensity depth profiles based on a direct correlation of Raman signal intensity and caffeine concentration in the surrogate, the attenuation based intensity decrease has to be mathematically corrected. Using the attenuation function (Equation 6-6), a signal re-attenuating algorithm is derived with $f(x)$ representing the detected Raman intensity at depth x and $R(x)$ representing the corrected signal.

$$R(x) = f(x) + 1 - (0.9997 * \exp\left(-\frac{x}{15.7581}\right) + (1 - 0.9997)) \qquad \text{Equation 6-7}$$

As the skin surrogate simulates the optical properties of human stratum corneum, the re-attenuation algorithm is supposed to correct drug intensity profiles in human skin samples.

For a proof of concept, the re-attenuation algorithm is used to recalculate caffeine intensity depth profiles in HSE samples. Figure Equation 6-9 shows mean drug intensity depth profiles of two different skin donors based on raw spectral data without any correction (solid line) and after processing the data with the re-attenuation algorithm (dashed line).

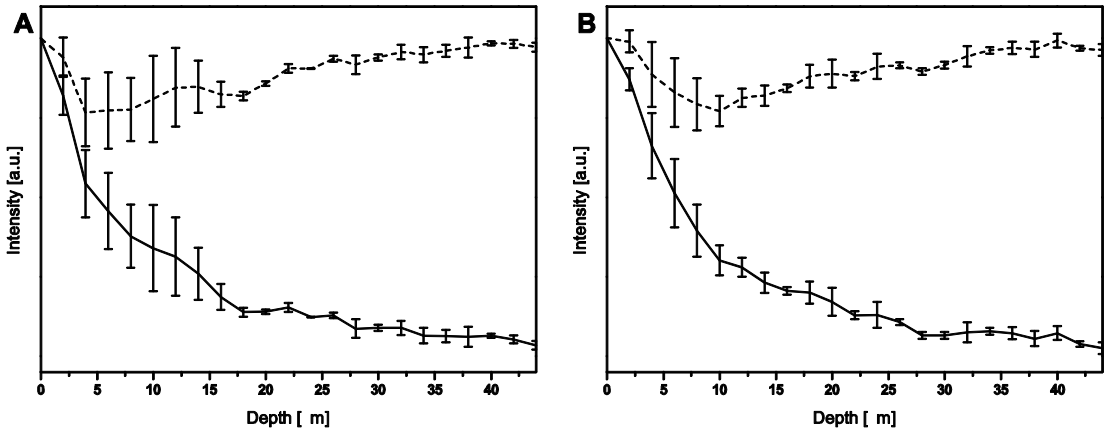

Figure 6-9 Raman mean intensity-depth-profile for donor A and B (solid line) and corrected profile (dashed line) mean +/- SD; n = 3

After correction, the drug intensity depth profiles exhibit a nearly constant Raman intensity, which is directly related to the drug concentration within the whole skin sample. A slight deviance in the first part of the corrected profile is based on a less accurate fit in the steep part of the profile as discussed above. Incubating the skin samples in caffeine solution bypasses the stratum corneum barrier function and facilitates complete soaking with drug solution. Assuming that the caffeine concentration is constant in each depth in the HSE, a calculated constant intensity of the caffeine related Raman peak over depth in HSE is plausible. These results indicate the suitability of the correction algorithm to correct intensity depth profiles for Raman signal attenuation. So far, most studies relied on a relative method to deal with Raman signal attenuation. By applying this method, the intensity of a drug representing Raman peak is related to a skin derived Raman peak [52, 196]. Inconsistencies in Raman peak intensity due to inhomogenities in skin composition are potentially causing uncertainties in depth profiling. Against this background, our novel approach to quantify Raman signal attenuation in a chemical skin surrogate with similar optical properties as skin and to generate a mathematical algorithm for correction of attenuation within skin samples bares many advantages. This approach potentially allows direct quantification of drug in skin tissue solely based on Raman peak intensities. Furthermore, the influence of skin inhomogenities on concentration depth profiles is reduced. On the contrary to the existing qualitative and semi-quantitative studies, this facilitates the acquisition of quantitative concentration depth profiles [52, 193]. However, future studies will investigate the applicability of the developed algorithm on a larger set of different drug depth profiles including a

comparison of Raman spectroscopy results and established standard techniques for the acquisition of drug depth profiles.

6.3.4 Conclusion

A mathematical function for the description of Raman signal attenuation in the skin surrogate was derived from an incubation study with a homogeneously distributed model drug and successfully applied to correct drug intensity depth profiles in human skin. This novel mathematical approach serves as a first step towards a reliable acquisition of drug concentration profiles by confocal Raman microscopy.

7 Summary

Mathematical models for the simulation and prediction of transdermal absorption can be considered as an alternative to ethically problematic in-vivo experiments on humans and animals. Reasonable approaches for prediction are typically based on previously generated experimental data – either to verify the model against a validation set or to use statistical methods to estimate model input parameters. For both cases, high quality *in-vitro* or *in-vivo* data is needed. In the presented work, various studies on the improvement and correction of experimental data were elaborated. Furthermore, mathematical models were developed to provide a better *in-vitro* and *in-vivo* prediction of substance transport through the skin.

First, the influence of the application area on finite dose permeation kinetics was investigated. Here, the *in-vitro* absorption of two model compounds (hydrophilic caffeine (CAF) and lipophilic flufenamic acid (FFA)) was analyzed for finite dosing. By application of different dyes the surface distribution of the different formulations could be visually determined. Using an automated, computer-controlled approach, it was possible to characterize and quantify the exact wetting of formulation. Using this information, the experimental permeation data could be corrected by the area of application. It was found that the permeation of the hydrophilic caffeine is highly dependent on the application area and a correction of the experimental data yielded a significant decrease in the variability of the experimental data. However, a correction of the experimental data of the lipophilic flufenamic acid greatly increased the variability. Skin biopsies after application of the formulations showed that caffeine – in contrast to flufenamic acid – did not distribute laterally. Thus, it can be said that a correction of experimental finite dose permeation data should be conditioned on the chemical properties of the active compound (likely lipophilicity).

During the investigation of the surface distribution of substance formulations, additionally, preliminary studies on the effect of skin topography on the absorption behavior were conducted. Here, a two-dimensional, numerical diffusion model was developed to investigate the *in-vivo* situation applying formulations on wrinkled skin. It could be shown that wrinkles might have an influence on the permeability.

In comparison to an idealized, smooth skin surface without skin furrows and wrinkles simulations have shown a significant increase in the calculated permeability for a wrinkled skin model when assuming perfect formulation coverage of the skin surface. This effect was independent of lipophilicity and size of the permeant. Differences in lag-time were negligible from a therapeutic point of view. If only part of skin surface were covered by formulation, the decrease in permeability for the wrinkled skin model was much more pronounced in comparison to the idealized, smooth skin model.

When investigating finite dosing, a complete mass balance is of great importance to obtain a complete picture of the underlying kinetic processes. In studies concerning in- vitro finite dose penetration of FFA and CAF using a Franz diffusion cell, a mass balance covering various (skin) compartments (donor SC, DSL, lateral skin part) was conducted. For both compounds high amounts of substance were found in the so-called lateral part (part of the test skin outside of the application area). Subsequently, the experimental setup was examined using three mathematical models: A pharmacokinetic model, a microscopic diffusion model and a homogenized diffusion model. The pharmacokinetic model was fitted to the data. The two diffusion models used experimentally determined model input parameters gathered from studies on infinite dosing. All models were able to satisfactorily describe and predict the experimental data. However, in comparison to the other models, the microscopic diffusion model showed the worst performance - the only model without a modeled lateral part. These findings provided evidence not to elide the lateral compartment when modeling *in-vitro* finite dosing.

Since the collection of necessary input parameters for microscopic diffusion models is a difficult and work-intense process, a simple-to-use strategy for the prediction of *in-vivo* penetration was developed. Here, *in-vitro* and *in-vivo* skin penetration experiments of the model compound flufenamic acid solved in an ointment was investigated by means of a mathematical model. Experimental *stratum corneum* concentration-depth profiles (SC-CDP) for various time intervals using two different *in-vitro* systems (Franz diffusion cell, Saarbruecken penetration model) were examined and simulated with the help of a highly optimized three compartment numerical diffusion model and compared to findings of SC-CDPs of the *in-vivo* scenario. Fitted model input parameters (diffusion coefficient and partition coefficient with respect

to the *stratum corneum*) for the *in-vitro* infinite dose case could be used to predict in-use conditions *in-vitro*. Despite apparent differences in calculated partition coefficients between *in-vivo* and *in-vitro* studies, prediction of *in-vivo* scenarios from input parameters calculated from the *in-vitro* case yielded reasonable results.

Traditional techniques for the determination of skin concentration-depth profiles are invasive and lack spatial resolution. Optical methods could overcome these disadvantages. Confocal Raman microscopy bares the potential due to its non-destructive, label-free and chemically selective properties. However, the quantification of a substance inside the skin is impeded by attenuation of the Raman signal. A first try was made to solve this problem. Here, the signal attenuation was corrected for a skin surrogate using a simple algorithm. Subsequently, its applicability was demonstrated by correcting human concentration-depth profiles.

When modeling skin absorption, often the reversible binding to keratins within the skin is neglected. This may have consequences for the determination of partition and diffusion coefficients. A relationship between binding affinity of a drug and its octanol/water partition coefficient has been known for some time. However, the known model to predict binding affinity was only validated using a very limited dataset. Therefore, we extended the known record for binding data with respect to different keratin sources (delipidized SC, bovine hoof and horn, human hair, human nail and sheep wool). It was shown that only keratins originated from delipidized SC, bovine hoof and horn as well as human nail represent useful keratin sources. Moreover, we could confirm the former mentioned relationship for our extended database on keratin binding. It was also possible to predict the binding of ionizable compounds by using the pH-corrected *logD*.

8 Zusammenfassung

Mathematische Modelle zur Simulation und Vorhersage transdermaler Absorption stellen eine Alternative zu ethisch problematischen in-vivo Versuchen an Mensch und Tier dar. Sinnvolle Konzepte zur Vorhersage stützen sich in den allermeisten Fällen auf vorher generierte experimentelle Daten – sei es, um die Qualität des Modells gegen ein Validierungsset zu testen oder um mit Hilfe statistischer Methoden Modelleingabeparameter abzuschätzen. In beiden Fällen ist eine hohe Qualität der erhobenen *in-vitro* oder *in-vivo* Daten von großer Notwendigkeit. Im Rahmen dieser Arbeit wurden verschiedene Studien zur Verbesserung und Korrektur experimenteller Daten erarbeitet und mathematische Modelle entwickelt, um eine bessere *in-vivo* und *in-vitro* Vorhersage des Substanztransports durch die Haut zu ermöglichen.

Zuerst wurde der Einfluss der Applikationsfläche bei finiter Dosierung auf die Permeationskinetik untersucht. Hierbei wurde die Absorption zweier Modellsubstanzen (das hydrophile Kaffein (CAF) und die lipophile Flufenaminsäure (FFA)) in finiter Dosierung in einem in-vitro Aufbau untersucht. Durch eine Einfärbung der wässrigen Substanzformulierungen konnte die Oberflächenbenetzung der aufgetragenen Formulierungen visuell bestimmt werden. Mit Hilfe eines automatisierten, computergesteuerten Ansatzes war es möglich, die genaue Benetzung zu charakterisieren und zu quantifizieren. Mithilfe dieser Informationen konnten die experimentellen Permeationsdaten anhand der Applikationsfläche korrigiert werden. Es zeigte sich, dass die Permeation des hydrophilen Koffeins stark von der Applikationsfläche abhängig ist und eine Korrektur der Daten zu einer deutlichen Abnahme der Variabilität der experimentellen Daten führte. Eine Korrektur der experimentellen Daten der lipophilen Flufenaminsäure erhöhte jedoch die Variabilität dieser Daten stark. Hautbiopsien nach dem Auftragen der Formulierungen zeigten, dass Koffein - im Gegensatz zur Flufenaminsäure - keine laterale Verteilung aufweist. Zusammenfassend kann somit gesagt werden, dass eine Korrektur experimenteller Permeationsdaten bei finiter Dosierung von den chemischen Eigenschaften (wahrscheinlich Lipophilie) abhängig gemacht werden sollte.

Im Rahmen der Untersuchung der Oberflächenverteilung von Substanzformulierungen wurden außerdem erste Untersuchungen zur Auswirkung der Hauttopographie auf das Absorptionsverhalten gemacht. Hierbei wurde ein zweidimensionales, numerisches Diffusionsmodell entwickelt, um die *in-vivo* Situation bei der Applikation von Formulierungen auf faltige Haut zu untersuchen. Es konnte gezeigt werden, dass Hautfalten einen Einfluss auf die Permeabilität haben könnten. Im Vergleich mit einer idealisierten, glatten Hautoberfläche ohne Hautfurchen konnten Simulationen bei einer vollständigen Benetzung der Hautoberfläche eine deutliche Erhöhung der berechneten Permeabilität für ein faltiges Hautmodell zeigen. Dieser Effekt war unabhängig von Lipophilie und Größe des Permeaten. Unterschiede in der Lag-Zeit waren aus therapeutischer Sicht unbedeutend. Bei einer nur teilweisen Benetzung der Hautoberfläche war die Abnahme der Permeabilität für das faltige Hautmodell wesentlich stärker ausgeprägt, als für das idealisierte, glatte Hautmodell.

Bei finiter Dosierung ist eine vollständige Massenbilanz von großer Bedeutung, um ein vollständiges Bild des zugrundeliegenden kinetischen Prozesses zu erhalten. Bei Untersuchungen von in-vitro Penetration von FFA und CAF in finiter Dosierung mit Hilfe einer Franz-Diffusionszelle wurde eine Massenbilanz in verschiedenen (Haut)Kompartimenten (Donor, SC, DSL, lateraler Hautteil) angefertigt. Für beide Substanzen wurden hohe Substanzmengen im sogenannten lateralen Hautteil (Teil der genutzten Versuchshaut außerhalb der Applikationsfläche) gefunden. Der experimentelle Versuchsaufbau wurde anschließend mit Hilfe dreier mathematischer Modelle untersucht: Ein pharmakokinetisches Modell, ein mikroskopisches Diffusionsmodell und ein homogenisiertes Diffusionsmodell. Hierbei wurde das pharmakokinetische Modell an die Daten mit Hilfe einer Fitting-Routing angepasst. Die beiden Diffusionsmodelle nutzten experimentell bestimmte Modelleingabeparameter aus Untersuchungen mit infiniter Dosierung. Alle Modelle konnten die experimentellen Daten zufriedenstellend beschreiben und vorhersagen. Jedoch konnte das mikroskopische Diffusionsmodell die Daten am schlechtesten Beschreiben - das einzige eingesetzte Modell ohne modellierten Lateralteil. Dies gab Hinweise, dass der laterale Hautteil bei der Simulation von finiter Dosierung *in-vitro* nicht vernachlässigt werden sollte.

Da die Bestimmung der notwendigen Eingangsparameter für mikroskopische Diffusionsmodelle einen schwierigen und arbeitsintensiven Prozess darstellt, wurde eine einfach anzuwendende Strategie für die Vorhersage von in-vivo Penetration entwickelt. Hierbei wurden *in-vitro* und *in-vivo* Haut-Penetrationsexperimente der Modellverbindung Flufenaminsäure, die in einer Salbe gelöst war, mittels eines mathematischen Modells untersucht. Hierzu wurden experimentelle *stratum corneum* Konzentrations-Schicht-Tiefenprofile (SC-CDP) für verschiedene Zeitpunkte unter Verwendung von zwei verschiedenen *in-vitro* Testsystemen (Franz-Diffusionszelle, Saarbruecken Penetrationsmodell) untersucht und mit Hilfe eines hochoptimierten, numerischen, drei-Kompartiment Diffusionsmodells simuliert. Diese Ergebnisse wurden anschließend mit *in-vivo* SC-CDPs verglichen. Hierbei konnten Modelleingangsparameter (Diffusionskoeffizienten und Verteilungskoeffizienten) stammend aus Fittings mit in-vitro Experimenten (infinite Dosierung) genutzt werden um eine finite Dosierung *in-vitro* vorherzusagen. Trotz offensichtlicher Unterschiede in den bestimmten Verteilungskoeffizienten für den *in-vivo* und *in-vitro* Fall, konnte eine vernünftige Vorhersage des *in-vivo*-Szenarios von der Eingangsparameter aus dem *in-vitro* Fall berechnet werden.

Traditionelle Techniken zur Bestimmung von Konzentration-Schicht-Tiefenprofilen sind invasiv und bereiten Schwierigkeiten bei der Tiefenbestimmung eines extrahierten Hautsegments. Optische Methoden könnten diese Nachteile überwinden. Die konfokale Raman-Mikroskopie zeigt hierbei durch ihre nicht-destruktiven, markerfreien und chemisch selektiven Eigenschaften ein vielversprechendes Potential. Jedoch wird die Quantifizierung einer Substanz in der Hauttiefe durch die Dämpfung des Raman-Signals behindert. Erste Ansätze zur Lösung dieses Problems wurden erarbeitet. Hierbei wurde die Signaldämpfung in einem Hautsurrogat mit Hilfe eines einfachen Algorithmus korrigiert und seine Anwendbarkeit durch die Korrektur von Humanhaut-Konzentration-Schicht-Tiefenprofilen demonstriert.

Bei der Modellierung von Hautabsorption wird oft die reversible Bindung an Keratin innerhalb der Haut vernachlässigt. Dies kann Konsequenzen für die Bestimmung von Verteilungs- und Diffusionskoeffizienten haben. Ein Verhältnis zwischen Bindungsaffinität eines Wirkstoffes und dessen Oktanol/Wasser-Verteilungskoeffizienten ist schon seit einiger Zeit bekannt. Jedoch wurde ein Vorhersagemodell zur Bindungsaffinität nur auf einem sehr limitierten Datensatz vali-

diert. Deshalb erweiterten wir den bekannten Datensatz um Bindungsdaten bezüglich verschiedenster Keratinquellen (entfettetes SC, Keratin aus Rinderhuf und Horn, Keratin aus menschlichem Haar, Keratin aus menschlichem Nagel und Keratin aus Schafwolle). Es konnte gezeigt werden, dass nur entfettetes SC, Keratin aus Rinderhuf und Horn und Keratin aus dem menschliches Nagel brauchbare Keratinquellen darstellen. Weiterhein konnte das bekannten Verhältnisses zwischen Bindungsaffinität eines Wirkstoffes und dessen Oktanol/Wasser-Verteilungskoeffizienten bestätigt werden. Außerdem war es möglich, die Bindung von ionisierbaren Verbindungen durch Verwendung der pH-korrigierten l*ogD* vorherzusagen.

9 References

[1] K.A. Walters, M.S. Roberts, The Structure and Function of the Skin, in: K.A. Walters (Ed.) Dermatological and Transdermal Formulations, Marcel Dekker, New York Basel, 2002, pp. 1-40.

[2] H. Wagner, N. Zghoul, C.M. Lehr, U.F. Schaefer, Human Skin and Skin Equivalents to Study Dermal Penetration and Permeation, in: C.-M. Lehr (Ed.) Cell Culture Models of Biological Barriers. In-vitro Test Systems for Drug Absorption and Delivery, Taylor & Francis, London, New York, 2002, pp. 289-309.

[3] T.P. Banning, C.M. Heard, Binding of Doxycycline to Keratin, Melanin and Human Epidermal Tissue, Int J Pharm, 235 (2002) 219-227.

[4] R.C. Scott, P.H. Dugard, A.W. Doss, Permeability of Abnormal Rat Skin, J Invest Dermatol, 86 (1986) 201-207.

[5] P.M. Elias, E.R. Cooper, A. Korc, B.E. Brown, Percutaneous Transport in Relation to Stratum Corneum Structure and Lipid Composition, J Invest Dermatol, 76 (1981) 297-301.

[6] P.M. Elias, Epidermal Lipids , Barrier Function, and Desquamation, J Invest Dermatol, 80 (1983) 44-49.

[7] G.B. Kasting, N.D. Barai, Equilibrium Water Sorption in Human Stratum Corneum, J Pharm Sci, 92 (2003) 1624-1631.

[8] H. Gray, Anatomy of the Human Body, Lea & Febiger, Philadelphia, 1918.

[9] H.R. Moghimi, B.W. Barry, A.C. Williams, Stratum Corneum and Barrier Performance: A Model Lamellar Structural Approach, in: R.L. Bronaugh, H. Maibach (Eds.) Drugs – Cosmetics – Mechanisms – Methodology, Marcel Dekker, New York, Basel, Hong Kong, 1999, pp. 515-553.

[10] J. Lademann, H. Richter, U.F. Schaefer, U. Blume-Peytavi, A. Teichmann, N. Otberg, W. Sterry, Hair Follicles – A Long-Term Reservoir for Drug Delivery, Skin Pharmacol Phys, 19 (2006) 232-236.

[11] J. Lademann, H. Richter, A. Teichmann, N. Otberg, U. Blume-Peytavi, J. Luengo, B. Weiß, U.F. Schaefer, C.M. Lehr, R. Wepf, W. Sterry, Nanoparticles – An Efficient Carrier for Drug Delivery into the Hair Follicles, Eur J Pharm Biopharm, 66 (2007) 159-164.

[12] A. Patzelt, H. Richter, F. Knorr, U. Schaefer, C.-M. Lehr, L. Daehne, W. Sterry, J. Lademann, Selective Follicular Targeting by Modification of the Particle Sizes, J Control Release, 150 (2011) 45-48.

[13] T.W. Prow, J.E. Grice, L.L. Lin, R. Faye, M. Butler, W. Becker, E.M.T. Wurm, C. Yoong, T.A. Robertson, H.P. Soyer, M.S. Roberts, Nanoparticles and Microparticles for Skin Drug Delivery, Adv Drug Deliv Rev, 63 (2011) 470-491.

[14] S.K. Rastogi, J. Singh, Lipid Extraction and Transport of Hydrophilic Solutes through Porcine Epidermis, Int J Pharm, 225 (2001) 75-82.

[15] N.A. Monteiro-Riviere, A.O. Inman, V. Mak, P. Wertz, J.E. Riviere, Effect of Selective Lipid Extraction from Different Body Regions on Epidermal Barrier Function, Pharm Res, 18 (2001) 992-998.

[16] P. Talreja, N.K. Kleene, W.L. Pickens, T.F. Wang, G.B. Kasting, Visualization of the Lipid Barrier and Measurement of Lipid Pathlength in Human Stratum Corneum, AAPS PharmSci, 3 (2001) 48-56.

[17] M.R. Prausnitz, S. Mitragotri, R. Langer, Current Status and Future Potential of Transdermal Drug Delivery, Nat Rev Drug Discov, 3 (2004) 115-124.

[18] A.C. Watkinson, J. Hadgraft, K.A. Walters, K.R. Brain, Measurement of Diffusional Parameters in Membranes using ATR-FTIR Spectroscopy, Int J Cosmet Sci, 16 (1994) 199-210.

[19] European Commission, Council Directive on the Approximation of the Laws of the Member States Relating to Cosmetic Products (76/768/EEC), in: OJ L 262, 1976, pp. 169-200.

[20] M.R. Rossignol, The 7th Amendment to the Cosmetics Directive., Atla-Altern Lab Anim, 33 (2005) 19-22.

[21] European Comission, Regulation (EC) No 1907/2006 of the European Parliament and of the Council Concerning the Registration, Evaluation, Authorisation and Restriction of Chemicals (REACH), 2006.

[22] EFSA, EFSA Panel on Plant Protection Products and their Residues (PPR), Guidance on Dermal Absorption, 10 (2012).

[23] European Comission, Review Report for the Active Substance Propineb, in: E.C.H.C.P.D.-. General (Ed.), 2003.

[24] NAFTA, Detailed Review and Harmonisation of Dermal Absorption Practices – Position Paper on Use of in vitro Dermal Absorption Data in Risk Assessment, (2009).

[25] T.J. Franz, Percutaneous Absorption. On the Relevance of In Vitro Data, J Investig Dermatol, 64 (1975) 190-195.

[26] R.L. Bronaugh, R.F. Stewart, Methods for In Vitro Percutaneous Absorption Studies. IV: The Flow-Through Diffusion Cell, J Pharm Sci, 74 (1985) 64-67.

[27] K.R. Brain, K.A. Walters, A.C. Watkinson, Methods for Studying Percutaneous Absorption, in: K.A. Walters (Ed.) Dermatological and Transdermal Formulations, Marcel Dekker AG, New York, 2002, pp. 197-270.

[28] C. Gummer, H. Maibach, Diffusion Cell Design, in: R.L. Bronaugh, H.I. Maibach (Eds.) In Vitro Percutaneous Absorption: Principles, Fundamentals, and Applications, CRC Press Boca Raton, FL, 1991, pp. 7-16.

[29] R.C. Scott, H.M. Clowes, In Vitro Percutaneous Absorption Experiments: A Guide to the Technique for Use in Toxicology Assessments, Toxicol Mech Methods, 2 (1992) 113-123.

[30] J. Krüse, D. Golden, S. Wilkinson, F. Williams, S. Kezic, J. Corish, Analysis, Interpretation, and Extrapolation of Dermal Permeation Data Using Diffusion-based Mathematical Models, J Pharm Sci, 96 (2007) 682-703.

[31] Y.G. Anissimov, M.S. Roberts, Diffusion Modeling of Percutaneous Absorption Kinetics. 1. Effects of Flow Rate, Receptor Sampling Rate, and Viable Epidermal Resistance for a Constant Donor Concentration, J Pharm Sci, 88 (1999) 1201-1209.

[32] D.R. Friend, In Vitro Skin Permeation Techniques, J Control Release, 18 (1992) 235-248.

[33] L.K. Pershing, J. Corlett, C. Jorgensen, In Vivo Pharmacokinetics and Pharmacodynamics of Topical Ketoconazole and Miconazole in Human Stratum Corneum, Antimicrob Agents Chemother, 38 (1994) 90-95.

[34] V.P. Shah, G.L. Flynn, A. Yacobi, H.I. Maibach, C. Bon, N.M. Fleischer, T.J. Franz, S.A. Kaplan, J. Kawamoto, L.J. Lesko, J.P. Marty, L.K. Pershing, H. Schaefer, J.A. Sequeira, S.P. Shrivastava, J. Wilkin, R.L. Williams, Bioequivalence of Topical Dermatological Dosage Forms - Methods of Evaluation of Bioequivalence, Pharm Res, 15 (1998) 167-171.

[35] A. Rougier, D. Dupuis, C. Lotte, In Vivo Correlation Between Stratum Corneum Reservoir Function and Percutaneous Absorption, J Invest Dermatol, 81 (1983) 275-278.

[36] L.M. Russell, R.H. Guy, Measurement and Prediction of the Rate and Extent of Drug Delivery into and through the Skin, Expert Opin Drug Deliv, 6 (2009) 355-369.

[37] T. Hahn, S. Hansen, D. Neumann, K.H. Kostka, C.M. Lehr, L. Muys, U.F. Schaefer, Infrared Densitometry: A Fast and Non-Destructive Method for Exact Stratum Corneum Depth Calculation for in vitro Tape-Stripping, Skin Pharmacol Phys, 23 (2010) 183-192.

[38] H. Wagner, K.H. Kostka, C.M. Lehr, U.F. Schaefer, Drug distribution in Human Skin Using Two Different In Vitro Test Systems: Comparison With In Vivo Data, Pharm Res, 17 (2000) 1475-1481.

[39] A. Melero, T. Hahn, U.F. Schaefer, M. Schneider, In Vitro Human Skin Segmentation and Drug Concentration-Skin Depth Profiles, in: K. Turksen (Ed.) Permeability barrier, Humana Press, 2011, pp. 33-50.

[40] J.J. Escobar-Chavez, V. Merino-Sanjuán, M. López-Cervantes, Z. Urban-Morlan, E. Piñón-Segundo, D. Quintanar-Guerrero, A. Ganem-Quintanar, The Tape-Stripping Technique as a Method for Drug Quantification in Skin, J Pharm Pharm Sci, 11 (2008) 104-130.

[41] C.S. King, S.P. Barton, S. Nicholls, R. Marks, The Change in Properties of the Stratum Corneum as a Function of Depth, Br J Dermatol, 100 (1979) 165-172.

[42] S.J. Bashir, A.-L. Chew, A. Anigbogu, F. Dreher, H.I. Maibach, Physical and Physiological Effects of Stratum Corneum Tape Stripping, Skin Res Technol, 7 (2001) 40-48.

[43] U. Jacobi, H.J. Weigmann, J. Ulrich, W. Sterry, J. Lademann, Estimation of the Relative Stratum Corneum Amount Removed by Tape Stripping, Ski Res Technol, 11 (2005) 91-96.

[44] H. Wagner, K.H. Kostka, C.M. Lehr, U.F. Schaefer, Human Skin Penetration of Flufenamic Acid: In Vivo/In Vitro Correlation (Deeper Skin Layers) for Skin Samples From the Same Subject, J Invest Dermatol, 118 (2002) 540-544.

[45] H. Wagner, K.H. Kostka, C.M. Lehr, U.F. Schaefer, Interrelation of Permeation and Penetration Parameters Obtained from In Vitro Experiments with Human Skin and Skin Equivalents, J Control Release, 75 (2001) 283-295.

[46] R. Alvarez-Román, A. Naik, Y. Kalia, H. Fessi, R. Guy, Visualization of Skin Penetration Using Confocal Laser Scanning Microscopy, Eur J Pharm Biopharm, 58 (2004) 301-316.

[47] N. Dayan, E. Touitou, Carriers for Skin Delivery of Trihexyphenidyl Hcl: Ethosomes vs. Liposomes, Biomaterials, 21 (2000) 1879-1885.

[48] P.J. Caspers, G.W. Lucassen, G.J. Puppels, Combined In Vivo Confocal Raman Spectroscopy and Confocal Microscopy of Human Skin, Biophys J, 85 (2003) 572-580.

[49] J. Wohlrab, A. Vollmann, S. Wartewig, W.C. Marsch, R. Neubert, Noninvasive Characterization of Human Stratum Corneum of Undiseased Skin of Patients with Atopic Dermatitis and Psoriasis as Studied by Fourier Transform Raman Spectroscopy, Biopolymers, 62 (2001) 141-146.

[50] A. Nijssen, T.C. Bakker Schut, F. Heule, P.J. Caspers, D.P. Hayes, M.H.A. Neumann, G.J. Puppels, Discriminating Basal Cell Carcinoma from its Surrounding Tissue by Raman Spectroscopy, J Invest Dermatol, 119 (2002) 64-69.

[51] A. Tfayli, O. Piot, M. Manfait, Confocal Raman Microspectroscopy on Excised Human Skin: Uncertainties in Depth Profiling and Mathematical Correction Applied to Dermatological Drug Permeation, J Biophotonics, 1 (2008) 140-153.

[52] A. Tfayli, O. Piot, F. Pitre, M. Manfait, Follow-Up of Drug Permeation through Excised Human Skin with Confocal Raman Microspectroscopy, Eur Biophys J, 36 (2007) 1049-1058.

[53] S.E. Cross, R. Jiang, H.A.E. Benson, M.S. Roberts, Can Increasing the Viscosity of Formulations be Used to Reduce the Human Skin Penetration of the Sunscreen Oxybenzone?, J Invest Dermatol, 117 (2001) 147-150.

[54] OECD, Guideline for the Testing of Chemicals. Skin Absorption: In Vitro Method, 428, (2004).

[55] OECD, Guidance Document for the Conduct of Skin Absorption Studies. OECD Series on Testing and Assessment. Number 28, (2004).

[56] European Commission, Basic Criteria for the In Vitro Assessement of Dermal Absorption of Cosmetic Ingredients, in: S.C.o.C. Products (Ed.), 2006.

[57] H.E. Buist, J.A. van Burgsteden, A.P. Freidig, W.J.M. Maas, J.J.M. van de Sandt, New In Vitro Dermal Absorption Database and the Prediction of Dermal Absorption Under Finite Conditions for Risk Assessment Purposes, Regul Toxicol Pharmacol, 57 (2010) 200-209.

[58] H.F. Frasch, A.M. Barbero, J.M. Hettick, J.M. Nitsche, Tissue Binding Affects the Kinetics of Theophylline Diffusion Through the Stratum Corneum Barrier Layer of Skin, J Pharm Sci, 100 (2011) 2989-2995.

[59] R.H. Guy, J. Hadgraft, D.A.W. Bucks, Transdermal Drug Delivery and Cutaneous Metabolism, Xenobiotica, 17 (1987) 325-343.

[60] M.B. Reddy, R.H. Guy, A.L. Bunge, Does Epidermal Turnover Reduce Percutaneous Penetration?, Pharm Res, 17 (2000) 1414-1419.

[61] Y. Dancik, Y.G. Anissimov, O.G. Jepps, Convective Transport of Highly Plasma Protein Bound Drugs Facilitates Direct Penetration Into Deep Tissues After Topical Application, Brit J Clin Pharmaco, 73 (2012) 564-578.

[62] Y.G. Anissimov, M.S. Roberts, Diffusion Modeling of Percutaneous Absorption Kinetics: 3. Variable Diffusion and Partition Coefficients, Consequences for Stratum Corneum Depth Profiles and Desorption Kinetics, J Pharm Sci, 93 (2004) 470-487.

[63] J. Crank, in: The Mathematics of Diffusion, Oxford University Press, London, 1975, pp. 49-53.

[64] B.D. Anderson, P. Raykar, Solute Structure–Permeability Relationships in Human Stratum Corneum, J Invest Dermatol, 93 (1989) 280-286.

[65] S. Hansen, L. C-M, U.F. Schaefer, Improved Input Parameters for Diffusion Models of Skin Absorption, Adv Drug Deliv Rev, 65 (2013) 251-264.

[66] Y.G. Anissimov, O.G. Jepps, Y. Dancik, M.S. Roberts, Mathematical and Pharmacokinetic Modelling of Epidermal and Dermal Transport Processes, Adv Drug Deliv Rev, (2012) 1-22.

[67] B. Anderson, W. Higuchi, P. Raykar, Heterogeneity Effects on Permeability–Partition Coefficient Relationships in Human Stratum Corneum, Pharm Res, 5 (1988) 566-573.

[68] R.J. Scheuplein, Mechanism of Percutaneous Absorption. II. Transient Diffusion and the Relative Importance of Various Routes of Skin Penetration, J Invest Dermatol, 48 (1967) 79-88.

[69] A.S. Michaels, S.K. Chandrasekaran, J.E. Shaw, Drug Permeation Through Human Skin: Theory and In Vitro Experimental Measurement., AIChE J, 21 (1975) 985-996.

[70] K. Sloan, S. Wasdo, J. Rautio, Design for Optimized Topical Delivery: Prodrugs and a Paradigm Change, Pharm Res, 23 (2006) 2729-2747.

[71] Q. Zhang, P. Li, M.S. Roberts, Maximum Transepidermal Flux for Similar Size Phenolic Compounds is Enhanced by Solvent Uptake into the Skin, J Control Release, 154 (2011) 50-57.

[72] V. Fiserova-Bergerova, J.T. Pierce, P.O. Droz, Dermal Absorption Potential of Industrial Chemicals: Criteria for Skin Notation, Am J Ind Med, 17 (1990) 617-635.

[73] T.E. McKone, R.A. Howd, Estimating Dermal Uptake of Nonionic Organic Chemicals from Water and Soil: I. Unified Fugacity-Based Models for Risk Assessments, Risk Anal, 12 (1992) 543-557.

[74] R.O. Potts, R.H. Guy, Predicting Skin Permeability, Pharm Res, 9 (1992) 663-669.

[75] B.M. Magnusson, Y.G. Anissimov, S.E. Cross, M.S. Roberts, Molecular Size as the Main Determinant of Solute Maximum Flux Across the Skin, J Invest Dermatol, 122 (2004) 993-999.

[76] E.R. Cooper, B. Berner, Finite Dose Pharmacokinetics of Skin Penetration, J Pharm Sci, 74 (1985) 1100-1102.

[77] H.S. Carslow, J.C. Jaeger, Conduction of Heat in Solids, Clarendon Press, Oxford, 1959.

[78] G.B. Kasting, Kinetics of Finite Dose Absorption Through Skin 1. Vanillylnonanamide, J Pharm Sci, 90 (2001) 202-212.

[79] R.P. Brent, Algorithms for Minimization Without Derivatives, in, Prentice-Hall, Englewood Cliffs, 1973.

[80] R.J. Scheuplein, L.W. Ross, Mechanism of Percutaneous Absorption. V. Percutaneous Absorption of Solvent Deposited Solids, J Invest Dermatol, 62 (1974) 353-360.

[81] A. Naegel, S. Hansen, D. Neumann, C.M. Lehr, U.F. Schaefer, G. Wittum, M. Heisig, In-silico Model of Skin Penetration Based on Experimentally Determined Input Parameters. Part II: Mathematical Modelling of In-Vitro Diffusion Experiments. Identification of Critical Input Parameters, Eur J Pharm Biopharm, 68 (2008) 368-379.

[82] A. Naegel, T. Hahn, U.F. Schaefer, C.M. Lehr, M. Heisig, G. Wittum, Finite Dose Skin Penetration: A Comparison of Concentration-Depth Profiles from Experiment and Simulation, Comput Visual Sci, 14 (2012) 327-339.

[83] K. McCarley, A. Bunge, Pharmacokinetic Models of Dermal Absorption, J Pharm Sci, 90 (2001) 1699-1719.

[84] Y. Seta, A.H. Ghanem, W.I. Higuchi, S. Borsadia, C.R. Behl, A.W. Malick, Physical Model Approach to Understanding Finite Dose Transport and Uptake of Hydrocortisone in Hairless Guinea-pig Skin, Int J Pharm, 81 (1992) 89-99.

[85] R. Guy, J. Hadgraft, H. Maibach, A Pharmacokinetic Model for Percutaneous Absorption, Int J Pharm, 11 (1982) 119-129.

[86] K. Kubota, A Compartment Model for Percutaneous Drug Absorption, J Pharm Sci, 80 (1991) 502-504.

[87] R.H. Guy, J. Hadgraft, Transdermal Drug Delivery: A Simplified Pharmacokinetic Approach, Int J Pharm, 24 (1985) 267-274.

[88] S.M. Wallace, G. Barnett, Pharmacokinetic Analysis of Percutaneous Absorption: Evidence of Parallel Penetration Pathways for Methotrexate, J Pharmacokinet Biopharm, 6 (1978) 315-325.

[89] M. Davies, R.U. Pendlington, L. Page, C.S. Roper, D.J. Sanders, C. Bourner, C.K. Pease, C. MacKay, Determining Epidermal Disposition Kinetics for Use in an Integrated Nonanimal Approach to Skin Sensitization Risk Assessment, Toxicol Sci, 119 (2011) 308-318.

[90] K. McCarley, A. Bunge, Physiologically Relevant Two-compartment Pharmacokinetic Models for Skin, J Pharm Sci, 89 (2000) 1212-1235.

[91] M. Reddy, K. McCarley, A. Bunge, Physiologically Relevant One-Compartment Pharmacokinetic Models for Skin. 2. Comparison of Models when Combined with a Systemic Pharmacokinetic Model, J Pharm Sci, 87 (2000) 482-490.

[92] K. George, A Two-Dimensional Mathematical Model of Non-Linear Dual-Sorption of Percutaneous Drug Absorption, Biomed Eng Online, 4 (2005) 15.

[93] L.L. Wearley, K. Tojo, Y.W. Chien, A Numerical Approach to Study the Effect of Binding on the Lontophoretic Transport of a Series of Amino Acids, J Pharm Sci, 79 (1990) 992-998.

[94] K. Kubota, F. Dey, S.A. Matar, E.H. Twizell, A Repeated-Dose Model of Percutaneous Drug Absorption, Appl Math Model 26 (2002) 529-544.

[95] R.T. Kurnik, R.O. Potts, Modeling of Diffusion and Crystal Dissolution in Controlled Release Systems, J Control Release, 45 (1997) 257-264.

[96] S. Hansen, A. Naegel, M. Heisig, G. Wittum, D. Neumann, K.H. Kostka, P. Meiers, C.M. Lehr, U.F. Schaefer, The Role of Corneocytes in Skin Transport Revised - A Combined Computational and Experimental Approach, Pharm Res, 26 (2009) 1379-1397.

[97] I. Muha, A. Naegel, S. Stichel, A. Grillo, M. Heisig, G. Wittum, Effective Diffusivity in Membranes with Tetrakaidekahedral Cells and Implications for the Permeability of Human Stratum Corneum, J Membr Sci, 368 (2010) 18-25.

[98] J.M. Nitsche, H.F. Frasch, Dynamics of Diffusion with Reversible Binding in Microscopically Heterogeneous Membranes: General Theory and Applications to Dermal Penetration, Chem Eng Sci, 66 (2011) 2019-2041.

[99] A.M. Barbero, H.F. Frasch, Modeling of Diffusion with Partitioning in Stratum Corneum Using a Finite Element Model, Ann Biomed Eng, 33 (2005) 1281-1292.

[100] M. Heisig, R. Lieckfeldt, G. Wittum, G. Mazurkevich, G. Lee, Non Steady-State Descriptions of Drug Permeation Through Stratum Corneum. I. The Biphasic Brick-And-Mortar Model, Pharm Res, 13 (1996) 421-426.

[101] A. Naegel, M. Heisig, G. Wittum, Detailed Modeling of Skin Penetration—An Overview, Adv Drug Deliver Rev, 65 (2013) 191-207.

[102] F. Frasch, A.M. Barbero, Application of Numerical Methods for Diffusion-based Modeling of Skin Permeation, Adv Drug Deliver Rev, (2012) 1-13.

[103] G. Flynn, Physicochemical Determinants of Skin Absorption, in: T. Gerrity, C. Henry (Eds.) Principle of Route-to-route Extrapolation for Risk Assessment., Elsevier, New York, 1990, pp. 93-127.

[104] A. Wilschut, W.F. ten Berge, P.J. Robinson, T.E. McKone, Estimating Skin Permeation. The Validation of Five Mathematical Skin Permeation Models, Chemosphere, 30 (1995) 1275-1296.

[105] H. Patel, W.t. Berge, M.T.D. Cronin, Quantitative Structure–activity Relationships (QSARs) for the Prediction of Skin Permeation of Exogenous Chemicals, Chemosphere, 48 (2002) 603-613.

[106] M.S. Roberts, W.J. Pugh, J. Hadgraft, Epidermal Permeability: Penetrant Structure Relationships. 2. The Effect of H-bonding Groups in Penetrants on their Diffusion through the Stratum Corneum, Int J Pharm, 132 (1996) 23-32.

[107] W.J. Pugh, M.S. Roberts, J. Hadgraft, Epidermal Permeability — Penetrant Structure Relationships: 3. The Effect of Hydrogen Bonding Interactions and Molecular Size on Diffusion Across the Stratum Corneum, Int J Pharm, 138 (1996) 149-165.

[108] W.J. Pugh, I.T. Degim, J. Hadgraft, Epidermal Permeability–penetrant Structure Relationships: 4, QSAR of Permeant Diffusion Across Human Stratum Corneum in Terms of Molecular Weight, H-bonding and Electronic Charge, Int J Pharm, 197 (2000) 203-211.

[109] T. Değïm, J. Hadgraft, S. İlbasmiş, Y. Özkan, Prediction of Skin Penetration Using Artificial Neural Network (ANN) modeling, J Pharm Sci, 92 (2003) 656-664.

[110] C.W. Lim, S.-i. Fujiwara, F. Yamashita, M. Hashida, Prediction of Human Skin Permeability Using a Combination of Molecular Orbital Calculations and Artificial Neural Network, Biol Pharm Bull, 25 (2002) 361-366.

[111] D. Neumann, O. Kohlbacher, C. Merkwirth, T. Lengauer, A Fully Computational Model for Predicting Percutaneous Drug Absorption, J Chem Inf Model 46 (2005) 424-429.

[112] F. Yamashita, M. Hashida, Mechanistic and Empirical Modeling of Skin Permeation of Drugs, Adv Drug Deliv Rev, 55 (2003) 1185-1199.

[113] A. Henning, D. Neumann, K.H. Kostka, C.M. Lehr, U.F. Schaefer, Influence of Human Skin Specimens Consisting of Different Skin Layers on the Result of in vitro Permeation Experiments, Skin Pharmacol Phys, 21 (2008) 81-88.

[114] G.B. Kasting, M.A. Miller, Kinetics of Finite Dose Absorption through Skin 2: Volatile Compounds, J Pharm Sci, 95 (2006) 268-280.

[115] Scientific Committee on Consumer Products, Basic Criteria for the In Vitro Assessment of Dermal Absorption of Cosmetic Ingredients, in, 2006.

[116] J.J.M. van de Sandt, J.A. van Burgsteden, S. Cage, P.L. Carmichael, I. Dick, S. Kenyon, G. Korinth, F. Larese, J.C. Limasset, W.J.M. Maas, L. Montomoli, J.B. Nielsen, J.P. Payan, E. Robinson, P. Sartorelli, K.H. Schaller, S.C. Wilkinson, F.M. Williams, In Vitro Predictions of Skin Absorption of Caffeine, Testosterone, And Benzoic Acid: A Multi-Centre Comparison Study, Regul Toxicol Pharmacol., 39 (2004) 271-281.

[117] J. Lademann, A. Rudolph, U. Jacobi, H.J. Weigmann, H. Schaefer, W. Sterry, M. Meinke, Influence of Nonhomogeneous Distribution of Topically Applied UV Filters on Sun Protection Factors, J Biomed Opt, 9 (2004) 1358-1362.

[118] A. Teichmann, M. Pissavini, H. Richter, J. Lademann, L. Ferrero, A. Dehais, L. Zastrow, Investigation of the Homogeneity of the Distribution of Sunscreen Formulations on the Human Skin: Characterization and Comparison of Two Different Methods, J Biomed Opt, 11 (2006) 064005-064005-064008.

[119] J. Lademann, H. Richter, K. Golz, L. Zastrow, W. Sterry, A. Patzelt, Influence of Microparticles on the Homogeneity of Distribution of Topically Applied Substances, Skin Pharmacol Phys, 21 (2008) 274-282.

[120] S.M. Harrison, B.W. Barry, P.H. Dugard, Effects of Freezing on Human Skin Permeability, J Pharm Pharmacol, 36 (1984) 261-262.

[121] S. Schreiber, A. Mahmoud, A. Vuia, M.K. Ruebbelke, E. Schmidt, M. Schaller, H. Kandárová, A. Haberland, U.F. Schaefer, U. Bock, H.C. Korting, M. Liebsch, M. Schaefer-Korting, Reconstructed Epidermis Versus Human and Animal Skin in Skin Absorption Studies, Toxicol in Vitro, 19 (2005) 813-822.

[122] J. Swarbrick, G. Lee, J. Brom, Drug Permeation Through Human Skin: I. Effect of Storage Conditions of Skin, J Invest Dermatol, 78 (1982) 63-66.

[123] A.M. Kligman, E. Christophers, Preparation of Isolated Sheets of Human Stratum Corneum, Arch Dermatol, 88 (1963) 702-705.

[124] M. Schaefer-Korting, U. Bock, W. Diembeck, H.-J. Duesing, A. Gamer, E. Haltner-Ukomadu, C. Hoffmann, M. Kaca, H. Kamp, S. Kersen, M. Kietzmann, H.C. Korting, H.-U. Kraechter, C.-M. Lehr, M. Liebsch, A. Mehling, C. Mueller-Goymann, F. Netzlaff, F. Niedorf, M.K. Ruebbelke, U. Schaefer, E. Schmidt, S. Schreiber, H. Spielmann, A. Vuia, M. Weimer, The Use of Reconstructed Human Epidermis for Skin Absorption Testing: Results of the Validation Study, Altern Lab Anim, 36 (2008) 161-187.

[125] S. Hansen, A. Henning, A. Naegel, M. Heisig, G. Wittum, D. Neumann, K.H. Kostka, J. Zbytovska, C.M. Lehr, U.F. Schaefer, In-Silico Model of Skin Penetration Based on Experimentally Determined Input Parameters. Part I: Experimental Determination of Partition and Diffusion Coefficients, Eur J Pharm Biopharm, 68 (2008) 352-367.

[126] G.H. Joblove, Color spaces for computer graphics, SIGGRAPH Comput Graph., 12 (1978) 20-25.

[127] H. Okamoto, M. Hashida, H. Sezaki, Structure-activity Relationship of 1-Alkyl- or 1-Alkenylazacycloalkanone Derivatives as Percutaneous Penetration Enhancers, J Pharm Sci, 77 (1988) 418-424.

[128] Y.G. Anissimov, M.S. Roberts, Diffusion Modeling of Percutaneous Absorption Kinetics: 2. Finite Vehicle Volume and Solvent Deposited Solids, J Pharm Sci, 90 (2001) 504-520.

[129] E. Jones, T. Oliphant, P. Peterson, SciPy: Open Source Scientific Tools for Python, in, 2001.

[130] S.C. Wilkinson, W.J.M. Maas, J.B. Nielsen, L.C. Greaves, J.J.M. van de Sandt, F.M. Williams, Interactions of Skin Thickness and Physicochemical Properties of Test Compounds in Percutaneous Penetration Studies, Int Arch Occup Environ Health, 79 (2006) 405-413.

[131] S. Majumdar, J. Thomas, S. Wasdo, K.B. Sloan, The Effect of Water Solubility of Solutes on their Flux through Human Skin In Vitro, Int J Pharm, 329 (2007) 25-36.

[132] J. Thomas, S. Majumdar, S. Wasdo, A. Majumdar, K.B. Sloan, The Effect of Water Solubility of Solutes on their Flux through Human Skin In Vitro: An Extended Flynn Database Fitted to the Roberts-Sloan Equation, Int J Pharm, 339 (2007) 157-167.

[133] M.E. Johnson, D.A. Berk, D. Blankschtein, D.E. Golan, R.K. Jain, R.S. Langer, Lateral Diffusion of Small Compounds in Human Stratum Corneum and Model Lipid Bilayer Systems, Biophys J, 71 (1996) 2656-2668.

[134] P.A. Lehman, S.G. Raney, T.J. Franz, Percutaneous Absorption in Man: In Vitro-in vivo Correlation, Skin Pharmacol Phys, 24 (2011) 224-230.

[135] S.A. Hotchkiss, M.A.J. Chidgey, S. Rose, J. Caldwell, Percutaneous Absorption of Benzyl Acetate through Rat Skin In Vitro. 1. Validation of an In Vitro Model Against In Vivo Data, Food Chem Toxicol, 28 (1990) 443-447.

[136] F. Dreher, F. Fouchard, C. Patouillet, M. Andrian, J.T. Simonnet, F. Benech-Kieffer, Comparison of Cutaneous Bioavailability of Cosmetic Preparations Containing Caffeine or Alpha-Tocopherol Applied on Human Skin Models or Human Skin Ex Vivo at Finite Doses, Skin Pharmacol Appl Skin Physiol, 15 (2002) 40-58.

[137] C.M. Gee, J.A. Nicolazzo, A.C. Watkinson, B.C. Finnin, Assessment of the Lateral Diffusion and Penetration of Topically Applied Drugs in Humans Using a Novel Concentric Tape Stripping Design, Pharm Res, (2012).

[138] U. Jacobi, S. Schanzer, H.J. Weigmann, A. Patzelt, T. Vergou, W. Sterry, J. Lademann, Pathways of Lateral Spreading, Skin Pharmacol Phys, 24 (2011) 231-237.

[139] G. Schicksnus, C.C. Muller-Goymann, Lateral Diffusion of Ibuprofen in Human Skin During Permeation Studies, Skin Pharmacol Phys, 17 (2004) 84-90.

[140] G.B. Kasting, M.A. Miller, V.D. Bhatt, A Spreadsheet-Based Method for Estimating the Skin Disposition of Volatile Compounds: Application to N,N-Diethyl-m-Toluamide (DEET). J Occup Environ Hyg, 5 (2008) 633-644.

[141] M.S. Roberts, S.E. Cross, Y.G. Anissimov, Factors Affecting the Formation of a Skin Reservoir for Topically Applied Solutes, Skin Pharmacol Phys, 17 (2004) 3-16.

[142] A.F. Ourique, A. Melero, C. de Bona da Silva, U.F. Schaefer, A.R. Pohlmann, S.S. Guterres, C.M. Lehr, K.H. Kostka, R.C. Beck, Improved Photostability and Reduced Skin Permeation of Tretinoin: Development of a Semisolid Nanomedicine, Eur J Pharm Biopharm, 79 (2011) 95-101.

[143] J. Luengo, B. Weiss, M. Schneider, A. Ehlers, F. Stracke, K. Konig, K.H. Kostka, C.M. Lehr, U.F. Schaefer, Influence of Nanoencapsulation on Human Skin Transport of Flufenamic Acid, Skin Pharmacol Phys, 19 (2006) 190-197.

[144] U. Schaefer, An Ex-Vivo Model for the Study of Drug Penetration into Human Skin, Pharm Res, 13 (Suppl.) (1996).

[145] T. Hahn, D. Selzer, D. Neumann, K.H. Koska, C.M. Lehr, U.F. Schaefer, Influence of the Application Area on Finite Dose Permeation in Relation to Drug Type Applied, Exp Dermatol, 21 (2012) 221–235.

[146] E.E. Bolton, Y. Wang, P.A. Thiessen, S.H. Bryant, Chapter 12 PubChem: Integrated Platform of Small Molecules and Biological Activities, in: A.W. Ralph, C.S. David (Eds.) Annu Rep Comput Chem, Elsevier, 2008, pp. 217-241.

[147] D.R. Lide, Handbook of Chemistry and Physics, CRC Press Inc, 2008.

[148] R. Manitz, W. Lucht, K. Strehmel, R. Weiner, R. Neubert, On Mathematical Modeling of Dermal and Transdermal Drug Delivery, J Pharm Sci, 87 (1998) 873–879.

[149] J.E. Rim, P.M. Pinsky, W.W. van Osdol, Multiscale Modeling Framework of Transdermal Drug Delivery, Ann Biomed Eng, 37 (2009) 1217-1229.

[150] Y.G. Anissimov, M.S. Roberts, Diffusion Modelling of Percutaneous Absorption Kinetics: 4. Effects of A Slow Equilibration Process Within Stratum Corneum on Absorption and Desorption Kinetics, J Pharm Sci, 98 (2009) 772-781.

[151] M.A. Miller, V. Bhatt, G.B. Kasting, Dose and Airflow Dependence of Benzyl Alcohol Disposition on Skin, J Pharm Sci, 95 (2006) 281-291.

[152] A. Santhanam, M.A. Miller, G.B. Kasting, Absorption and Evaporation of N,N-diethyl-m-toluamide from Human Skin In Vitro, Toxicol Appl Pharm, 204 (2005) 81-90.

[153] M.A. Miller, G.B. Kasting, Toward a Better Understanding of Pesticide Dermal Absorption: Diffusion Model Analysis of Parathion Absorption in Vitro and in Vivo, J Toxicol Environ Health – Part A, Current Issues, 73 (2010) 284-300.

[154] K. Kubota, Finite Dose Percutaneous Drug Absorption: A BASIC Program for the Solution of the Diffusion Equation., Comput Biomed Res, 24 (1991) 196-207.

[155] K. Kubota, T. Yamada, Finite Dose Percutaneous Drug Absorption: Theory and Its Application to In Vitro Timolol Permeation, J Pharm Sci, 79 (1990) 1015-1019.

[156] C.G.J. Hayden, S.E. Cross, C. Anderson, N.A. Saunders, M.S. Roberts, Sunscreen Penetration of Human Skin and Related Keratinocyte Toxicity after Topical Application, Skin Pharmacol Phys, 18 (2005) 170-174.

[157] D. Kim, M.E. Andersen, L.A. Nylander-French, Dermal Absorption and Penetration of Jet Fuel Components in Humans, Toxicol Lett, 165 (2006) 11-21.

[158] European Comission, Review report for the active substance flufenacet, in: E.C.H.C.P. Directorate-General (Ed.), 2003.

[159] T.J. Franz, P.A. Lehman, S.F. Franz, H. North-Root, J.L. Demetrulias, C.K. Kelling, S.J. Moloney, S.D. Gettings, Percutaneous Penetration of N-Nitrosodiethanolamine Through Human Skin (in Vitro): Comparison of Finite and Infinite Dose Applications from Cosmetic Vehicles, Fund Appl Toxicol, 21 (1993) 213-221.

[160] D. Selzer, M.M.A. Abdel-Mottaleb, T. Hahn, U.F. Schaefer, D. Neumann, Finite and Infinite Dosing: Difficulties in Measurements, Evaluations and Predictions, Adv Drug Deliver Rev, 65 (2013) 278-294.

[161] H. Wagner, Charakterisierung des Arzneistofftransportes in Humanhaut unter In-vitro und In-vivo Bedingungen Sowie unter Beruecksichtigung des Einflusses Zweier In-vitro Testsysteme, in: PhD Thesis, Saarland University, Saarbruecken, Germany, 2001, pp. 235.

[162] OECD, Guidance Notes on Dermal Absorption, 428, (2010).

[163] World Health Organization, Dermal Absorption, in: Environmental Health Criteria 235, 2006, pp. 90-103.

[164] European Food Safety Authority, Guidance on Dermal Absorption, EFSA J, 10 (2012) 1-30.

[165] D. Selzer, T. Hahn, A. Naegel, M. Heisig, K.H. Kostka, C.M. Lehr, D. Neumann, U.F. Schaefer, G. Wittum, Finite Dose Skin Mass Balance Including the Lateral Part: Comparison Between Experiment, Pharmacokinetic Modeling and Diffusion Models, J Control Release, 165 (2013) 119-128.

[166] D. Borchert, Methoden zur Untersuchung der Simultanen Penetration von Arzneistoffen und Vehikelbestandteilen aus Salben in Exzidierter Humanhaut, in: PhD Thesis, Saarland University, Saarbruecken, 1994.

[167] F. Theobald, In-vitro Methoden zur Biopharmazeutischen Qualitaetspruefung von Dermatika unter Beruecksichtigung der Lipidzusammensetzung des Stratum Corneum., in: PhD Thesis, Saarland University, Saarbruecken, 1998.

[168] FDA, Guidance for Industry. Topical Dermatological Drug Product NDAs and ANDAs – In-vivo Bioavailability, Bioequivalance, In-vitro Release, and Associated Studie, in: C.f.D.E.a. Research (Ed.), 1998, pp. 1-19.

[169] W.I. Higuchi, Analysis of Data on the Medicament Release from Ointments, J Pharm Sci, 51 (1962) 802-804.

[170] A. Babucke, M.J. Kloker, U. Rist, Accuracy Analysis of the Fundamental Finite-difference Methods on Non-uniform Grids (Internal Report), in, Institut fuer Aerodynamik und Gasdynamik, Stuttgart University, Germany, Stuttgart Germany, 2009.

[171] R Core Team, R: A Language and Environment for Statistical Computing, in, R Foundation for Statistical Computing, Vienna, Austria, 2012.

[172] P.M. Elias, G.K. Menon, S. Grayson, B.E. Brown, Membrane Structural Alterations in Murine Stratum Corneum: Relationship to the Localization of Polar Lipids and Phospholipases, J Investig Dermatol, 91 (1988) 3-10.

[173] D. Southwell, B.W. Barry, R. Woodford, Variations in Permeability of Human Skin Within and Between Specimens, Int J Pharm, 18 (1984) 299-309.

[174] C. Herkenne, A. Naik, Y.N. Kalia, J. Hadgraft, R.H. Guy, Ibuprofen Transport Into and Through Skin from Topical Formulations: In Vitro-In Vivo Comparison, J Invest Dermatol, 127 (2006) 135-142.

[175] E. Jaeckle, U.F. Schaefer, H. Loth, Comparison of Effects of Different Ointment Bases on the Penetration of Ketoprofen Through Heat-separated Human Epidermis and Artificial Lipid Barriers, J Pharm Sci, 92 (2003) 1396-1406.

[176] F. Pirot, Y.N. Kalia, A.L. Stinchcomb, G. Keating, A. Bunge, R.H. Guy, Characterization of the Permeability Barrier of Human Skin In Vivo, Proc Natl Acad Sci USA, 94 (1997) 1562-1567.

[177] C. Herkenne, A. Naik, Y.N. Kalia, J. Hadgraft, R.H. Guy, Dermatopharmacokinetic Prediction of Topical Drug Bioavailability In Vivo, J Invest Dermatol, 127 (2006) 887-894.

[178] S. Hansen, D. Selzer, U.F. Schaefer, G.B. Kasting, An Extended Database of Keratin Binding, J Pharm Sci, 100 (2011) 1712-1726.

[179] P.V. Raykar, M.-C. Fung, B.D. Anderson, The Role of Protein and Lipid Domains in the Uptake of Solutes by Human Stratum Corneum, Pharm Res, 5 (1988) 140-150.

[180] D.C. Schwartzendruber, P. Wertz, D.T. Downing, Evidence that the Corneocyte Has a Chemically Bound Lipid Envelope, J Invest Dermatol, 88 (1987) 709-713.

[181] U. Hagedorn-Leweke, B.C. Lippold, Accumulation of Sunscreens and Other Compounds in Keratinous Substrates, Eur J Pharm Biopharm, 46 (1998) 215-221.

[182] G.B. Kasting, N.D. Barai, T.F. Wang, J.M. Nitsche, Mobility of Water in Human Stratum Corneum, J Pharm Sci, 92 (2003) 2326-2340.

[183] S. Yadav, N.G. Pinto, G.B. Kasting, Thermodynamics of Water Interaction with Human Stratum Corneum I: Measurement by Isothermal Calorimetry, J Pharm Sci, 96 (2007) 1585-1597.

[184] D. Weininger, Smiles, a Chemical Language and Information System. 1. Introduction to Methodology and Encoding Rules, P Edinburgh Math Soc, 17 (1970) 1-14.

[185] R. Guha, M.T. Howard, G.R. Hutchinson, P. Murray-Rust, H. Rzepa, C. Steinbeck, J.K. Wegner, E. WIllighagen, The Blue Obelisk Interoperability in Chemical Informatics, J Chem Inf Model, 46 (2006) 991-998.

[186] D. Selzer, DSkin – A Graphical Software Application to Model Dermal Absorption, in, Saarland University, Saarbruecken, 2010.

[187] T.C. Rohner, D. Staab, M. Stoeckli, MALDI Mass Spectrometric Imaging of Biological Tissue Sections, Mech Ageing Dev, 126 (2005) 177-185.

[188] L. Franzen, D. Selzer, J.W. Fluhr, U.F. Schaefer, M. Windbergs, Towards Drug Quantification in Human Skin With Confocal Raman Microscopy, Eur J Pharmaceut Biopharmaceut, 84 (2013) 437-444.

[189] H. Wagner, K.-H. Kostka, W. Adelhardt, U.F. Schaefer, Effects of Various Vehicles on the Penetration of Flufenamic Acid into Human Skin, Eur J Pharm Biopharm, 58 (2004) 121-129.

[190] Y.Y. Grams, L. Whitehead, P. Cornwell, J.A. Bouwstra, Time and Depth Resolved Visualisation of the Diffusion of a Lipophilic Dye into the Hair Follicle of Fresh Unfixed Human Scalp Skin, J Control Release, 98 (2004) 367-378.

[191] B. Yu, K.H. Kim, P.T.C. So, D. Blankschtein, R. Langer, Visualization of Oleic Acid-induced Transdermal Diffusion Pathways Using Two-photon Fluorescence Microscopy, J Investig Dermatol, 120 (2003) 448-455.

[192] P.J. Caspers, G.W. Lucassen, H.A. Bruining, G.J. Puppels, Automated Depth-Scanning Confocal Raman Microspectrometer for Rapid In Vivo Determination of Water Concentration Profiles in Human Skin, J Raman Spectrosc, 31 (2000) 813-818.

[193] M. Mélot, P.D.A. Pudney, A.-M. Williamson, P.J. Caspers, A. Van Der Pol, G.J. Puppels, Studying the Effectiveness of Penetration Enhancers to Deliver Retinol Through the Stratum Cornum by In Vivo Confocal Raman Spectroscopy, J Control Release, 138 (2009) 32-39.

[194] J. Lademann, P.J. Caspers, A. van der Pol, H. Richter, A. Patzelt, L. Zastrow, M. Darvin, W. Sterry, J.W. Fluhr, In Vivo Raman Spectroscopy Detects Increased Epidermal Antioxidative Potential with Topically Applied Carotenoids, Laser Phys Lett, 6 (2009) 76-79.

[195] G. Zhang, C.R. Flach, R. Mendelsohn, Tracking the Dephosphorylation of Resveratrol Triphosphate in Skin by Confocal Raman Microscopy, J Control Release, 123 (2007) 141-147.

[196] M. Förster, M.-A. Bolzinger, D. Ach, G. Montagnac, S. Briançon, Ingredients Tracking of Cosmetic Formulations in the Skin: A Confocal Raman Microscopy Investigation, Pharm Res, 28 (2011) 858-872.

10 List of publications

Publications in peer-reviewed journals (original articles)

Hansen, S., Selzer, D., Schaefer, U. F., Kasting, G. B. (2011). An Extended Database of Keratin Binding. *J Pharm Sci*, 100(5), 1712–1726.

Hahn, T., Selzer, D., Neumann, D., Kostka, K. H., Lehr, C.-M., Schaefer, U. F. (2012). Influence of the Application Area on Finite Dose Permeation in Relation to Drug Type Applied. *Exp Dermatol,* 21(3), 233–235.

Selzer, D., Hahn, T., Naegel, A., Heisig, M., Kostka, K. H., Lehr, C.-M., Neumann, D., Schaefer, U. F., Wittum, G. (2013). Finite Dose Skin Mass Balance Including the Latral Part: Comparison Between Experiment, Pharmacokinetic Modeling and Diffusion Models. *J Control Release,* 165(2), 119–128.

Franzen, L., Selzer, D., Fluhr, J. W., Schaefer, U. F., Windbergs, M. (2013). Towards Drug Quantification in Human Skin with Confocal Raman Microscopy. *Eur J Pharmaceut Biopharmaceut*, 84(2), 437–444.

Selzer, D., Neumann, D., Neumann, H., Kostka, K. H., Lehr, C.-M., Schaefer, U. F. (2014). A Strategy for In-Silico Prediction of Skin Absorption in Man. *(submitted)*

Publications in peer-reviewed journals (reviews)

Selzer, D., Abdel-Mottaleb, M. M. A., Hahn, T., Schaefer, U. F., & Neumann, D. (2013). Finite and Infinite Dosing: Difficulties in Measurements, Evaluations and Predictions. *Adv Drug Deliver Rev,* 65(2), 278–294.

Book chapters

Selzer, D., Schaefer, U. F., Lehr, C.-M., Hansen, S. (2013) Basic Mathematics in Skin Absorption. In H. Maibach (Ed.), Percutaneous Penetration Enhancers: *Springer Press* (in press)

Schaefer, U. F., Selzer, D., Hansen, S., Lehr, C.-M. (2013) Human native and reconstructed skin preparations for in vitro penetration and permeation studies. In H. Maibach (Ed.), Percutaneous Penetration Enhancers: *Springer Press* (in press)

Other publications

Hahn, T., Selzer., D., Neumann, D., Schaefer, U. F. (2011) Das geht unter die Haut – Aufbau der humanen Haut und mögliche Invasionswege. *PZ Prisma,* 1, 35–43

Conference contributions – oral presentations

Selzer, D., Hahn, T., Neumann, D., Lehr C.-M., Schäfer, U. F. The Role of the Lateral Compartment for Finite Dose Skin Penetration Experiments in Vitro. *Modeling Biological Membranes,* Frankfurt am Main (Germany), February 22–24th 2011

Selzer, D., Naegel, A., Hahn, T., Heisig, M., Neumann, D., Lehr C.-M., Wittum, G., Schäfer, U. F. Finite Dose Skin Mass Balance Including a Lateral Part – Comparison Between In-silico Modeling and Experiment. *Skin and Formulation 4th Symposium,* Lyon (France), June 4–5th 2012

Selzer, D., Schaefer U. F. Advanced In-silico Models for Skin Absorption. *2nd MoSiPS Meeting – Modeling of complex biological systems,* Saarbrücken (Germany), October 7th 2013

Conference contributions – poster presentations

Selzer, D., Hahn, T., Neumann, D., Lehr C.-M., Schaefer U. F. Finite Dose Skin Penetration Experiments In Vitro: The Role of the Lateral Compartment. *DPhG Jahrestagung*, Braunschweig (Germany), October 4–7th 2010.

Selzer, D., Schaefer U. F., Lehr C.-M., Neumann, D. DSkin – A Graphical Software Application to Simulate Dermal Absorption. *Skin Forum 12th Annual Meeting*, Frankfurt (Germany), March 28–29th 2011

Hahn, T., Selzer, D., Neumann, D., Lehr, C.-M., Schaefer, U. F. The Role of Donor Surface Distribution in Finite Dose Skin Absorption Experiments. *Occupational and Environmental Exposure of Skin to Chemicals*, Toronto, Canada, June 5–8th 2011

Selzer, D., Naegel, A., Hahn, T., Heisig, M., Neumann, D., Lehr C.-M., Wittum, G., Schäfer, U. F. Finite Dose Skin Mass Balance Including a Lateral Part – Comparison Between In-silico Modeling and Experiment. *Skin and Formulation 4th Symposium*, Lyon (France), June 4–5th 2012

Selzer, D., Schaefer U. F., Lehr C.-M., Neumann, D. DSkin – A Graphical Software Application to Simulate Dermal Absorption. *9th International Conference and Workshop on Biological Barriers*, Saarbrücken (Germany), February 29th – March 9th 2012

Franzen, L., Selzer, D., Hahn, T., Fluhr, J., Schaefer, U. F., Windbergs M. Utilizing Confocal Raman Microscopy as Advanced Technique for Drug Follow Up Studies in Human Skin. *9th International Conference and Workshop on Biological Barriers*, Saarbrücken (Germany), February 29th – March 9th 2012

11 Acknowledgement

I would like to thank my advisors, Professors Claus-Michael Lehr and Ulrich F. Schäfer, for supporting me during all these years and giving me the opportunity to work with them. Both did a remarkable job in keeping me motivated and focused - especially in times when I tend to lose track in my research. Furthermore, I would like to thank Prof. Stefan Diebels on his opinion regarding this thesis and the other members of the examination board. During my time at the institute I met a lot of smart and kind people, and I am grateful for this experience. I had the opportunity to be involved in a broad range of research projects and learned a lot from people that came from various fields of life sciences, mathematics and computer sciences. A special thanks goes out to my colleagues Dr. Steffi Hansen, Dr. Tsambika Hahn, Dr. Julian Kirsch and Dr. Sandra Gantzsch from Saarland University, as well as Dr. Arne Nägel and Dr. Michael Heisig from Frankfurt University. It was a pleasure to support and advice Jan Riehm working on his well received master's thesis. Furthermore, I would like to thank Dr. Dirk Neumann, who introduced me (together with Professor Schäfer) in the field of modeling the skin barrier - a topic I deeply felt in love with. I am grateful for the support and encouragement provided by my family and friends. They all gave me the room to ask, to try, to fail and to succeed. Science can be cruel at times, and it is important to have people on your side to reset your focus and bump you in the right direction at times.

Appendix A

Table A-1 Parameters for simulations with the homogenized diffusion model. A) For the model with one regression parameter (HOM1), all parameters except for D_{SC} are taken from [125]. B) For the model with three regression parameters (HOM3), all parameters except for D_{DON} were optimized according to the parameterization provided in the text. The optimized parameters are labeled with an asterisk. The regression parameters and standard errors for both models are reported in Table A-3.

	Times [min]		FFA	CAF (1mg/ml)	CAF (12.5 mg/ml)	Reference
A	D_{DON}	[cm²/h]	2.47E-02	2.92E-02	2.92E-02	Equation 4-4
	$D^{*}_{SC,rr}$	[cm²/h]	2.00E-05	3.70E-05	3.70E-05	Equation 4-6
	$D^{*}_{SC,zz}$	[cm²/h]	10.43E-07	1.69E-07	2.29E-07	Equation 4-6
	D_{DSL}	[cm²/h]	4.90E-03	2.30E-03	2.30E-03	[125]
	$K_{SC/DON}$		5.88	4.70	4.70	[125]
	$K_{SC/DSL}$		3.0	27.00	27.00	[125]
B	D_{DON}	[cm²/h]	2.47E-02	2.92E-02	2.92E-02	Equation 4-4
	$D^{*}_{SC,rr}$	[cm²/h]	1.98E-05	3.70E-05	3.73E-05	Equation 4-6
	$D^{*}_{SC,zz}$	[cm²/h]	7.72E-07	1.54E-07	5.97E-07	Equation 4-6
	D^{*}_{DSL}	[cm²/h]	3.26E-03	1.87E-03	10.72E-03	
	$K^{*}_{SC/DON}$		8.54	5.77	2.57	
	$K^{*}_{SC/DSL}$		4.36	33.13	14.75	

Table A-2 Rate constants and standard errors (SE) of the pharmacokinetic model

Parameter	FFA		Caffeine (1mg/ml)		Caffeine (12.5 mg/ml)	
	Mean [%/min]	SE	Mean [%/min]	SE	Mean [%/min]	SE
k_1	3,70E-02	3,45E-03	3,81E-03	2,09E-04	5,92E-03	5,68E-04
k_2	4,52E-02	5,29E-03	5,73E-03	4,66E-04	2,11E-02	3,08E-03
k_3	6,78E-03	2,80E-04	2,76E-04	3,14E-04	4,35E-03	1,55E-03
k_4	2,29E-04	2,42E-04	1,52E-03	1,90E-03	2,38E-03	2,68E-03
k_5	1,00E-03	8,42E-04	1,96E-03	7,79E-04	4,52E-03	1,78E-03
k_6	7,12E-04	1,15E-04	1,50E-03	4,06E-04	5,53E-03	1,61E-03
k_7	-	-	1,05E-03	4,30E-04	2,13E-03	4,37E-04

Table A-3 Regression parameters for simulations with the homogenized diffusion model.

	Parameter		FFA	CAF (1mg/ml)	CAF (12.5mg/ml)	Reference
A	Homogenized model with one regression parameter.					
	D_{LIP}	[cm^2/h]	1.10E-04	2.10E-04	2.10E-04	[125]
	θ1		-4.91E+00 ± 9.93E-02	-9.72E+00 ± 1.68E+00	-8.12E+00 ± 6.65E-01	
	ξ		7.39E-03 ± 7.33E-04	6.00E-05 ± 1.01E-04	2.98E-04 ± 1.98E-04	
	$\alpha_{SC,rr}$		1.82E-01	1.76E-01	1.76E-01	
	$\alpha_{SC,zz}$		9.48E-03	8.06E-04	1.09E-03	
B	Homogenized model with three regression parameters.					
	D_{LIP}	[cm^2/h]	1.10E-04	2.10E-04	2.10E-04	[125]
	θ1		-5.24 ± 0.11	---	-6.33 ± 0.29	
	θ2		-0.41 ± 0.27	1.08 ± 0.37	1.54 ± 0.32	
	θ3		-0.37 ± 0.09	-0.20 ± 0.07	0.60 ± 0.16	
	ξ		5.31E-03 ± 5.65E-04	---	1.78E-03 ± 5.21E-04	
	$\alpha_{SC,rr}$		1.80E-01	1.76E-01	1.77E-01	
	$\alpha_{SC,zz}$		7.02E-03	7.35E-04	2.85E-03	